Subterranean Biology 33: 87–108 (2020)
doi: 10.3897/subtbiol.33.48721
http://subtbiol.pensoft.net

RESEARCH ARTICLE

A peer-reviewed open-access journal
Subterranean Biology
Published by The International Society for Subterranean Biology

Troglomorphism in the brittle star *Ophionereis commutabilis* Bribiesca-Contreras et al., 2019 (Echinodermata, Ophiuroidea, Ophionereididae)

Francisco Márquez-Borrás[1], Francisco A. Solís-Marín[2], Luis M. Mejía-Ortiz[3]

1 *Posgrado en Ciencias del Mar y Limnología, Instituto de Ciencias del Mar y Limnología (ICML), Universidad Nacional Autónoma de México (UNAM), Apdo. Post. 70-305, Ciudad de México 04510, México* **2** *Laboratorio de Sistemática y Ecología de Equinodermos, Instituto de Ciencias del Mar y Limnología, Universidad Nacional Autónoma de México, Circuito Universitario s/n, Ciudad de México 04510, México* **3** *Laboratorio de Bioespeleología y Carcinología, Universidad de Quintana Roo, División de Desarrollo Sustentable, Av. Andrés Quintana Roo s/n, Cozumel 77600, Quintana Roo, México*

Corresponding author: *Márquez-Borrás* (marquez@ciencias.unam.mx)

Academic editor: *Oana T. Moldovan* | Received 23 November 2019 | Accepted 27 January 2020 | Published 5 March 2020

http://zoobank.org/EBDB477C-A272-4ECF-8682-CCB256CE2EA0

Citation: Márquez-Borrás F, Solís-Marín FA, Mejía-Ortiz LM (2020) Troglomorphism in the brittle star *Ophionereis commutabilis* Bribiesca-Contreras et al., 2019 (Echinodermata, Ophiuroidea, Ophionereididae). Subterranean Biology 33: 87–108. https://doi.org/10.3897/subtbiol.33.48721

Abstract

Due to their peculiar and sometimes bizarre morphology, cave fauna (across invertebrates and vertebrates from both aquatic and terrestrial cave habitats) have fascinated researchers throughout history. Despite their success in colonizing most marine ecosystems, the adaptations of cave brittle stars (Ophiuroidea) to a stygobiotic lifestyle have been scarcely examined. Employing comparative methods on a data set of two species belonging to the genus *Ophionereis*, this study addresses whether a cave-dwelling species from Cozumel exhibited similar troglomorphic traits as those of other taxa inhabiting caves. Our work demonstrated that some characters representing potential morphological cave adaptations in *O. commutabilis* were: bigger sizes, elongation of arms and tube feet and the presence of traits potentially paedomorphic. In addition, an element of ophiuroid's photoreceptor system, as well as pigmentation, was observed to be peculiar in this stygobiotic species, plausibly as a result of inhabiting a low light-energy environment. Finally, we add evidence to the statement that *O. commutabilis* is a cave endemic species, already supported by demography, distribution and origin of this species, and now by a typical array of troglomorphisms.

Keywords

adaptation, Aerolito, anchialine system, cave, Cozumel, ophiuroid, stygobiotic

Introduction

Several traits are often associated with cave-dwellers, which are also known as troglomorphisms, defined as a morphological modification in cave fauna (Culver et al. 1995; Romero 2009). These modifications or morphological traits could be expressed as reductive or constructive traits, such as the lack of photoreceptors or depigmentation in the case of the former and as the hypertrophy of appendages for the latter (Mejía-Ortíz et al. 2006, Gonzalez et al. 2018). All these traits allow organisms to survive in caves, environments that constitute isolated and harsh habitats (Culver and Pipan 2009).

According to Bishop et al. (2015), anchialine caves are "a tidally-influenced subterranean estuary located within crevicular and cavernous karst and volcanic terrains that extends inland to the limit of seawater penetration". These environments are thought to be food-limited, with detritus and dissolved organic matter being the most important nutritional sources (Mejía-Ortíz et al. 2013). However, several caves have an important contribution of food from bacterial activity (Sarbu et al. 1996; Pohlman et al. 1997; Brankovits et al. 2017). The limitation of food is related to the fact that caves are completely devoid of sunlight and lack of sources of primary productivity (Culver et al. 1995; Gonzalez et al. 2018).

Although cave fauna is mainly composed by crustaceans, several studies have reported organisms of other taxa inhabiting these ecosystems (Sket 1996; Gibert and Deharveng 2002; Calderón-Gutiérrez et al. 2017). Concerning echinoderms, 58 species have been reported inhabiting cave environments, distributed into the five classes of the phylum: Crinoidea (2 species), Asteroidea (8), Ophiuroidea (39), Echinoidea (5) and Holothuroidea (4) (Martínez García et al. 2009; Pomory et al. 2011; Bribiesca-Contreras et al. 2013; Tan et al. 2014; Okanishi and Fujita 2019; Okanishi et al. 2019). However, only five of these species have been described as stygobiotic species (restricted aquatic cave-dwelling organism), the starfish *Copidaster cavernicola* Solís-Marín & Laguarda-Figueras, 2010 and the ophiuroids *Amphicutis stygobita* Pomory, Carpenter & Winter, 2011, *Ophiozonella cavernalis* Okanishi & Fujita, 2018, *Ophionereis commutabilis* Bribiesca-Contreras et al., 2019 and *Ophiopsila xmasilluminans* Okanishi, Oba & Fujita, 2019. This is surprising considering that there are over 7,500 species of echinoderms that live in a wide variety of habitats (Zhang 2011). Also striking is the fact that although Ophiuroidea is the largest class of echinoderms (about 2100 described species according to O'Hara et al. (2018)) and are generally photonegative (Stöhr et al. 2012; O'Hara et al. 2018), only a few (39) species have been found in caves.

Troglomorphism has been investigated mainly on arthropods and vertebrates from both aquatic and terrestrial caves (Poulson and White 1969; Mejía-Ortíz and Hartnoll 2005; White and Culver 2012; Mejía-Ortíz et al. 2013; Rizzato and Bichuette 2017). Despite the existence of some studies about troglomorphism on other taxa (White and Culver 2012; Gonzalez et al. 2018), no extensive study has been conducted on stygobiotic echinoderms. Instead, only a few remarks have been made on the morphology of species of echinoderms and its relation with the cave-habitat (Mejía-Ortíz et al. 2007;

Solís-Marín and Laguarda-Figueras 2010; Pomory et al. 2011; Brom et al. 2015; Carpenter 2016; Okanishi and Fujita 2018; Bribiesca-Contreras et al. 2019).

Thus, the aim of this study is the identification of morphological adaptations of *O. commutabilis*. To test the hypothesis that *O. commutabilis* shows troglomorphisms, we carried out a comparative study between *O. commutabilis* and its epigean congener *O. reticulata*. A comparison with other epigean congeners for several traits, as well as the similarities among cave-dwelling brittle stars are discussed. As this is one of the first studies to investigate troglomorphism in brittle stars, our assumptions are mainly based on the analogy to previously identified troglomorphic traits throughout other stygobiotic taxa. Implications for troglomorphism are discussed with respect to concepts of cave biology.

Methods

Species selection

Ophionereis reticulata (Say, 1825) was selected to use as a reference for comparison, based on both morphological and genetic resemblance between Caribbean *Ophionereis* species with *O. commutabilis* (Bribiesca-Contreras et al. 2013, 2019). Therefore, specimens of *O. commutabilis* (*N* = 46) from the anchialine system El Aerolito, Cozumel Island (20°27'58.4"N, 86°58'41.2"W) (details in Bribiesca-Contreras et al. 2019) were compared with their reef relatives, *O. reticulata* (*N*= 59) from localities in Quintana Roo, Mexico. All the analysed material is deposited in the "Colección Nacional de Equinodermos Dra. María Elena Caso", at Instituto de Ciencias del Mar y Limnología, of Universidad Nacional Autónoma de México (**UNAM**).

Selection of morphological traits

Morphological traits were chosen based on the previous studies on other taxa, and from our personal observations. We sampled and compared the morphological traits described below. A detailed discussion of each character is provided.

Arms and tube feet length

Elongation of body appendages are well documented traits in cave fauna, as they affect both sensorial and feeding structures in aquatic and terrestrial environments (Turk et al. 1996; Mejía-Ortíz et al. 2006, 2013). Arms of brittle stars are used mainly for locomotion and present tube feet and spines, both being the only known sensorial organs of this taxa (Hajduk 1992; Zueva et al. 2018). Spines and tube feet also participate in the acquisition of food by suspension feeding (Stöhr et al. 2012). Cave brittle stars show unique patterns of tube feet and arm length, proposed to be the result of differ-

ent forms of locomotion and feeding in these environments (Bribiesca-Contreras et al. 2019; Pomory et al. 2011).

Here we evaluate the elongation of arms and tube feet as a potential morphological adaptation to the cave. Measures of the structure's length were correlated with the disc diameter of each specimen. Length of arms was measured from the first to the last segment, considering only complete arms without regenerating scars. Tube feet and oral tentacle length were measured from the base (at the tentacle pore or tentacle basin, respectively) to the tip of the structure. Tube feet were considered from proximal, middle and distal portions of the arm (based on Munday (1993)), and were measured using image analysis software (ADOBE PHOTOSHOP CC: RRID: SCR_014199) calibrated with scaled photographs of fixed organisms.

Regeneration frequency

Regeneration is a common process on brittle stars, caused by damage of arms through sub-lethal predation. As a result, regeneration rate of arms is often used as an estimate of predation pressure (Sköld and Rosenberg 1996; Dupont and Thorndyke 2006; Yokoyama and Amaral 2010), which in caves decreases in importance or is absent (Gibert and Deharveng 2002). The regeneration frequencies of each specimen were registered by counting the regenerating scars on the oral side. To identify the scars, we compared differences in colour and size patterns between regenerated portions and old sections.

Paedomorphic traits

Morphological juvenile traits retained by sexually mature organisms have been reported for cave-dwellers, also known as paedomorphic features (Culver 1982; Sket 1996; Culver and Pipan 2009). Cave brittle stars could show some paedomorphic traits related to organization, size and calcification of skeletal plates of arms and disc (Pomory et al. 2011). For this reason, external morphology and microstructure of arm plates (dorsal, ventral, lateral, spines, tentacle scales) from proximal, middle and distal portions of the arm of mature and juvenile specimens were analysed. Likewise, radial shields and buccal skeleton (oral and adoral shields; oral and dental plates, as well as teeth) were considered.

The arm ossicles used for microstructure examination were obtained from one arm of each specimen selected. Tissue was removed by soaking two segments of each portion in 5% sodium hypochlorite and later washed with MilliQ water. Ossicles were mounted on a stub and coated with gold for taking micrographs using a Hitachi SU1510 scanning electron microscope (SEM).

Images of the external face of dorsal, ventral and lateral arm plates were analysed using both geometric morphometrics and morphological approaches. For geometric morphometrics, TPS, MAKEFAN8 and MORPHOJ *v*2.0 software (MorphoJ, RRID: SCR_016483) were used. Landmarks (LM) were digitized to describe the perimeter of the plates (Suppl. materials 1, Fig. S1). Madreporic oral shields, teeth, spines and tentacle scales were examined by comparing the morphology of outer face between

species. Oral, radial and adoral shields, as well as oral and dental plates, were analysed by comparing porosity of external stereom.

Photoreceptors

Brittle stars have a photoreceptor system consisting of nerve bundles, chromatophores and expanded peripheral trabeculae (EPT) (Hendler and Byrne 1987; Aizenberg et al. 2001). EPTs are hemispheres on the outer face of arm plates and have been suggested to be a structural adaptation relating to chromatophore activity (Sumner-Rooney et al. 2018). Considering that caves exhibit total darkness, processes like photoreception and bioluminescence, as well as the involved structures, could be modified. Therefore, we estimated the EPTs density of the central region of the dorsal arm plates by using SEM images.

In addition to morphological traits, spectral transmittance of isolated dorsal arm plates was estimated by coupling a source of white light (LS-1-II Ocean Optics) to an HR4000 spectrophotometer. We used two optical fibres of 50 and 100 μm on different positions to obtain readings of three dorsal-proximal arm plates of each species (*O. reticulata* and *O. commutabilis*). Data were normalized and analysed on ORIGIN PRO 9.1 software (Origin, RRID: SCR_014212).

Statistical analyses

We analyzed the number of arms and specimens regenerating as well as arm and tube feet ratios between the two species considered. Data and R-scripts used throughout this work are available on the supporting information. All analyses were performed under software RSTUDIO *v*3.5.0. (Team 2016).

Concerning geometric morphometrics analysis, after the Procrustes fit of the sample, canonical variate analysis (CVA) was performed to explore morphological differences among species using geometric morphometric analysis of arm plates. *P* values were calculated using a permutation test based on 100,000 iterations of the Mahalanobis distances for differences. CVA, including estimation of the significance of Mahalanobis distances using a parametric approach (Procrustes ANOVA), was also performed to assess the statistical robustness of the groups delineated in the CVA.

Results

Appendages length

A remarkable arm elongation is observed in *O. commutabilis*, with arms up to 20 times the disc diameter and a mean of 13.2 in comparison to 6.6 of *O. reticulata*. This ratio showed statistical differences between species (ANOVA, $F_{1, 105}=559.3$; $p<0.001$). Furthermore, we found that arms of specimens of equal size from both cave and epigean

species are integrated by segments of similar length (Suppl. materials 2, Table S1), hence, cave species having more segments. No differences of oral tentacle nor tube feet length were found among species in either proximal or middle portions of arms. Distal tube feet showed statistical differences in length (ANOVA, $F_{1, 48}$=18.1; p <0.001), where the stygobiotic specimens had longer tube feet than *O. reticulata*. These results are summarized in Table 1.

After measuring the disc diameter, we observed that stygobiotic specimens showed bigger sizes. For the disc diameter, we observed between mature *O. reticulata* and *O. commutabilis*, statistical differences (ANOVA, F1, 88= 4.54; p <0.05). Cave-dwelling specimens having a disc diameter 14% bigger than its epigean congener.

Regeneration frequency

Based on recorded observations of specimens of *O. commutabilis*, 32% (n= 46) showed signs of arm regeneration. Besides, 14% of arms observed (n= 196) were damaged. In comparison, from the 51 individuals of *O. reticulata* analyzed, 70% showed signs of arm regeneration. Correspondingly, 35% of arms (n= 213) were damaged in specimens of *O. reticulata*.

The average of arms regenerating per individual in cave-dweller specimens was 0.7 (14.42%) while in reef individuals was 1.6 arms (33.16%). Statistical analysis showed a difference between species for these data (ANOVA, $F_{1, 95}$= 12.52; p <0.001).

Microstructures

Dorsal arm plates (DAP) of both species are different in form, being hexagonal in mature *O. commutabilis* and trapezoid in *O. reticulata* (Fig. 1). Meanwhile, DAP of juvenile specimens of *O. reticulata* are hexagonal (Fig. 1c). Geometric morphometric analyses allowed us to confirm the statistical significance of differences in form between plates of mature specimens of both species (Table 2). Deformation grids in the DAP shape showed the mentioned change based on LM displacement vectors (Fig. 1d). Although ventral arm plates (VAP) of *O. reticulata* are slightly wider than those of *O. commutabilis*, the general shape is similar in both species (Fig. 2). Ventral arm plates (VAP) of mature *O. reticulata* specimens are also wider than juveniles of this species (Fig. 2c). Differences in form of VAP between species were confirmed with CVA ($P < 0.001$) and deformation grid exhibited the difference in width among species (Fig. 2d). Both DAP and VAP of juvenile specimens of *O. commutabilis* show the same shape than plates of mature specimens. Finally, lateral arm plates showed significant differences in form between species (Table 4) but no clear pattern associated (Fig. 3). Examination of arm plates allowed us to corroborate the correlation between serial and ontogenetic variation, that is to say, distal plates analogous to plates of juvenile specimens.

Table 1. Summary of morphometric results showing significant (S) and not significant (NS) differences for each trait. For traits with statistically significant differences the result of it with respect to the cave species is expressed as longer/bigger than *O. reticulata* (↑). NT: not statistically tested.

Trait	Differences	Result
Arm length	S	*O. commutabilis* ↑
Number of arm segments	NT	*O. commutabilis* ↑
Oral tentacle length	NS	-
Proximal tube feet length	NS	-
Middle tube feet length	NS	-
Distal tube feet length	S	*O. commutabilis* ↑

Table 2. Geometric morphometrics results for DAP. *Ophionereis* spp. dorsal arm plates Procrustes ANOVA and P values based on permutation test results with environment (Reef for *O. reticulata* and Cave for *O. commutabilis*) as covariate (Mahalanobis distance in parenthesis).

		Procrustes ANOVA			
Effect	**SS**	**MS**	***df***	***F***	***P*(param.)**
Individual	0.06245164	0.0052043037	12	3.01	0.0005
Residual	0.53979931	0.0017301260	312		
		***P* value based on permutation test**			
	Environment			Cave	
	Reef			<0.0002(2.39)	

Table 3. Geometric morphometrics results for VAP. *Ophionereis* spp. ventral arm plates Procrustes ANOVA and P values based on permutation test results with environment (Reef for *O. reticulata* and Cave for *O. commutabilis*) as covariate (Mahalanobis distance in parenthesis).

		Procrustes ANOVA			
Effect	**SS**	**MS**	***df***	***F***	***P*(param.)**
Individual	0.02209517	0.0012275093	18	5.00	<0.0001
Residual	0.11482214	0.0002453465	468		
		***P* value based on permutation test**			
	Environment			Cave	
	Reef			<0.0001(7.34)	

Table 4. Geometric morphometrics results for LAP. *Ophionereis* spp. lateral arm plates Procrustes ANOVA and P values based on permutation test results with environment (Reef for *O. reticulata* and Cave for *O. commutabilis*) as covariate (Mahalanobis distance in parenthesis).

		Procrustes ANOVA			
Effect	**SS**	**MS**	***df***	***F***	***P*(param.)**
Individual	0.11434060	0.0043977153	26	7.58	<0.0001
Residual	0.73910392	0.0005801444	1274		
		***P* value based on permutation test**			
	Environment			Cave	
	Reef			<0.0001(6.27)	

Concerning microstructures qualitatively analyzed, *O. commutabilis* tentacle scales are ovoid and longer than wide, which resembles the same plates of juvenile *O. reticulata* (Fig. 4a–c). On the other hand, spines showed no clear differences in form among species. All examined microstructures exhibited differences in porosity, with

Table 5. Comparison of several traits between a stygobiotic *Ophionereis* species and its closest epigean relatives. dd: disc diameter; al: arm length; DAP: dorsal arm plate; VAP: ventral arm plates; ND: No data.

Species	Habitat	dd (mm) [Max]	Avg ratio (al/dd) [Max]	Avg segment length (mm)	Regeneration frequency (%) [for arms]	DAP shape	VAP shape	Reference
Ophionereis commutabilis	Cave-dwelling	11.4 [17]	13.2 [20]	0.58	32 [14]	Hexagonal	Longer than wide	Present study
O. reticulata	Epigean	11.4 [15]	6.6 [8]	0.55	70 [35]	Trapezoid	Quadrangular	Bribiesca-Contreras et al. 2013, Hendler et al. 1995, Present study
O. vittata	Epigean	6.7 [10]	8 [13]	ND	ND	Rounded hexagonal	Bell shaped	Bribiesca-Contreras et al. 2013, Hendler et al. 1995, Present study
O. squamulosa	Epigean	5 [6]	8 [ND]	ND	ND	Rounded hexagonal	Bell shaped	Bribiesca-Contreras et al. 2013, 2019, Pomory 2007
O. olivacea	Epigean	4.5 [6]	5 [ND]	ND	ND	Roughly hexagonal	Bell shaped	Bribiesca-Contreras et al. 2013, 2019, Hendler et al. 1995

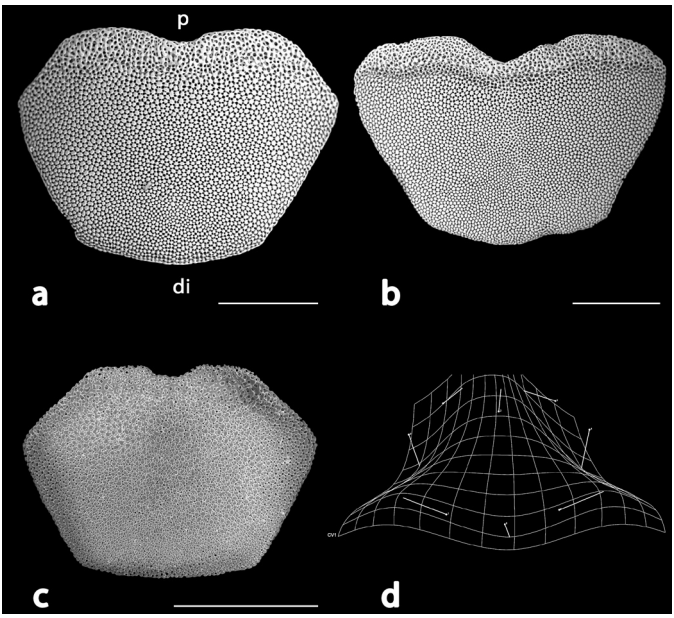

Figure 1. Scanning electron micrograph (SEM) of dorsal arm plates from mature *Ophionereis commutabilis* (**a**) and *O. reticulata* (**b**). SEM of dorsal arm plate of juvenile *O. reticulata* (**c**). Deformation grid of DAP shape showing deformation vectors (**d**). Orientation (p: proximal, di: distal). Scale bars: 400 µm.

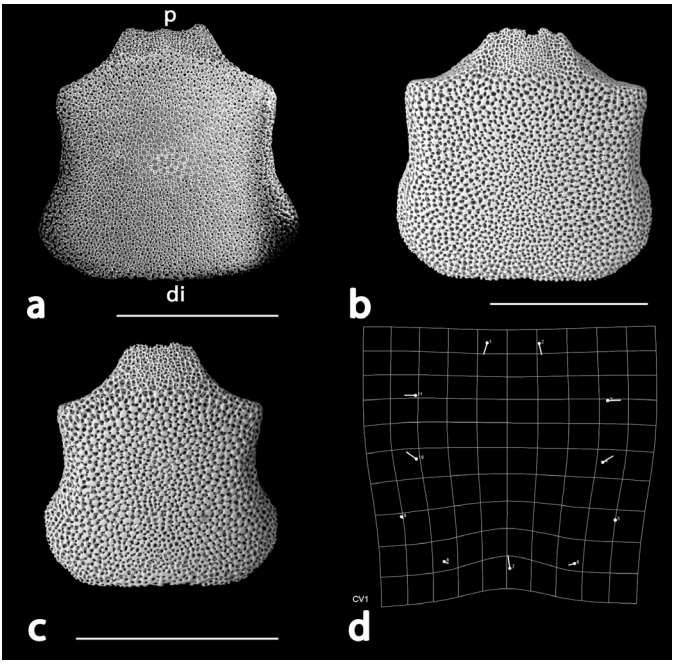

Figure 2. Scanning electron micrograph (SEM) of ventral arm plates from mature *Ophionereis commutabilis* (**a**) *and O. reticulata* (**b**). SEM of ventral arm plate of juvenile *O. reticulata* (**c**). Deformation grid of VAP shape showing deformation vectors (**d**). Orientation (p: proximal, di: distal). Scale bars: 500 µm.

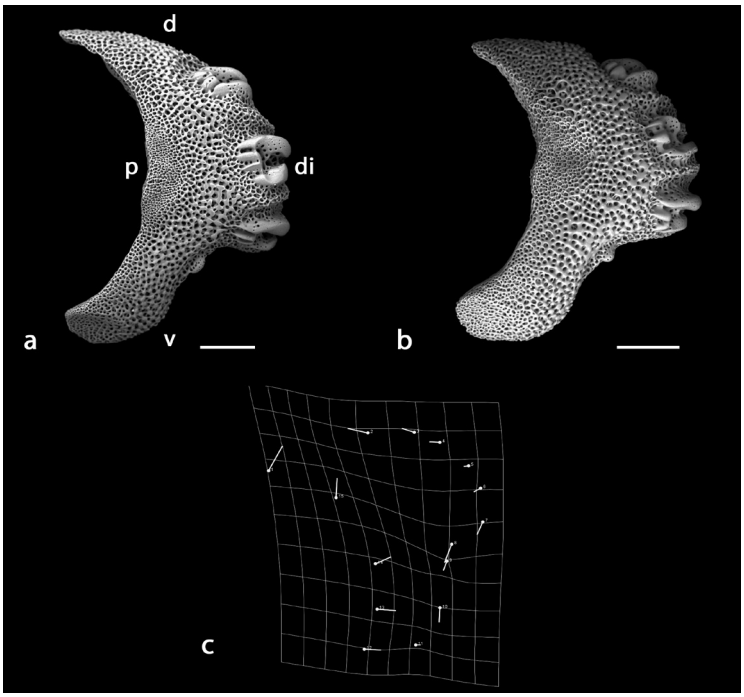

Figure 3. Scanning electron micrograph (SEM) of lateral arm plates from mature *Ophionereis commutabilis* (**a**) and *O. reticulata* (**b**). Deformation grid of lateral arm plate shape showing deformation vectors (**c**). Orientation (p: proximal, di: distal, d: dorsal, v: ventral). Scale bars: 200 μm.

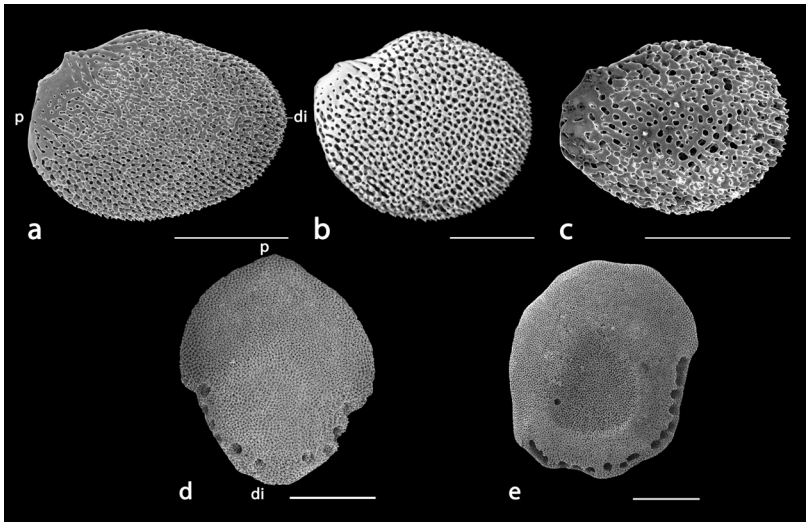

Figure 4. Scanning electron micrograph (SEM) of tentacle scales from mature *Ophionereis commutabilis* (**a**) *and O. reticulata* (**b**). SEM of tentacle scale of juvenile *O. reticulata* (**c**). SEM of madreporite of *O. commutabilis* (**d**) and *O. reticulata* (**e**). Orientation (p: proximal, di: distal). Scale bars: 200 μm (**a**–**c**); 500 μm (**d**–**e**).

the ossicles of the stygobiotic specimens being slightly more porous than its epigean congener (e.g. 5 to 9 pores surrounding each EPT in *O. commutabilis* and 4–7 in *O. reticulata* as shown in Figs 1, 5). Although these differences in porosity are observed in all ossicles, it is especially remarkable in distal arm plates, spines, tentacle scales and dental plates (Fig. 4 and Suppl. materials 1, Fig. S2). Madreporites between both species differ in form and in the number of hydropores (around eight in *O. commutabilis* and 17 in *O. reticulata*) (Fig. 4d–e). Lastly, though teeth showed great intraspecific variation, a clear pattern allowed us to distinguish between species. While *O. reticulata* possesses compound teeth, *O. commutabilis* reveals both uniform and compound teeth (Suppl. materials 1, Fig. S3).

Photoreceptors

Dorsal arm plates (DAP) of *O. commutabilis* exhibit a pattern of EPTs agglomeration, however, this pattern is only present on some DAP from the distal portion of the arm of *O. reticulata* (Fig. 5a–c). This pattern decreases the EPT density (increasing its size) on the stygobiotic specimens in comparison to its epigean congener. The EPT density of DAP relativized with the disc diameter in *O. reticulata* (498 EPT/mm^2) almost doubled that of *O. commutabilis* (251 EPT/mm^2).

Differences in the arrangement and size of the EPT in both species corresponds to a different pattern of the inner stereom through a cross-section. DAP of *O. commuta-*

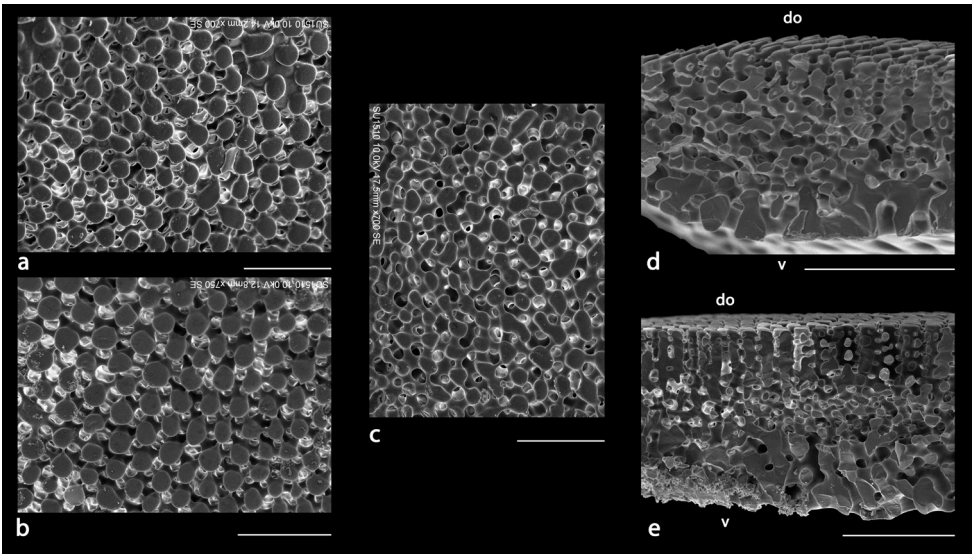

Figure 5. Scanning electron micrographs (SEM) of central region of dorsal arm plates (DAP) of *Ophionereis* brittle stars. SEM of a DAP from mature *Ophionereis commutabilis* (**a**) and *O. reticulata* (**b**). SEM of a DAP of juvenile *O. reticulata* (**c**). SEM of a cross-section of a fractured DAP from mature *O. commutabilis* (**d**) and *O. reticulata* (**e**). Orientation (do: dorsal, v: ventral). Scale bars: 50 μm (**a**–**c**); 100 μm (**d**–**e**).

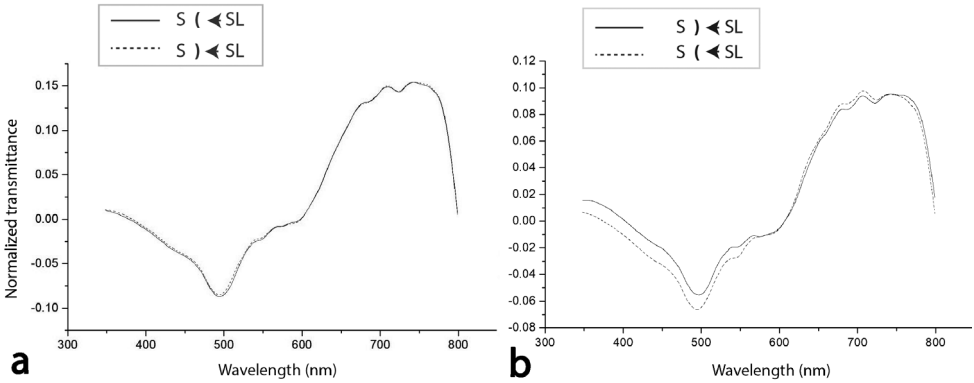

Figure 6. Dorsal arm plates transmittance of *Ophionereis reticulata* (**a**) and *O. commutabilis* (**b**). Two different arrangements between spectrophotometer (S), source light (SL) and plates are presented with concave section representing the inner face and convex the outer face]-(].

bilis show a nearly uniform disorganized pattern across the plate, while DAP of the epigean specimens exhibit two clear patterns depending on the side of the plate: (1) a dorsal half with an organized stereom associated with EPT and (2) a ventral half with unsystematic stereom (Fig. 5d–e).

Correspondingly with the differences on the microstructure of DAP, transmittance values of DAP showed differences among species. The values of epigean specimens did not differ depending on the position of optical fibres. Meanwhile, differences were observed along the spectra between the two arrangements in the transmittance values of DAP of *O. commutabilis*. For both species, the transmittance was lower around 500 nm and greater for wavelengths between 600 and 780 nm (Fig. 6). In general, plates of stygobionts showed slightly lower values of transmittance than those isolated from epigean specimens.

Discussion

Using a comparative morphological approach, we provide evidence of cave adaptation in *O. commutabilis*. This study quantified the main morphological differences observed between *O. commutabilis* and its epigean congener *O. reticulata*. Our findings were similar to those known in arthropods and are characteristic of changes considered as troglomorphism (Culver et al. 1995; Pérez-Moreno et al. 2016; Gonzalez et al. 2018).

Arm length is the most conspicuous trait of *O. commutabilis*, here we provide, for the first time, direct and quantitative evidence of this. As previously mentioned, elongation of body appendages is well documented in cave fauna as a troglomorphic trait, hence, arm elongation represents a potential morphological cave adaptation in *O. commutabilis*. The larger number of segments in *O. commutabilis* suggests that elongation is the result of having more segments than its epigean congener. Each segment has two

tentacle pores, thus cave-dwelling individuals have more tentacle pores and therefore more tube feet, as well as more spines. It has been proposed that appendage elongation increases the ability of cave fauna to locate food, avoid predation or improve sensory capability (Iliffe and Kornicker 2009; Mejía-Ortíz et al. 2006, 2013). Given that both spines and tube feet are important structures in sensory reception of ophiuroids (Hajduk 1992; Zueva et al. 2018), our results are relevant in giving a plausible explanation about the origin and function of adapted elongated arms. Additionally, these results confirm quantitively the first report of a species of Ophionereididae having arms that long (Stöhr et al. 2012; Bribiesca-Contreras et al. 2019) in average and as maximum (Table 5). This is valid not only for Caribbean species but also for species from the Pacific Ocean (e.g. *Ophionereis variegata* with an arm length average of five times the size of the disc or *O. amoyensis* with arms ten times the size of the disc) (Clark 1953).

Distal tube feet play an important role on detritus and suspension feeding (Warner 1982), which could explain *O. commutabilis* having longer distal tube feet than *O. reticulata*, suggesting that detritus and suspended particles are also (Mejía-Ortíz et al. 2013) an important source of food in the cave El Aerolito. On the other hand, oral tentacle, as well as proximal and middle tube feet, are commonly less specialized (Keogh and Keegan 2006), which provides an explanation for cave species not having longer structures than epigean congeners.

The tube feet, as well as their relation with arms in cave ophiuroids, need to be studied more deeply, as these structures probably play an important role in the evolution of cave ophiuroids. This is suggested by the striking differences in length and function among cave species and their epigean congeners demonstrated in *A. stygobita* (Carpenter 2016; Pomory et al. 2011), *O. xmasilluminans* (Okanishi et al. 2019) and *O. commutabilis* (Table 5), and between the cave species itself. Concerning arm length, the results obtained in this study are similar to that observed in *O. xmasilluminans* (Okanishi et al. 2019) and contrast with those observed in *A. stygobita* which have shorter arms (Pomory et al. 2011). Given that abiotic conditions are expected to be similar in the three caves, these differences could support the theory that elongation is associated with food-finding abilities or colonization times rather than specific abiotic factors (Delić et al. 2016).

Our results allowed us to confirm that *O. commutabilis* is distinguished by reaching big sizes in comparison to other Caribbean species of the genus (Bribiesca-Contreras et al. 2019) (Table 5). This is striking on a cave species, given that usually this fauna has a reduction in size as a response to a diminished food supply or quality (Culver et al. 1995; Culver and Pipan 2009). This could respond to the low predation rate expected for a cave environment (Gibert and Deharveng 2002) and the high population density of *O. commutabilis* in El Aerolito (Calderón-Gutiérrez and Solís-Marín 2014), factors that have been proposed to favor the survival of bigger organisms (Gage 1990; Bishop and Iliffe 2009). Larger bodies could also be advantageous in terms of energy economy and fecundity, important aspects in a cave (Trontelj et al. 2012). Interestingly, two species inhabiting similar environments show opposite patterns of population densities (low in *A. stygobita* and high in *O. commutabilis*) (Carpenter 2016) and relative sizes (small in *A. stygobita* and big in *O. commutabilis*) with respect to their epigean congeners.

The contrasting results of this study (*O. commutabilis*) compared with those obtained by Pomory et al. (2011) in *A. stygobita* point out the need for more studies on stygobiotic echinoderms. This will improve our understanding of troglomorphisms in the phylum and it would provide useful information to understand the evolution of marine organisms in caves.

Regeneration frequency was lower in *O. commutabilis* (32% of specimens and 14% of arms) than *O. reticulata* (70% and 35%). *O. commutabilis* shows similar percentages to *A. stygobita* (35% and 14%) (Carpenter 2016), another cave species. On the other hand, the regeneration frequency of *O. reticulata* is similar to that observed in other populations of this species and other epigean species (Lawrence and Vasquez 1996; Yokoyama and Amaral 2010). Therefore, the low incidence of damage in *O. commutabilis* indicates that sub-lethal predation is low inside El Aerolito as expected. This could be related with specimens inside the cave being usually found exposed rather than hidden (Bribiesca-Contreras et al. 2019: supplementary video 3), corresponding to the reduced escape behaviour observed on cave fauna (White and Culver 2012).

Stereom organization and porosity is the most conspicuous trait potentially considered as paedomorphic, being more porous in all the analysed ossicles of the cave species. Similar patterns have been proposed as an adaptive trait for deep-sea and cave brittle stars, improving feeding and gas exchange mechanisms and enhancing chemo and mechanoreception in harsh environments (Pomory et al. 2011; Carpenter 2016; Stöhr and Martynov 2016). We suggest that tentacle scales, DAP and VAP shape of *O. commutabilis* are paedomorphic traits based on the resemblance between mature cave specimen's ossicles and that of juvenile *O. reticulata*. Moreover, Bribiesca-Contreras et al. (2019) described conspicuous primary plates as a usual trait of *O. commutabilis*, which has been suggested as a paedomorphic trait in ophiuroids (Pomory et al. 2011; Martynov et al. 2015). Therefore, it seems evident that like cave brittle stars from Bahamas (Pomory et al. 2011), *O. commutabilis* specimens show paedomorphic traits on skeletal plates, as previously reported for the size in *O. olivacea* (Byrne 1991). It must be noted that *O. commutabilis* does not show some typical paedomorphic traits such as segment length-to-width ratio close to 10 (Stöhr and Martynov 2016). Moreover, some of the traits here reported as paedomorphic could be the result of other factors affecting the biology of this stygobiotic species (e.g. stereom development could be explained by abiotic factors in the cave). However, it must be considered that there are different levels of heterochronic changes affecting ophiuroids, which implies different levels of difficulty to recognize this characters, as well as different evolutionary effects on the species (Stöhr and Martynov 2016). The resemblance in DAP and VAP shape between *O. commutabilis* and the other Caribbean species (Table 5) should be studied more deeply to understand the evolutionary patterns of this structures in the group as well as the impact of a harsh environment such as caves in this. More species should be compared concerning the potentially paedomorphic traits presented in this work to define whether *O. commutabilis* present paedomorphosis.

The number of hydropores is equal among species of highly different geographical distribution, but inhabiting similar environments as *O. reticulata* and *O. schayeri* (Ezhova et al. 2016). However, that number is very different between closely related

species *as O. reticulata* and *O. commutabilis*, which inhabit very dissimilar environments. This is consistent with the hypothesis claiming that madreporites are ecologically informative (Ezhova et al. 2016). The differences among species in the type of teeth are relevant if we consider that teeth types have been used as an indicator of feeding preferences (uniform teeth for macrophagous feeders and compound for microphagous) (Medeiros-Bergen 1996; Brogger et al. 2015). Five ophionereidids have been reported to possess only compound teeth (Medeiros-Bergen 1996), while *O. commutabilis* shows both compound and uniform teeth, which could represent an adaptation, increasing the importance of omnivorous feeding in this cave system (as suggested by Bribiesca-Contreras et al. (2019) for other food sources). An alternative explanation for the presence of uniform teeth in *O. commutabilis* could be that they represent underdeveloped teeth, either for being ventral (the youngest according to Hendler (2018) or for the slow growth rate of cave organisms (Carpenter 2016). Though all the teeth were obtained from the ventral and dorsal portions of specimens of similar size, this explanation (being underdeveloped teeth) must be considered in further studies.

The presence of EPTs on DAP is conspicuous across the genus *Ophionereis*, not only in Caribbean species like *O. reticulata* but also in the Indo-Pacific species *O. porrecta* and *O. degeneri* (figures 15c and 16c in: Stöhr (2011)). Furthermore, based on figures from available literature, ophionereidids have higher EPT densities than species of the genus *Ophiocoma* (e.g. 15 vs 498) (Hendler and Byrne 1987) and *Ophiopsila* (e.g. 96 vs 498) (Deheyn et al. 2015). Though *O. commutabilis* shows expanded peripheral trabeculae on dorsal arm plates, these structures show a different pattern that decreases in density in contrast to its epigean congeners. These differences could suggest the effects of low energy and darkness typical of caves, in the photoreceptor system of this species. Moreover, the cave specimens DAP show a disorganized inner mesh, further suggesting stereom organization being reduced as an expensive or dispensable trait, as proposed for cave-dwelling taxa (Klaus et al. 2013). Concerning inner stereom it is especially relevant since it affects chromatophore activity (Hendler and Byrne 1987; Sumner-Rooney et al. 2018), suggesting an important impact of darkness in *O. commutabilis* life as previously discussed for the diversity of colouration of this species (Bribiesca-Contreras et al. 2019).

Stereom of cave specimens are similar to that of deep-sea ophiuroids in having less defined expanded peripheral trabeculae (Hendler and Byrne 1987), both environments having similar conditions (e.g. absence of light and low energy). On the other hand, agglomeration of EPT has been reported for bioluminescent species, particularly conspicuous in *Ophiopsila californica* (Deheyn et al. 2015). In addition, transmittance differences (due to whether the light beam passes through EPT first or last) on DAP of the cave species are similar to differences observed among bioluminescent (*Ophiopsila californica and Amphipholis squamata*) and non-bioluminescent (*Amphipholis pugetana*) species (Deheyn et al. 2015). Therefore, our results suggest that both photoreception and bioluminescence processes have affected the evolution of this species and confirm that differences in morphology of DAP between both species have an impact on light transmittance.

The lower transmittance peak observed in the two analyzed species corresponds to wavelengths that activate phototaxis in ophiuroids (Delroisse et al. 2016). This

adds evidence to the hypothesis that this species diverged from a shallow water lineage (Bribiesca-Contreras et al. 2019). On the other hand, the highest peak is usual in ophiuroids, since it corresponds to wavelengths attenuated on the first 10-20 cm depth (Deheyn et al. 2015). Finally, these results highlight the necessity of more studies to understand if the phototaxis in ophiuroids is related to their relative success in caves (in comparison with the other classes of the phylum).

Cave fauna shows particular morphological traits that could be considered to be troglomorphisms if they allow organisms to successfully colonize these harsh environments (Culver and Pipan 2009; Gonzalez et al. 2018). This paper demonstrates that brittle stars inhabiting an anchialine cave in Cozumel show troglomorphic traits such as arm (through the adding of segments) and distal tube feet elongation, increase in size, and possibly paedomorphic traits. This is, to our knowledge, the second study investigating troglomorphic adaptations in a group of echinoderms; our work confirms *that O. commutabilis* can be characterized as a stygobiotic species as demography, distribution and origin of this species suggested (Bribiesca-Contreras et al. 2013, 2019).

Conclusion

In conclusion, troglomorphic traits of *Ophionereis commutabilis* include elongation of arms (as a result of the addition of segments) and increased sizes, similar to those observed for other cave fauna. Additionally, potentially paedomorphic traits are reported for an ophionereidid. Finally, the morphology of *O. commutabilis* confirms it as a stygobiotic species as demography, distribution and origin of this species previously suggested.

The authors have declared that no competing interests exist.

Acknowledgements

We are grateful to Alicia Duran for the loan of specimens and Berenit Mendoza for taking the SEM photographs; Susana Guzmán for technical assistance in photography. Thanks to Arodi Farrera for help on geometric morphometrics analysis. To Juan Hernández and Amado Velazquez for assistance with the optical proofs. Thanks to Jill Yager, Laura Arroyo and Tania Pineda for their helpful comments and corrections that greatly improved the manuscript. We are grateful to Guadalupe Bribiesca-Contreras and an additional anonymous reviewer for providing valuable comments that improved considerably the content of this contribution. This work was funded by CONACYT (746189).

References

Aizenberg J, Tkachenko A, Weiner S, Addadi L, Hendler G (2001) Calcitic microlenses as part of the photoreceptor system in brittlestars. Nature 412(6849): 819–822. https://doi.org/10.1038/35090573

Bishop RE, Humphreys WF, Cukrov N, Žic V, Boxshall GA, Cukrov M, Iliffe TM, Kršinić F, Moore WS, Pohlman JW, Sket B (2015) 'Anchialine' redefined as a subterranean estuary in a crevicular or cavernous geological setting. Journal of Crustacean Biology 35(4): 511–514. https://doi.org/10.1163/1937240X-00002335

Bishop RE, Iliffe TM (2009) Metabolic rates of stygobiontic invertebrates from the Túnel de la Atlántida, Lanzarote. Marine Biodiversity 39 (3): 189–194. https://doi.org/10.1007/s12526-009-0018-3

Brankovits D, Pohlman JW, Niemann H, Leigh MB, Leewis MC, Becker KW, Iliffe TM, Alvarez F, Lehmann MF, Phillips B (2017) Methane-and dissolved organic carbon-fueled microbial loop supports a tropical subterranean estuary ecosystem. Nature Communications 8 (1). https://doi.org/10.1038/s41467-017-01776-x

Bribiesca-Contreras G, Pineda-Enríquez T, Márquez-Borrás F, Solís-Marín FA, Verbruggen H, Hugall AF, O'Hara T (2019) Dark offshoot: phylogenomic data sheds light on the evolutionary history of a new species of cave brittle star. Molecular Phylogenetics and Evolution 136: 151–163. https://doi.org/10.1016/j.ympev.2019.04.014

Bribiesca-Contreras G, Solís-Marín FA, Laguarda-Figueras A, Zaldívar-Riverón A (2013) Identification of echinoderms (Echinodermata) from an anchialine cave in Cozumel Island, Mexico, using DNA barcodes. Molecular Ecology Resources 13(6): 1137–1145. https://doi.org/10.1111/1755-0998.12098

Brogger MI, Martinez MI, Cadierno MP, Penchaszadeh PE (2015) Tooth microstructure and feeding biology of the brittle star *Ophioplocus januarii* (Echinodermata: Ophiuroidea) from northern Patagonia, Argentina. Revista de Biologia Tropical 63: 353–360. https://doi.org/10.15517/rbt.v63i2.23169

Brom KR, Brachaniec T, Salamon MA (2015) Troglomorphism in the middle Triassic crinoids from Poland. The Science of Nature 102(9–10): 60. https://doi.org/10.1007/s00114-015-1310-7

Byrne M (1991) Reproduction, development and population biology of the Caribbean ophiuroid *Ophionereis olivacea*, a protandric hermaphrodite that broods its young. Marine Biology 111 (3): 387–399. https://doi.org/10.1007/BF01319411

Calderón-Gutiérrez F, Solís-Marín FA (2014) Anchialine ecosystem El Aerolito (Cozumel, Mexico): paradise of cave dweller echinoderms. In: Whitmore E (Ed.) Echinoderms: Ecology, Habitats and Reproductive Biology. Nova Publishers, New York, 167–181.

Calderón-Gutiérrez F, Solís-Marín FA, Gómez P, Sánchez C, Hernández-Alcántara P, Álvarez-Noguera F, Yáñez-Mendoza G (2017) Mexican anchialine fauna — With emphasis in the high biodiversity cave El Aerolito. Regional Studies in Marine Science 9: 43–55. https://doi.org/10.1016/j.rsma.2016.11.001

Carpenter JH (2016) Observations on the biology and behavior of *Amphicutis stygobita*, a rare cave brittle star (Echinodermta: Ophiuroidea) from Bernier Cave, San Salvador Island, Bahamas. In: Erdman R, Morrison R (Eds) The 15th Symposium on the Natural History of the Bahamas. A & A, 31–44.

Clark A (1953) A revision of the genus *Ophionereis* (Echinodermata, Ophiuroidea). Proceedings of the Zoological Society of London 123(1): 65–94. https://doi.org/10.1111/j.1096-3642.1953.tb00157.x

Culver DC (1982) Cave Life: Evolution and Ecology. Harvard University Press, Cambridge, 189 pp. https://doi.org/10.4159/harvard.9780674330214

Culver DC, Kane TC, Fong DW (1995) Adaptation and natural selection in caves: the evolution of *Gammarus minus*. Harvard University Press, 223 pp. https://doi.org/10.4159/harvard.9780674419070

Culver DC, Pipan T (2009) The Biology of Caves and other Subterranean Habitats. Oxford University Press, 254 pp.

Deheyn DD, Allen MC, De Meulenaere E (2015) On the biophotonic properties of brittlestar ossicles. Organic Photonic Materials and Devices 17(9360): 936004. https://doi.org/10.1117/12.2084665

Delić T, Trontelj P, Zakšek V, Fišer C (2016) Biotic and abiotic determinants of appendage length evolution in a cave amphipod. Journal of Zoology 299(1): 42–50. https://doi.org/10.1111/jzo.12318

Delroisse J, Mallefet J, Flammang P (2016) *De novo* adult transcriptomes of two European brittle stars: spotlight on opsin-based photoreception. PLoS ONE 11(4): e0152988. https://doi.org/10.1371/journal.pone.0152988

Dupont S, Thorndyke MC (2006) Growth or differentiation? Adaptive regeneration in the brittlestar *Amphiura filiformis*. Journal of Experimental Biology 209(19): 3873–3881. https://doi.org/10.1242/jeb.02445

Ezhova OV, Malakhov VV, Martynov AV (2016) Madreporites of Ophiuroidea: are they phylogenetically informative? Zoomorphology 135(3): 333–350. https://doi.org/10.1007/s00435-016-0315-x

Gage JD (1990) Skeletal growth bands in brittle stars: microstructure and significance as age markers. Journal of the Marine Biological Association of the United Kingdom 70(1): 209–224. https://doi.org/10.1017/S0025315400034329

Gibert J, Deharveng L (2002) Subterranean Ecosystems: A Truncated Functional Biodiversity. BioScience 52(6): 473–481. https://doi.org/10.1641/0006-3568(2002)052[0473:SEATFB]2.0.CO;2

Gonzalez BC, Worsaae K, Fontaneto D, Martínez A (2018) Anophthalmia and elongation of body appendages in cave scale worms (Annelida: Aphroditiformia). Zoologica Scripta 47(1): 106–121. https://doi.org/10.1111/zsc.12258

Hajduk SL (1992) Ultrastructure of the tube-foot of an ophiuroid echinoderm, *Hemipholis elongata*. Tissue and Cell 24 (1): 111–119. https://doi.org/10.1016/0040-8166(92)90085-L

Hendler G (2018) Armed to the teeth: a new paradigm for the buccal skeleton of brittle stars (Echinodermata: Ophiuroidea). Contributions in Science 526: 189–311.

Hendler G, Byrne M (1987) Fine structure of the dorsal arm plate of *Ophiocoma wendti*: Evidence for a photoreceptor system (Echinodermata, Ophiuroidea). Zoomorphology 107: 261–272. https://doi.org/10.1007/BF00312172

Iliffe TM, Kornicker LS (2009) Worldwide diving discoveries of living fossil animals from the depths of anchialine and marine caves. Smithsonian Contributions to the Marine Sciences 38: 269–280. https://doi.org/10.5479/si.1943667X.0

Keogh JK, Keegan BF (2006) Ultrastructure of the podia of *Amphiura chiajei* and *Amphiura filiformis* and their role in feeding. Journal of the Marine Biological Association of the United Kingdom 86(4): 817–822. https://doi.org/10.1017/S0025315406013737

Klaus S, Mendoza JCE, Liew JH, Plath M, Meier R, Yeo DCJ (2013) Rapid evolution of troglomorphic characters suggests selection rather than neutral mutation as a driver of

eye reduction in cave crabs. Biology Letters 9(2): 20121098. https://doi.org/10.1098/rsbl.2012.1098

Lawrence JM, Vasquez J (1996) The effect of sublethal predation on the biology of echinoderms. Oceanologica Acta 19 (3–4): 431–440.

Martínez GA, Palmero AM, Brito MC, Núñez J, Worsaae K (2009) Anchialine fauna of the Corona lava tube (Lanzarote, Canary Islands): diversity, endemism and distribution. Marine Biodiversity 39(3): 169–182. https://doi.org/10.1007/s12526-009-0023-6

Martynov A, Ishida Y, Irimura S, Tajiri R, O'Hara T, Fujita T (2015) When ontogeny matters: A new Japanese species of brittle star illustrates the importance of considering both adult and juvenile characters in taxonomic practice. PLoS ONE 10: e0139463. https://doi.org/10.1371/journal.pone.0139463

Medeiros-Bergen DE (1996) On the stereom microstructure of ophiuroid teeth. Ophelia 45(3): 211–222. https://doi.org/10.1080/00785326.1996.10432473

Mejía-Ortíz LM, Hartnoll RG (2005) Modifications of Eye Structure and Integumental Pigment in Two Cave Crayfish. Journal of Crustacean Biology 25(3): 480–487. https://doi.org/10.1651/C-2569

Mejía-Ortíz LM, Hartnoll RG, López-Mejía M (2006) Progressive troglomorphism of ambulatory and sensory appendages in three Mexican cave decapods. Journal of Natural History 40 (5–6): 255–264. https://doi.org/10.1080/00222930600628382

Mejía-Ortíz LM, López-Mejía M, Pakes J, Hartnoll RG, Zarza-González E (2013) Morphological adaptations to anchialine environments in species of five shrimp families (*Barbouria yanezi*, *Agostocaris bozanici*, *Procaris mexicana*, *Calliasmata nohochi* and *Typhlatya pearsei*). Crustaceana 86(5): 578–593. https://doi.org/10.1163/15685403-00003197

Mejía-Ortíz LM, Yánez G, López-Mejía M (2007) Echinoderms in an anchialine cave in Mexico. Marine Ecology 28 (1): 31–34. https://doi.org/10.1111/j.1439-0485.2007.00174.x

Munday BW (1993) Field survey of the occurrence and significance of regeneration in *Amphiura chiajei* (Echinodermata: Ophiuroidea) from Killary Habrour, west coast of Ireland. Marine Biology 115(4): 661–668. https://doi.org/10.1007/BF00349374

O'Hara TD, Stöhr S, Hugall AF, Thuy B, Martynov A (2018) Morphological diagnoses of higher taxa in Ophiuroidea (Echinodermata) in support of a new classification. European Journal of Taxonomy 416: 1–35. https://doi.org/10.5852/ejt.2018.416

Okanishi M, Fujita Y (2018) First finding of anchialine and submarine cave dwelling brittle stars from the Pacific Ocean, with descriptions of new species of *Ophiolepis* and *Ophiozonella* (Echinodermata: Ophiuroidea: Amphilepidida). Zootaxa 4377(1): 1–20. https://doi.org/10.11646/zootaxa.4377.1.1

Okanishi M, Fujita Y (2019) A comprehensive taxonomic list of brittle stars (Echinodermata: Ophiuroidea) from submarine caves of the Ryukyu Islands, southwestern Japan, with a description of a rare species, *Dougaloplus echinatus* (Amphiuridae). Zootaxa 4571(1): 73. https://doi.org/10.11646/zootaxa.4571.1.5

Okanishi M, Oba Y, Fujita Y (2019) Brittle stars from a submarine cave of Christmas Island, northwestern Australia, with description of a new bioluminescent species *Ophiopsila xmas-illuminans* (Echinodermata: Ophiuroidea) and notes on its behaviour. Raffles Bulletin of Zoology 67: 421–439. https://doi.org/10.26107/RBZ-2019-0034

Pérez-Moreno JL, Iliffe TM, Bracken-Grissom HD (2016) Life in the Underworld: Anchialine cave biology in the era of speleogenomics. International Journal of Speleology 45(2): 149–170. https://doi.org/10.5038/1827-806X.45.2.1954

Pohlman JW, Iliffe TM, Cifuentes LA (1997) A stable isotope study of organic cycling and the ecology of an anchialine cave ecosystem. Marine Ecology Progress Series 155: 17–27. https://doi.org/10.3354/meps155017

Pomory CM, Carpenter JH, Winter JH (2011) *Amphicutis stygobita*, a new genus and new species of brittle star (Echinodermata: Ophiuroidea: Ophiurida: Amphilepididae) found in Bernier Cave, an anchialine cave on San Salvador Island, Bahamas. Zootaxa 3133: 50–68. https://doi.org/10.11646/zootaxa.3133.1.3

Poulson TL, White WB (1969) The cave environment. Science 165(3897): 971–981. https://doi.org/10.1126/science.165.3897.971

Rizzato PP, Bichuette ME (2017) The laterosensory canal system in epigean and subterranean *Ituglanis* (Siluriformes: Trichomycteridae), with comments about troglomorphism and the phylogeny of the genus. Journal of Morphology 278(1): 4–28. https://doi.org/10.1002/jmor.20616

Romero A (2009) Cave Biology, Life in Darkness. Cambridge University Press, 306. https://doi.org/10.1017/CBO9780511596841

Sarbu SM, Kane TC, Kinkle BK (1996) A Chemoautotrophically Based Cave Ecosystem. Science 272(5270): 1953–1955. https://doi.org/10.1126/science.272.5270.1953

Sket B (1996) The ecology of anchihaline caves. Trends in Ecology and Evolution 11(5): 221–225. https://doi.org/10.1016/0169-5347(96)20031-X

Sköld M, Rosenberg R (1996) Arm regeneration frequency in eight species of Ophiuroidea (Echinodermata) from European sea areas. Journal of Sea Research 35(4): 353–362. https://doi.org/10.1016/S1385-1101(96)90762-5

Solís-Marín FA, Laguarda-Figueras A (2010) A new species of starfish (Echinodermata: Asteroidea) from an anchialine cave in the Mexican Caribbean. Revista Mexicana de Biodiversidad 81(3): 663–668. https://doi.org/10.22201/ib.20078706e.2010.003.638

Stöhr S (2011) New records and new species of Ophiuroidea (Echinodermata) from Lifou, Loyalty Islands, New Caledonia. Zootaxa 3089 (1): 1. https://doi.org/10.11646/zootaxa.3089.1.1

Stöhr S, Martynov A (2016) Paedomorphosis as an evolutionary driving force: Insights from deep-sea brittle stars. PLoS ONE 11(11): 1–24. https://doi.org/10.1371/journal.pone.0164562

Stöhr S, O'Hara TD, Thuy B (2012) Global diversity of brittle stars (Echinodermata: Ophiuroidea). PLoS ONE 7 (3): 1–15. https://doi.org/10.1371/journal.pone.0031940

Sumner-Rooney L, Rahman IA, Sigwart JD, Ullrich-Lüter EM (2018) Whole-body photoreceptor networks are independent of 'lenses' in brittle stars. Proceedings of the Royal Society B 285(1871): 11–13. https://doi.org/10.1098/rspb.2017.2590

Tan HH, Tohru N, Fujita Y, Tan SK (2014) Observations on the fauna from submarine and associated anchialine caves in Christmas Island, Indian Ocean Territory, Australia. Raffles Bulletin of Zoology 30: 406–418.

Team Rs (2016) RStudio: Integrated Development Environment for R. Boston, MA. http://www.rstudio.com

Trontelj P, Blejec A, Fišer C (2012) Ecomorphological convergence of cave communities. Evolution: International Journal of Organic Evolution 66(12): 3852–3865. https://doi.org/10.1111/j.1558-5646.2012.01734.x

Turk S, Sket B, Sarbu S (1996) Comparison between some epigean and hypogean populations of *Asellus aquaticus* (Crustacea: Isopoda: Asellidae). Hydrobiologia 337(1–3): 161–170. https://doi.org/10.1007/BF00028517

Warner G (1982) Food and feeding mechanisms: Ophiuroidea. In: Jangoux M, Lawrence JM (Eds) Echinoderm Nutrition. CRC Press, Rotterdam, 161–182.

White W, Culver DC (2012) Encyclopedia of Caves. Academic Press, Amsterdam, 945 pp.

Yokoyama LQ, Amaral ACZ (2010) Arm regeneration in two populations of *Ophionereis reticulata* (Echinodermata, Ophiuroidea). Iheringia Serie Zoologia 100(2): 123–127. https://doi.org/10.1590/S0073-47212010000200006

Yokoyama LQ, Amaral ACZ (2011) Recruitment and growth variation of *Ophionereis reticulata* (Echinodermata: Ophiuroidea). Invertebrate Reproduction & Development 55(2): 73–81. https://doi.org/10.1080/07924259.2011.553402

Zhang ZQ (2011) Animal biodiversity: An outline of higher-level classification and survey of taxonomic richness. Zootaxa 3148: 1–237. https://doi.org/10.11646/zootaxa.3148.1.1

Zueva O, Khoury M, Heinzeller T, Mashanova D, Mashanov V (2018) The complex simplicity of the brittle star nervous system. Frontiers in Zoology 15(1): 1. https://doi.org/10.1186/s12983-017-0247-4

Supplementary material 1

Supplementary figures S1–S3

Authors: Francisco Márquez-Borrás, Francisco A. Solís-Marín, Luis M. Mejía-Ortiz

Data type: multimedia

Explanation note: **Figure S1.** Sets of Landmarks (LM) configurations designed to register the shape of the dorsal (A), ventral (B) and lateral (C–D) arm plates. Orientation (p: proximal, di: distal, do: dorsal, v: ventral). **Figure S2.** Scanning electron micrograph (SEM) of dental plates. SEM of dental plates from *Ophionereis commutabilis* (a-b) (modified from Bribiesca-Contreras et al. 2019) and *O. reticulata* (c-d), showing external (a, c) and internal faces (b, d). Scale bars: 500 μm. **Figure S3.** Scanning electron micrograph (SEM) of teeth from *Ophionereis commutabilis*, showing compound (a) and uniform teeth (b). Compound teeth from *O. reticulata* (c-d). Scale bars: a-c, 300 μm; c-d, 400 μm.

Link: https://doi.org/10.3897/subtbiol.33.48721.suppl1

Supplementary material 2

Supplementary table S1

Authors: Francisco Márquez-Borrás, Francisco A. Solís-Marín, Luis M. Mejía-Ortiz

Data type: table

Explanation note: Arm features of the stygobiotic species (*O. commutabilis*) and its epigean congener (*O. reticulata*).

Link: https://doi.org/10.3897/subtbiol.33.48721.suppl2

Supplementary material 3

R-scripts

Authors: Francisco Márquez-Borrás, Francisco A. Solís-Marín, Luis M. Mejía-Ortiz

Data type: statistical data

Link: https://doi.org/10.3897/subtbiol.33.48721.suppl3

Journal of Crustacean Biology

The Crustacean Society

Journal of Crustacean Biology

Journal of Crustacean Biology (2020) 1–11. doi:10.1093/jcbiol/ruaa037

Anchialine adjustments: an updated phylogeny and classification for the family Barbouriidae Christoffersen, 1987 (Decapoda: Caridea)

Robert E. Ditter[1], Luis M. Mejía-Ortíz[2] and Heather D. Bracken-Grissom[1]

[1]*Department of Biological Sciences, Florida International University, 3000 NE 151st St., MSB 330, North Miami, FL 33181, USA; and*
[2]*Laboratorio de Biospeología y Carcinología, Universidad de Quintana Roo, Av. Andrés Quintana Roo s/n, CON 110 Sur Col. San Gervasio, C.P. 77600, Cozumel, Quintana Roo, Mexico*

Correspondence: R.E. Ditter; e-mail: rditt003@fiu.edu

(Received 16 December 2019; accepted 15 May 2020)

ABSTRACT

Barbouriidae Christoffersen, 1987 is a family comprised of 4 genera and 11 species of enigmatic shrimps restricted to anchialine or marine caves whose evolutionary history and relationships remain elusive. We investigated the evolutionary relationships among members of Barbouriidae with the inclusion of four genera and nine species, and newly collected material from Belize, the Bahamas, and the Yucatán Peninsula, Mexico. Phylogenetic analyses based on seven mitochondrial and nuclear gene regions and genetic distances calculated using partial 16S gene regions have identified a need to revisit the relationships and classification within Barbouriidae. More specifically, we find evidence to suggest *Janicea* Manning & Hart, 1984 as a junior synonym of *Parhippolyte* Borradaile, 1900, *B. yanezi* Mejía, Zarza & López, 2008 as a synonym of *Barbouria cubensis* (von Martens, 1872), and define two new subfamilies, Calliasmatinae Holthuis, 1973 and Barbouriinae Christoffersen, 1987. Included is a dichotomous key for the species of Barbouriidae that summarizes previous literature and includes new morphological characters. Our findings shed light on existing inaccuracies and gaps in molecular data from barbouriids. We also provide further clarity into evolutionary relationships among genera of Barbouriidae and their allies, suggesting phylogeographic divisions within the family. Our findings suggest an early Atlantic-Pacific divide among genera originating from a shallow-water reef ancestor.

Key Words: cave shrimps, 28S, COI, enolase, H3, NaK, PEPCK, phylogeny, taxonomy

INTRODUCTION

Anchialine pools are a common feature throughout the tropical western Atlantic, and are broadly defined as land-locked pools with limited tidal connections to adjacent marine water bodies through a complex network of subterranean conduits (Bishop *et al.*, 2015). Anchialine systems are considered to be isolated due to their unique species assemblages and endemicity (Iliffe & Kornicker, 2009; Becking *et al.*, 2011; Pérez-Moreno *et al.*, 2016). Barbouriidae Christoffersen, 1987 (Fig. 1) is a family of caridean shrimps that commonly inhabits anchialine or coastal caves along tropical latitudes (Fig. 2). Barbouriidae is currently comprised of 4 genera and 11 species, but the genera within this family have undergone substantial revisions in recent years (Chace, 1972, 1997; Manning & Hart, 1984; Christoffersen, 1987, 1990; Fransen & Tomascik, 1996; Wicksten, 1996; De Grave *et al.*, 2014).

The evolutionary history of Barbouriidae remains unclear (De Grave *et al.*, 2014). Members of this family had previously been classified as monotypic genera within Hippolytidae Spence Bate, 1888 until Christoffersen (1987, 1990) proposed recognizing Barbouriidae as a family with six genera (*Ligur* Sarato, 1885; *Barbouria* Rathbun, 1912; *Janicea* Manning & Hart, 1984; *Parhippolyte* Borradaile, 1900; *Somersiella* Hart & Manning, 1981; and *Koror* Clark, 1989). Kemp (1914) synonymized *Parhippolyte* with *Ligur* without comment. Upon discovery of additional species with a multiarticulate carpus and propodus of the third to fifth pereiopods, *Parhippolyte* was removed from the synonymy of *Ligur* (Manning & Hart, 1984). *Ligur* became a monospecific genus with the removal of *P. uveae* Borradaile, 1900 and was transferred from Hippolytidae upon the resurrection of Lysmatidae Dana, 1852 (Manning & Hart, 1984; De Grave *et al.*, 2014). The

description of *Koror misticius* Clark, 1989 and *Somersiella sterreri* Hart & Manning, 1981 placed them within Hippolytidae, but a lack of morphological evidence at the genus level for both genera led them to be synonymized with *Parhippolyte* (Wicksten, 1996; Chace, 1997). With these exclusions and reclassifications, recent phylogenetic analyses have supported the recognition of the family Barbouriidae (Li *et al.*, 2011; De Grave *et al.*, 2014; Aznar-Cormano *et al.*, 2015). The current classification of Barbouriidae includes two species of *Barbouria* (*B. cubensis* (von Martens, 1872)) and *B. yanezi* Mejía, Zarza & López, 2008), one species of *Janicea* (*J. antiguensis* (Chace, 1972)), five species of *Parhippolyte* (*P. cavernicola* Wicksten, 1996; *P. misticia* (Clark, 1989); *P. rukuensis* Burukovsky, 2007; *P. sterreri* (Hart & Manning, 1981); and *P. uveae*), and the most recent addition of three species of *Calliasmata* Holthuis, 1973 (*C. nohochi* Escobar-Briones, Camacho & Alcocer, 1997; *C. pholidota* Holthuis, 1973; and *C. rimolii* Chace, 1975). *Barbouria cubensis* and *P. sterreri* (listed as *Somersiella sterreri*) are listed as critically endangered on the IUCN Red List (Iliffe, 1996).

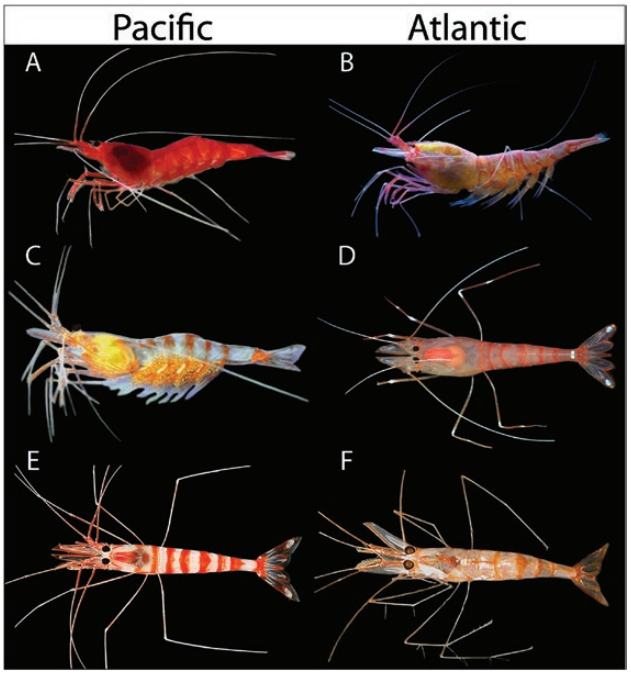

Figure 1. *Parhippolyte uveae* (photo by Meerwasser-Aquaristik-Studio-Korallenkiste, Rosbach vor der Höhe, Germany) (**A**); *Barbouria cubensis* (photo by HBG) (**B**); *Parhippolyte cavernicola* (photo by A. Kerstitch) (**C**); *Parhippolyte sterreri* (photo by RED) (**D**); *Parhippolyte misticia* (photo by J. Starmer in Legall & Poupin, 2018) (**E**); *Janicea antiguensis* (photo by T. Iliffe) (**F**). This figure is available in color at *Journal of Crustacean Biology* online.

Although the genus *Calliasmata* is presently placed within Barbouriidae, De Grave *et al.* (2014) questioned the inclusion of this group within the family. *Calliasmata* lacks all of the defining characters shared by genera of Barbouriidae, including the unique subocular tooth posterodorsal to the orbital angle, which has been previously considered as a synapomorphy of the family (Clark, 1989; Chace, 1997; De Grave *et al.*, 2014). Moreover, in spite of the troglodytic lifestyle of barbouriids, only *Calliasmata* exhibits characteristic adaptions of cave-dwelling animals, such as highly degenerate eyes (Pérez-Moreno *et al.*, 2016). The conflicting morphology of *Calliasmata* with the other members of Barbouriidae further complicates the evolutionary history of this family, and Barbouriidae presently lacks an accurate formal description (see De Grave *et al.*, 2014).

We also revisited the placement of the monospecific genus *Janicea* among other barbouriids. *Janicea* has the broadest distribution of the Atlantic species, ranging from the Canary Islands, Bermuda, and the Yucatán Peninsula, Mexico (Manning & Hart, 1984; Li *et al.*, 2011). *Janicea antiguensis* (Chace, 1972) has a gill compliment similar to that of *B. cubensis*, but multiarticulation of the carpus and propodus of the third to fifth pereiopods and a cornea wider than the eyestalk suggest an affinity to *Parhippolyte* (Manning & Hart, 1984). The first description of *J. antiguensis* placed it within *Barbouria* with the belief that *Barbouria* would eventually be synonymized with *Ligur*, but *Janicea* was later recognized as a monotypic genus (Chace, 1972; Buden & Felder, 1977; Manning & Hart, 1984). The taxonomic uncertainty surrounding *J. antiguensis* justifies a closer examination of the phylogenetic placement of this species within Barbouriidae.

Figure 2. Distribution of the genera *Barbouria, Calliasmata, Janicea*, and *Parhippolyte*. *Parhippolyte rukuensis* is excluded because it was described from a single female from Yeh-Him Island, Ryukyu Archipelago, Japan. This figure is available in color at *Journal of Crustacean Biology* online.

Barbouria yanezi Mejía, Zarza & López, 2008 is the most recently described species of Barbouriidae and has only been reported from Cenote Tres Potrillos, Cozumel Island, Mexico (Mejía *et al.* 2008). *Barbouria yanezi* differs from *Barbouria cubensis* (von Martens, 1872) in the length and number of teeth of the rostrum, the length to width ratio of the scaphocerite, the proportions of the first and second pereiopod, the number of articulations of the carpus and ischium of the second pereiopod, and the length and terminal spines of the appendix masculina (Mejía *et al.*, 2008). *Barbouria cubensis* has been more recently found to exhibit phenotypic hypervariation (PhyV), defined as the presence of extensive undescribed morphological variation at an uncommonly high frequency (Ditter *et al.*, 2019). The differences that distinguish *B. yanezi* from *B. cubensis* fall within the range of morphological variations documented for *B. cubensis* from the Bahamas (Ditter *et al.*, 2019). In light of PhyV, the need to revisit the relationship between *B. yanezi* and *B. cubensis* using molecular tools is clear.

Although past molecular phylogenies have enhanced our understanding of barbouriid relationships, they are hindered by limited sampling across genera or incomplete genetic datasets (Fiedler *et al.*, 2010; Li *et al.*, 2011; Baeza, 2013; De Grave *et al.*, 2014; Aznar-Cormano *et al.*, 2015). Recent collections have allowed us to include nine species across all genera and provides further insight into the evolutionary relationships among these enigmatic crustaceans. We investigated the evolutionary relationships across current members of Barbouriidae with particular attention to the above-mentioned genera and species using multi-locus phylogenetic methods.

MATERIALS AND METHODS

Sampling

We selected 7 genera and 16 species to be included in the phylogenetic analysis of Barbouriidae, including all four currently recognized genera of the family Barbouriidae (*Calliasmata*, *Barbouria*, *Parhippolyte* and *Janicea*). Species of the closely related genera *Latreutes* Stimposn, 1860, *Ligur*, and *Lysmata* Risso, 1816 are included as outgroups. *Barbouria cubensis* and *P. sterreri* were collected on the San Salvador, Bahamas using baited minnow traps between June 2014 and July 2015. Tissue samples of *B. yanezi* were provided by LMMO collected from Cenote Tres Potrillos, Cozumel, Mexico. Specimens of *J. antiguensis* and *C. nohochi* were donated to the Florida International Crustacean Collection (FICC) by Dr. Thomas Iliffe. Additional sequences for *J. antiguensis* and *L. fucorum* were generated from specimens housed in FICC located on the Biscayne Bay Campus of Florida International University. Several specimens of *Parhippolyte misticia* were received as a loan from Dr. Tin-Yam Chan, National Taiwan Ocean University (NTOU) and several *Parhippolyte uveae* specimens were received as a loan from the Muséum national d'Histoire naturelle, Paris (MNHN). *Parhippolyte cavernicola* and additional specimens of *P. uveae* were received as loans from the Smithsonian Institution, United States National Museum of Natural History (NMNH). Attempts to generate additional sequences for *L. ensiferus* were unsuccessful. Loci were selected based on previous studies that confirm their utility in caridean phylogenetics (Bracken-Grissom *et al.*, 2009a; Fiedler *et al.*, 2010; Li *et al.*, 2011; De Grave *et al.*, 2014; Aznar-Cormano *et al.*, 2015). To utilize taxa with sequences available in GenBank, loci were also selected so that individuals included in previous studies could be included. Loci included both protein coding and non-coding nuclear and mitochondrial gene regions. We generated 196 new sequences for seven partial gene regions from *Barbouria cubensis*, *B. yanezi*, *Calliasmata nohochi*, *Parhippolyte sterreri*, *P. cavernicola*, *P. misticia*, *P. uveae*, *Janicea antiguensis*, and *Latreutes fucorum* (Fabricius, 1798).

DNA extraction, PCR and sequencing

Total genomic DNA was extracted from muscle tissue of the abdomen, antennule or the third to fifth pleopod using DNeasy® Blood and Tissue Kits (Qiagen, Valencia, CA, USA). For incomplete tissue digestions, 10 µl of 10% DTT and 10 µl Proteinase K was added, and samples incubated until complete digestion was achieved. Total genomic DNA quality was visualized using 2% agarose gels and concentration was measured using the Qubit dsDNA HS Assay kit on the Qubit 2.0 Fluorometer (Invitrogen, Carlsbad, CA, USA) according to manufacturer's instructions.

We selected two partial mitochondrial genes and five partial nuclear genes for their utility in studies of phylogeny and genetic diversity among decapods (Bracken *et al.*, 2009b; Baeza, 2010; De Grave *et al.*, 2014; Aznar-Cormano *et al.*, 2015). The mitochondrial genes included the 16S large ribosomal subunit (~550 basepairs (bps)) and protein-coding cytochrome oxidase I (~600 bps, COI). The nuclear genes included the 28S large ribosomal subunit (~750 bps) and protein coding genes: phosphoenolpyruvate carboxykinase (PEPCK, ~585 bps), enolase (~375 bps), histone H3 (~350 bps), and sodium-potassium ATPase alpha-subunit (NaK, ~565 bps). The large ribosomal subunit (16S) was amplified with primers 16S-1471/1472 (Palumbi *et al.*, 1991; Crandall & Fitzpatrick 1996), COI was amplified with primers F/10, or LCO1490/HCO2198 (Folmer *et al.*, 1994; Bracken-Grissom *et al.*, 2014), 28S was amplified with primers 28S01/28SR-02 (Fiedler *et al.*, 2010), PEPCK with primers -for/-rev (Tsang *et al.*, 2008), enolase with primers EA2/ES2 (Li *et al.*, 2011), H3 with primers AF/AR (Li *et al.*, 2011), and NaK with primers N79/N610 (De Grave *et al.*, 2014). Amplification was performed in 25µl volume reactions containing 12.5µl GoTaq DNA polymerase (Promega, Madison, WI, USA), 1µl forward and reverse primer for each gene, 9.5µl sterile H_2O, and 1µl template DNA. The thermal cycling profile conformed to the following parameters: Initial denaturation for 5 min at 95 °C followed by 35 cycles of 30 sec at 94 °C, 45 sec at 48–56 °C, 45 sec at 72 °C, and a final extension of 5 min at 72 °C. PCR products were sent to Genewiz (South Plainfield, NJ, USA) for amplicon purification and subsequent sequencing.

All sequencing data was visually inspected, quality trimmed, manually cleaned, and assembled using Geneious 9.1.7 (Biomatters, Newark, NJ, USA). Once assembled, sequences were aligned using MAFFT v7.308 (Katoh & Standley, 2013). To identify potential pseudogenes, we translated protein-coding sequences and checked for insertions and deletions, stop codons, identified the open reading frames, and compared sequences among conspecifics following the protocol of Song *et al.* (2008).

Phylogenetic analyses

A dataset consisting of partial sequences of the 16S, 28S, COI, enolase, H3, NaK, and PEPCK gene regions (Table 1) was constructed to investigate generic and species level relationships across Barbouriidae. Missing data were designated as a "?" in our alignment. We constructed individual gene trees to compare topologies for both datasets. To improve resolution, multiple genes were concatenated into single alignments (Ahyong & O'Meally, 2004; Porter *et al.*, 2005; Robles *et al.*, 2007; Page *et al.*, 2008). We conducted a partition test of heterogeneity and incongruence length difference test to determine if the gene regions were appropriate to combine for analyses, as implemented in PartitionFinder 2.7.1 and PAUP*, respectively (Swofford, 2002; Lanfear *et al.*, 2016). The model of evolution that best fit the individual data sets was determined by Partitionfinder 2.7.1 (Felsenstein & Churchill, 1996). Independent models of evolution and parameters were partitioned in the Bayesian concatenated analysis.

The maximum likelihood (ML) analyses were conducted using RAxML (randomized accelerated maximum likelihood;

Table 1. Species used in phylogenetic reconstruction for the family Barbouriidae [see Material and Methods for the museum abbreviations]. Accession numbers for partial sequences of COI we generated using the LCO1490/HCO2198 and F/10 primers respectively. Individuals with successful amplification for both regions will have two accession numbers for the COI gene.

Taxon	Collection locality	Museum catalog no.	GenBank accession no.							
			16S	28S	Enolase	H3	NaK	PEPCK	COI	
Barbouria cubensis	San Salvador, Bahamas	HBG1937	MT505235	MT505191	MT527421	MT527448	MT527503	MT527477	MT524340	MT540990
B. cubensis	San Salvador, Bahamas	HBG2151	MT505236	MT505192	MT527422	MT527449	MT527504	MT527478	MT524341	MT540991
B. cubensis	San Salvador, Bahamas	HBG2198	MT505237	MT505193	MT527423	MT527450	MT527505	MT527479	MT524342	MT540992
B. cubensis	San Salvador, Bahamas	OUMNH.ZC.2010-05-003	KF023098	–	KF023142	–	KF023173	–	–	–
B. yanezi	Cozumel, Mexico	HBG9168	MT505238	–	–	MT527451	–	–	–	MT540993
B. yanezi	Cozumel, Mexico	HBG9180	MT505239	MT505194	MT527424	MT527452	MT527506	MT527480	–	MT540994
B. yanezi	Cozumel, Mexico	HBG9181	MT505240	MT505195	–	MT527453	–	MT527481	–	MT540995
Calliasmata pholidota	Hawaii, USA	OUMNH.ZC.2010-04-003	KF023119	–	KF023151	–	KF023182	–	–	–
C. nohochi	Mexico	A. Baeza, pers. coll.	–	–	KF178861	KF178838	–	–	–	–
C. nohochi	Mayaguana, Bahamas	HBG10007	MT505231	MT505187	MT527417	MT527444	MT527499	MT527473	MT524336	MT549845
C. nohochi	Mayaguana, Bahamas	HBG10008	MT505232	MT505188	MT527418	MT527445	MT527500	MT527474	MT524337	MT549846
C. nohochi	Mayaguana, Bahamas	HBG10009	MT505233	MT505189	MT527419	MT527446	MT527501	MT527475	MT524338	MT549847
C. nohochi	Mayaguana, Bahamas	HBG10010	MT505234	MT505190	MT527420	MT527447	MT527502	MT527476	MT524339	MT549848
Janicea antiguensis	Cape Verde, Africa	HBG66/OUMNH.ZC.2004-15-002	MT505241	MT505196	MT527425	MT527454	MT527507	MT527482	MT524343	–
J. antiguensis	Giant Cave, Belize	HBG9999	MT505242	MT505197	MT527426	MT527455	MT527508	MT527483	–	MT542150
J. antiguensis	Giant Cave, Belize	HBG10000	MT505243	MT505198	MT527427	MT527456	MT527509	MT527484	MT524344	MT542151
Parhippolyte cavernicola	Baja California Sur, Mexico	HBG10136/USNM-273315	MT505253	MT505208	MT527431	MT527470	MT527524	–	MT534287	–
P. misticia	Odo Point, Okinawa, Japan	Fiedler *et al*., 2010	HQ315615	HQ315560	–	–	–	–	–	–
P. misticia	Shagakko-mae, Japan	HBG10126/NTOU-M01157-E	–	MT505204	–	MT527465	MT527518	MT527491	MT524349	MT542196
P. misticia	Shagakko-mae, Japan	HBG10127/NTOU-M01157-F	–	MT505205	MT527436	MT527466	MT527519	MT527492	MT524350	MT542197
P. misticia	Shagakko-mae, Japan	HBG10128/NTOU-M01157-G	–	MT505206	MT527437	MT527467	MT527520	MT527493	–	MT542198
P. sterreri	San Salvador, Bahamas	HBG1941	MT505244	MT505199	MT527428	MT527457	MT527510	MT527485	MT524345	MT542201
P. sterreri	San Salvador, Bahamas	HBG1943	MT505245	MT505200	MT527429	MT527458	MT527511	MT527486	MT524346	MT542200
P. sterreri	San Salvador, Bahamas	HBG2149	MT505246	MT505201	MT527430	MT527459	MT527512	MT527487	MT524347	MT542199
P. sterreri	Iguana Cay, Exumas, Bahamas	MNHN-IU-2012-1057	KP725619	KP726001	–	KP726178	–	–	KP759480	–
Parahyppolyte sp.	Japan	NTOU M01675/TWH-2014	KF023096	–	KF023140	–	KF023171	–	–	–
P. cf. *uveae*	Okinawa, Japan	JAB-2013	KF178886	–	KF178877	KF178855	–	–	–	–
P. uveae	Society Islands, French Polynesia	HBG10114/MNHN-IU-2012-1001	MT505247	MT505202	MT527432	MT527460	MT527513	MT527488	–	MT542192
P. uveae	Society Islands, French Polynesia	HBG10115/MNHN-IU-2012-1002	MT505248	MT505203	MT527433	MT527461	MT527514	MT527489	–	MT542193
P. uveae	Coral Sea	HBG10117/MNHN-IU-2018-3568-B	MT505249	–	MT527434	MT527462	MT527515	MT527490	–	MT542194
P. uveae	Aldabra, Seychelles	HBG10130/ USNM-280216–85(1)	MT505251	–	MT527438	MT527468	MT527521	MT527494	MT524351	–
P. uveae	Aldabra, Seychelles	HBG10134/USNM-280216–85(2)	–	–	–	MT527469	MT527522	MT527495	MT524352	MT542202
P. uveae	Aldabra, Seychelles	HBG10135/USNM-280216–86(3)	MT505252	MT505207	MT527432	MT527460	MT527513	MT527488	MT524353	MT542203
Lysmata amboinensis	Not available	HBF395/KC9045	MT505229		MT527439	–	–	MT527472	–	MT542204
L. debelius	Not Available	MLP12l	DQ079718	DQ079793	–	DQ079681	–	–	–	–
L. hochi	Long Key, FL, USA	UMML32.9460	EU861507	–	KF178810	KF178848	–	–	KC962174	–
L. intermedia	Bocas Del Toro, Panama	UMML32.9461	EU861484	–	KF178871	KF178849	KF023169	–	KC962203	–
L. wurdemanni	Gulf of Mexico	HBG546/KC4529/ULLZ17433	MT505230	MT505186	MT527440	MT527443	MT527498	–	–	–
Ligur ensiferus	Guadeloupe	MNHN-IU-2012-1000	KP725542	KP725926	KF023141	KP726104	KF023172	–	–	–
Latreutes fucorum	Gulf of Mexico	HBG2764	MT505228	MT505184	MT527441	MT527442	MT527497	MT527471	–	MT563442

Stamatakis *et al.*, 2005) with computations performed on the high-performance computing cluster at Florida International University. Likelihood settings followed the general time reversible model with a gamma distribution and estimates of the proportion of invariable sites (GTR+I+G) and RAxML estimated all free parameters. Confidence in the resulting topologies was assessed using rapid bootstrapping and a search for the best-scoring tree with 1,000 replicates (Felsenstein, 1985). We performed Bayesian inference (BI) analyses using parameters selected by PartitionFinder 2.7.1 and conducted in MrBayes v3.2.6 (Huelsenbeck & Ronquist, 2001). A MCMC algorithm ran for 10,000,000 generations, sampling one tree every 1,000 generations. Observation of likelihood scores allowed us to determine burnins and stationary distributions. Once split frequency in the Bayesian analysis reached < 0.01, a 50% majority-rule consensus tree was obtained from the remaining trees. Posterior probabilities for clades were compared for congruence between analyses, bootstrap values > 70 for RAxML and > 0.90 for Bayesian are presented on the phylograms.

Genetic diversity and distance

We separately calculated nucleotide diversity (π) and Tajima's D (D) for each mitochondrial gene region in PopART v1.7 (Leigh & Bryant, 2015) to investigate genetic diversity and demographic history across the western Atlantic. To investigate genetic divergence between presently recognized genera of Barbouriidae, Nei's standard genetic distance (D_A) between partial 16S sequences were calculated using the Dnadist package of PHYLIP v3.695 (Felsenstein, 1989; Tuimala, 2004). All calculations were conducted following standard parameters.

RESULTS

Updated phylogeny of Barbouriidae

This combined analysis represents 39 terminals from the family Barbouriidae, representing all presently recognized genera, and seven outgroups, *Ligur ensiferus* (Risso, 1816), *Lysmata amboinensis* (De Man, 1888), *Lysmata debelius* Bruce, 1883, *Lysmata hochi* Baeza & Anker, 2009, *Lysmata intermedia* (Kingsley, 1878), *Lysmata wurdemanni* (Gibbes, 1850), and *Latreutes fucorum*. New sequences were generated for each gene region (16S, 28S, COI, enolase, H3, NaK, and PEPCK), for three *Barbouria cubensis*, three *B. yanezi*, four *Calliasmata nohochi*, three *Janicea antiguensis*, one *Parhippolyte cavernicola*, three *P. misticia*, three *P. sterreri*, five *P. uveae*, and one *Latreutes fucorum* individual. Individual gene phylogenies of 16S, 28S, enolase, H3, NaK, and PEPCK are without conflict (Supplementary material Figs. S1–S8). *Calliasmata* is recovered as sister to *Lysmata* in the COI phylogeny but has poor support at the conflicting nodes (bootstrap values < 50). All relationships within the concatenated phylogeny were recovered with significant support using ML and Bayesian analyses (Fig. 3). *Ligur* was the earliest branching lineage and a sister clade to Lysmatidae + Barbouriidae. *Calliasmata pholidota* and *C. nohochi* form a monophyletic group (clade 1) and is sister to the remaining barbouriids. Four individuals of *B. cubensis* and three of *B. yanezi* form a monophyletic group (clade 2) and is sister to a paraphyletic group of *Parhippolyte* + *Janicea antiguensis*. *Janicea antiguensis* is recovered as a sister species to *P. sterreri* (clade 3), which falls sister to a clade composed of remaining species of *Parhipplyte* (clades 4 and 5). Clade 4 represents *Parhippolyte uveae* (including *P.* cf. *uveae* from GenBank). *Parhippolyte cavernicola* is recovered as a sister species to *P. misticia* (clade 5). Several misidentifications or unidentified GenBank individuals were revealed during this study (denoted as * in Figure 3, and these can be found denoted in Table 2).

Genetic diversity and distance

Tajima's D and nucleotide diversity (π) was calculated due to of the lack of geographic clustering between of *B. cubensis* and *B. yanezi* in the phylogeny (clade 2; Fig. 3). The highest values for Tajima's D were negative (D = –2.34721, p_D = 0.998216). Genetic diversity was also found to be very low (π = 0.00209644). Mean and standard error values for Nei's D (D_A) for the 16S gene region are reported in Table 3, a heat map with all 16S D_A values in Supplementary material Table S9. Species within the same genus to have a mean genetic distance of 0.010–0.113 (Table 3). Genera within the same subfamily have genetic distances of 0.113–0.260. Individuals within the same family have distances of 0.260–0.311 (Table 3). For individuals within the same superfamily we find genetics distances > 0.311 (Table 3). We find similar patterns for the genetic distances for the COI partial gene region amplified with the F/10 primers as we find for the 16S partial gene region (Table 4). We find individuals of the same species have genetic distances < 0.01, and individuals within the same genus have genetic distances of ~0.01–0.25 (Table 4). We find individuals within the same family to have genetic distances of ~0.25–0.32 (Table 4). For individuals within the same superfamily we find genetic distances of > 0.33 (Table 4). Oddly, for this locus, we recover *Latreutes fucorum* to be more closely related to *Barbouria* and *Parhippolyte* than *Calliasmata nohochi* is to *Barbouria* and *Parhippolyte*.

Reclassification of Barbouriidae

The following classification is proposed for Barbouriidae. It is based on molecular evidence generated from this study and the accumulated morphological and molecular evidence in the literature.

Superfamily Alpheoidea Rafinesque, 1815

Family Barbouriidae Christoffersen, 1987

Subfamily Barbouriinae

Genus *Parhippolyte* Borradaile, 1900
Parhippolyte antiguensis (Chace, 1972)
Parhippolyte cavernicola Wicksten, 1996
Parhippolyte misticia (Clark, 1989)
Parhippolyte rukuensis Burukovsky, 2007
Parhippolyte sterreri (Hart & Manning, 1981)
Parhippolyte uveae Borradaile, 1900
Genus *Barbouria* Rathbun, 1912
Barbouria cubensis (von Martens, 1872)

Subfamily Calliasmatinae

Genus *Calliasmata* Holthuis, 1973
Calliasmata nohochi Escobar-Briones, Camacho & Alcocer, 1997
Calliasmata pholidota Holthuis, 1973
Calliasmata rimolii Chace, 1975

Subfamily Callismatinae

Diagnosis: Sensory dorsal organs of carapace, if present, highly reduced. Infraorbital angle of carapace depressed, inconspicuous below antennal tooth, subocular tooth absent. Rostrum, if present, highly reduced, unarmed. Carapace bearing minute scales or setules. Palp and incisor process of mandible, if present, highly reduced. Eyes highly degenerated, with eyestalks fused basally. First pereiopod and third maxilliped notably robust in comparison to other pereiopods.

Genera included: Calliasmata Holthuis, 1973.

Material examined: see Supplementary material Table S10.

Subfamily Barbouriinae

Diagnosis: Carapace with 2 moderately large and 2 small sensory dorsal organs (Fig. 4); first large organ associated with and posterior to epigastric tooth, second organ medial along dorsal margin located medially within cardiac region, small posterolateral pair juxtaposed to second large organ (Fig. 4). Cornea darkly pigmented, may be broader or narrower than eyestalk. Mandible with 3-jointed palp, incisor process absent. Pereiopods elongated, with or without arthrobranchs at bases of anterior 4 pairs of pereiopods. First pereiopods chelate; chelae slender, moderately small. Second pereiopods with carpus divided into articles, ischium and merus faintly subdivided. Third to fifth pereiopods with or without posterior segments subdivided into articles.

Genera included: *Parhippolyte* Borradaile, 1900 and *Barbouria* Rathbun, 1912.

Material examined: see Supplementary material Table S10.

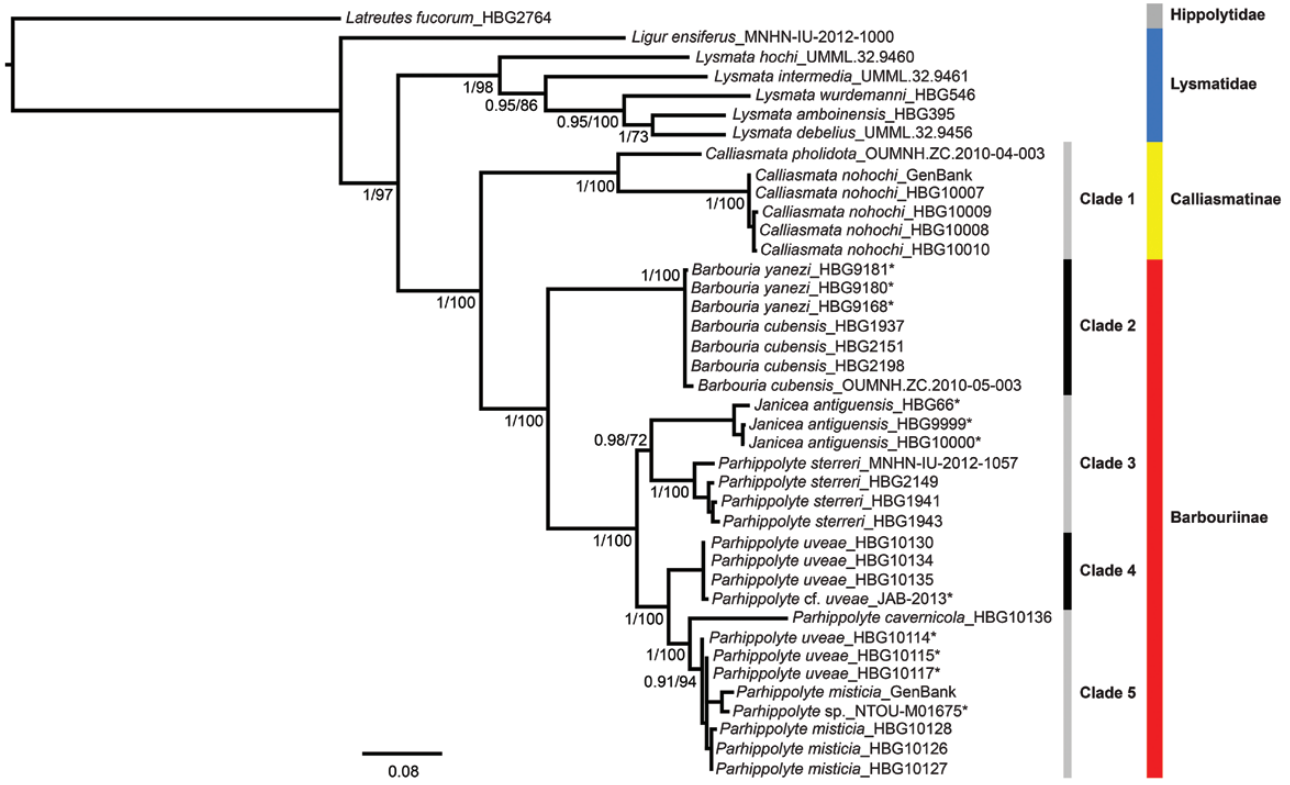

Figure 3. Bayesian phylogram for Barbouriidae ($N = 9$) based on a 16S, 28S, COI, enolase, H3, NaK and PEPCK concatenated data set. BI posterior probabilities and maximum likelihood (ML) bootstrap values noted above branches. Values > 0.7 for ML and > 90% for BI are shown and represented by percentages. Catalog numbers represent voucher specimens (whole or tissue) housed in the Florida International Crustacean Collection (FICC). *, misidentified, unresolved, or reclassified individuals (refer to Table 2 for correct identifications based on molecular data). This figure is available in color at *Journal of Crustacean Biology* online.

Table 2. Original and corrected identifications of taxa in Barbouriidae. See Material and Methods for museum abbreviations.

	Taxon	
Museum catalog no.	**Original**	**Corrected**
HBG9168	*Barbouria yanezi*	*Barbouria cubensis*
HBG9180	*Barbouria yanezi*	*Barbouria cubensis*
HBG9181	*Barbouria yanezi*	*Barbouria cubensis*
HBG66/OUMNH.ZC.2004-15-002	*Janicea antiguensis*	*Parhippolyte antiguensis*
HBG9999	*Janicea antiguensis*	*Parhippolyte antiguensis*
HBG10000	*Janicea antiguensis*	*Parhippolyte antiguensis*
HBG10114/MNHN-IU-2012-1001	*Parhippolyte uveae*	*Parhippolyte misticia*
HBG10115/MNHN-IU-2012-1002	*Parhippolyte uveae*	*Parhippolyte misticia*
HBG10117/MNHN-20018–3568	*Parhippolyte uveae*	*Parhippolyte misticia*
NTOU M01675/TWH-2014	*Parhippolyte* sp.	*Parhippolyte misticia*
JAB-2013	*Parhippolyte* cf. *uveae*	*Parhippolyte uveae*

Table 3. Mean (and standard error) of genetic distances between genera of Barbouriidae for the 16S partial gene regions.

	Ligur	*Lysmata*	*Calliasmata*	*Barbouria*	*Janicea*	*Parhippolyte*
Ligur	0.022 (0.025)	0.309 (0.024)	0.321 (0.006)	0.329 (0.000)	0.344 (0.010)	0.304 (0.027)
Lysmata	0.309 (0.024)	0.112 (0.104)	0.329 (0.015)	0.334 (0.021)	0.352 (0.018)	0.330 (0.029)
Calliasmata	0.331 (0.005)	0.344 (0.015)	0.099 (0.118)	0.311 (0.006)	0.303 (0.022)	0.300 (0.021)
Barbouria	0.329 (0.000)	0.334 (0.021)	0.311 (0.006)	0.000 (0.000)	0.260 (0.007)	0.238 (0.014)
Janicea	0.344 (0.010)	0.352 (0.018)	0.303 (0.022)	0.260 (0.007)	0.007 (0.009)	0.113 (0.018)
Parhippolyte	0.304 (0.027)	0.330 (0.029)	0.300 (0.021)	0.238 (0.014)	0.113 (0.018)	0.089 (0.054)

Table 4. Genetic distances for the CO1 partial gene region in species of Barbouriidae amplified with the F/10 primers. GenBank accession numbers and alternative museum catalog numbers are listed in Table 1. Individuals with asterisk (*) represent eclassified specimens. See Table 2 for the correct identifications.

	Latreutes fucorum	*Calliasmata nohochi*	*Barbouria cubensis*	*Barbouria yanezi*	*Parhippolyte sterreri*	*Parhippolyte uveae**	*Parhippolyte misticia*	*Parhippolyte uveae*	*Parhippolyte cavernicola*	*Janicea antiguensis*
Voucher	HBG2764	HBG10010	HBG1937	HBG9181	HBG2149	HBG10114	HBG10125	HBG10135	HBG10136	HBG10000
Latreutes fucorum	0	0.6878	0.4425	0.4425	0.4875	0.4338	0.4257	0.4302	0.4782	0.4031
Calliasmata nohochi	0.6878	0	0.5072	0.5072	0.5343	0.5007	0.5030	0.5074	0.6459	0.5014
Barbouria cubensis	0.4425	0.5072	0	0	0.2717	0.3173	0.3184	0.2760	0.2887	0.2904
B. yanezi	0.4425	0.5072	0	0	0.2717	0.3173	0.3184	0.2760	0.2887	0.2904
Parhippolyte sterreri	0.4875	0.5343	0.2717	0.2717	0	0.2241	0.2297	0.2180	0.2509	0.2041
*P. uveae**	0.4338	0.5007	0.3173	0.3173	0.2241	0	0.0073	0.2119	0.2556	0.2478
P. misticia	0.4257	0.5030	0.3184	0.3184	0.2297	0.0073	0	0.2126	0.2595	0.2437
P. uveae	0.4302	0.5074	0.2760	0.2760	0.2180	0.2119	0.2126	0	0.0300	0.2345
P. cavernicola	0.4782	0.6459	0.2887	0.2887	0.2509	0.2556	0.2595	0.0300	0	0.2674
Janicea antiguensis	0.4031	0.5014	0.2904	0.2904	0.2041	0.2478	0.2437	0.2345	0.2674	0

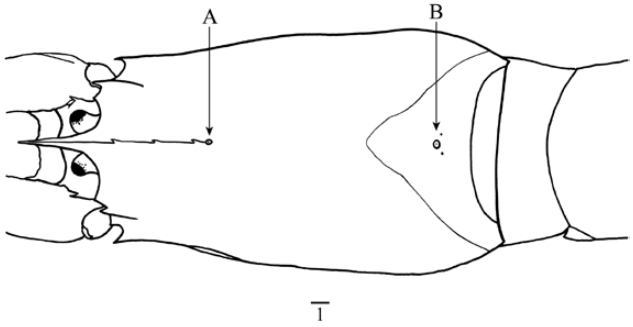

Figure 4. Sensory dorsal organs (SDO) of *Barbouria cubensis* (illustrated by RED). SDO associated with and posterior to the epigastric tooth (**A**), single large SDO within cardiac region and a small pair juxtaposed to the larger SDO (**B**). Scale bar = 1mm.

DISCUSSION

The classification of Barbouriidae has undergone numerous revisions and still lacks an accurate formal morphological definition (De Grave *et al.*, 2014). Our tree, based on multi-locus phylogenetic methods, includes representatives of all barbouriid genera (Fig. 3). The tree excludes *Parhippolyte rukuensis* and *Calliasmata rimolii* as no sequence data is available for these species and attempts to locate molecular-grade material failed. All previous studies have at least one representative of *Parhippolyte* and found support for the continued recognition of Barbouriidae, with the inclusion of *Barbouria*, *Parhippolyte*, and *Janicea* (Chace, 1997; Fiedler *et al.*, 2010; Baeza, 2013; De Grave *et al.*, 2014; Aznar-Cormano *et al.*, 2015). De Grave *et al.* (2014) found evidence for the inclusion of *Calliasmata* into Barbouriidae, based on their phylogenetic analysis of 16S, enolase and NaK, and because all species of *Calliasmata* are anchialine cave dwellers. While De Grave *et al.* (2014) advanced our understanding of hippolytid relationships, many generic- and species-level relationships within Barbouriidae remained unresolved due to limited sampling.

Anchialine species are often endemic and increasingly rare. It is important to examine evolutionary relationships between these species and their allies to improve management efforts. Our study presents the most comprehensive treatment to date of barbouriid phylogeny. Our results recover *Ligur* as the earliest branching lineage and is markedly outside of *Lysmata*. De Grave *et al.* (2014) found *Ligur* to be included within Lysmatidae, but our finding shows *Ligur* to be a distinct lineage, using *Latreutus fucorum* as the outgroup taxon. It is possible *Ligur* may need to be considered outside of Lysmatidae; however, further analyses with the inclusion of additional specimens of *L. ensiferus*, and species of Lysmatidae and Hippolytidae is required to resolve this relationship.

Calliasmata is the earliest branching lineage of Barbouriidae, which is in congruence with previous molecular findings (De Grave *et al.*, 2014). More surprising, the genetic distance separating *Calliasmata* from the remaining barbouriids is comparable to the family-level distances between Lysmatidae and Barbouriidae, suggesting that *Calliasmata* represents a separate taxonomic group (Tables 3, 4). From a morphological standpoint, *Calliasmata* lacks any significant synapomorphy previously identified for Barbouriidae as stated by De Grave *et al.* (2014). The genus differs from genera of Barbouriidae in having the rostrum formed by a simple spine, degenerate and immovable eyes that may or may not be fused, the scaphocerite not reaching beyond the distal margin of the third antennular peduncle and lacking a 3-jointed palp, and the presence of a single podobranch on the second maxilliped and a single arthrobranchs on the third maxilliped (Holthuis, 1973; Chace, 1975; Escobar-Briones *et al.*, 1997). The relationships formed within the multi-locus phylogenetic tree (Fig. 3), genetic distances and morphological evidence, provide strong support that Barbouriinae and Calliasmatinae be erected as a monogeneric subfamilies within Barbouriidae. Erecting these subfamilies resolves the disparity

Table 5. Comparison between diagnostic characters of Barbouriinae and Calliasmatinae.

	Barbouriinae	Calliasmatinae
1	Rostrum with dorsal and ventral margin armed, usually reaching beyond the eyestalk.	Rostrum, if present, highly reduced and unarmed, not reaching beyond eyestalk.
2	Carapace with subocular tooth.	Carapace without subocular tooth.
3	Carapace smooth, without setules.	Carapace and integument bearing setules.
4	Sensory dorsal organs of carapace well developed; (*1*) associated with epigastric tooth, (*2*) located within cardiac region (Fig. 4).	Sensory dorsal organs of carapace, if present, highly reduced.
5	Mandible with 3-jointed palp.	Palp of mandible, if present, highly reduced.
6	Cornea darkly pigmented and well developed.	Cornea, if present, highly degenerate.
7	Eyestalk not fused basally.	Eyestalk fused together basally.
8	Third maxilliped and first pereiopod narrow and elongated, slightly more robust compared to remaining pereiopods.	Third maxilliped and first pereiopod notably more robust compared to remaining pereiopods.

between morphological and molecular evidence as to the relationship between *Calliasmata* and other barbouriids (Fig. 3; Tables 3–5), but Barbouriidae still lacks a complete definition (De Grave *et al.*, 2014).

Another surprising result is the phylogenetic position of *Janicea antiguensis*, significantly supported within *Parhippolyte* and as the sister taxon to *P. sterreri* (clade 3; Fig. 3). In all phylogenetic trees, including single gene phylogenies, *J. antiguensis* was found nested within the genus *Parhippolyte*. *Janicea antiguensis* is similar to *Parhippolyte* in the subdivision of the three posterior pereiopods and having a cornea that is wider than the eyestalk, and is superficially most similar to *P. misticia* (Chace, 1972; Clark, 1989). *Janicea antiguensis* is similar to *Barbouria* in its gill compliment (Chace, 1972; Manning & Hart, 1984). Clark (1989) drew attention to the appendix masculina (AM) being longer than the appendix interna (AI) as a diagnostic character for *Janicea*. In the likely case that barbouriid genera are protandric simultaneous hermaphrodites similar to *P. misticia*, however, the length of the AM versus the AI will change as individuals transition from the male to female phase (Onaga *et al.*, 2012). This character and other similar sexually dimorphic characters are thus not viable characters to delineate among species. Morphologically, *Janicea* seems to represent an intermediate between *Parhippolyte* and *Barbouria*, but our molecular results suggest a clear affinity between species of *Parhippolyte* and *J. antiguensis* (clade 3; Fig. 3).

Our phylogeny (Fig. 3) finds *Parhippolyte* to be paraphyletic. The paraphyly can be resolved by either considering *Janicea* as a junior synonym of *Parhippolyte*, or by resurrecting the genus *Somersiella*. In our tree, *P. sterreri* is found to form a group with *J. antiguensis* (clade 3; Fig. 3) and is sister to a clade composed of *P. misticia* + *P. uweae* + *P. cavernicola* (clades 4 and 5; Fig. 3). It is noteworthy that *Parhippolyte sterreri* was first described as *Somersiella sterreri* (Hart & Manning, 1981) and *Somersiella* was considered distinct from *Parhippolyte* due to the lack of a podobranch on the second maxilliped (Manning & Hart, 1984), and whether or not the telson terminated in a sharp point (Christoffersen, 1987). The examination of material of *P. sterreri* revealed a podobranch on the second maxilliped previously diagnosed as being absent, and that characters that are distinct among genera are likely species-specific (Wicksten, 1996). There is no morphological evidence supporting the resurrection of *Somersiella* (Wicksten, 1996). The inclusion of more material, including *P. cavernicola*, has helped resolve the relationships among species of *Parhippolyte*. Based on a lack of morphological evidence and our multi-locus phylogeny, we find the best solution is to consider *Janicea* as a junior synonym of *Parhippolyte* and retain *P. sterreri* within the genus *Parhippolyte*.

The relationship between *P. misticia* and *P. uweae* could not be resolved using only the available sequences from GenBank. The inclusion of additional material of *P. misticia*, *P. cavernicola*, and *P. uweae* has revealed the evolutionary relationships within this genus and mistaken or unresolved identification of species within *Parhippolyte* (Table 2). Updating the GenBank and museum records for the corresponding sequences for these *Parhippolyte* species resolves the conflicts in the phylogenies created by the inclusion of these sequences (Table 2).

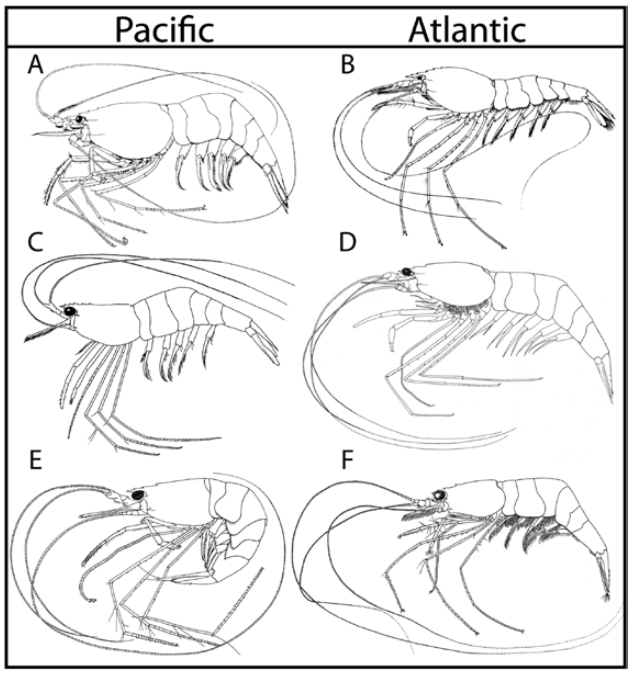

Figure 5. *Parhippolyte uweae* (from Fransen & Tomascik, 1996: fig. 1) (**A**); *Barbouria cubensis* (from Hobbs *et al.*, 1977: fig. 33) (**B**); *Parhippolyte cavernicola* (from Wicksten, 1996: fig. 1) (**C**); *Parhippolyte sterreri* formerly *Somersiella sterreri* (from Hart & Manning, 1981: fig. 1) (**D**); *Parhippolyte misticia* (from Clark, 1989: fig. 1) (**E**); *Janicea antiguensis* (from Chace, 1972: fig. 40b) (**F**).

Our phylogeny finds *Barbouria cubensis* and *Barbouria yanezi* form a single species, representing by a polytomy in our tree (Fig. 3). *Barbouria yanezi* was described as a distinct species within *Barbouria* based on the length of the rostrum, number and positioning of rostral teeth, length to width ratio of the scaphocerite, length ratios of the articles of the first and second pereiopod, length of the appendix masculina *versus* the appendix interna, number of terminal spines, and maximum recorded carapace length (Mejía *et al.*, 2008). All of the differences between *B. yanezi* and *B. cubensis* fall within the range of PhyV documented in *B. cubensis* (Ditter *et al.*, 2019). Based on the lack of genetic morphological differences we consider *Barbouria yanezi* to be a synonym of *B. cubensis*. This reverts *Barbouria* to a monotypic genus.

Some noteworthy phylogeographic patterns emerge in our barbouriid tree (Figs. 2, 3). *Barbouria cubensis* (Atlantic species) is the earliest branching lineage of Barbouriinae (clade 2; Fig. 3), sister to a clade comprised of *P. sterreri* + *J. antiguensis* (clade 3; Fig. 3) and *P. misticia* + *P. cavernicola* + *P. uveae* (clades 4 and 5; Fig. 3). This would suggest that Barbouriinae originated in the Atlantic after the invasion of caves. Pacific barbouriids also appear superficially similar to Atlantic counterparts, with similar a morphological appearance between *P. uveae* and *B. cubensis*, *P. cavernicola* and *P. sterreri*, and *P. misticia* and *J. antiguensis* (Figs. 1, 5). Our phylogeny also suggests that Barbouriidae likely originated from shallow-water reef species prior to invading caves, instead of deep-sea species, a hypothesis based on the close relationship of Barbouriidae with Lysmatidae. A cornea that is narrower than the eyestalk is a predominant troglodytic adaptation found in Barbouriinae but only present in *B. cubensis*. Only *B. cubensis* and *P. sterreri* have the propodus and carpus of the third to fifth pereiopods not articulated. *Barbouria cubensis* and *J. antiguensis* lack arthrobranchs on the first and second maxillipeds, whereas all species of Barbouriinae have two arthrobranchs on the first and second maxillipeds. These characters suggest that the ancestor of Barbouriinae likely possessed a greater number of troglodytic adaptations that have been lost over time. It is peculiar, however, that *J. antiguensis* shares characters with both Atlantic and Pacific species of Barbouriidae. Such distribution suggests that after *Barbouria* further diverged from its troglodytic ancestor barbouriids before invading the Pacific. It would be of particular interest to investigate the results of an ancestral state reconstruction to gain a better understanding when these invasions and divergences occurred.

Our results are not expected to fully resolve the classification of all barbouriids, but represents progress towards unraveling the relationships among these species, which have remained enigmatic to caridean systematists. This study is intended to provide clarity into the evolutionary history of Barbouriidae and provide a framework for future studies.

KEY FOR SUBFAMILIES BARBOURIINAE AND CALLIASMATINAE

Carapace armed with unique subocular tooth posterodorsal to the orbital angle; mandible with 3-jointed palp; carapace with sensory dorsal organs, the first associated and posterodorsal to the epigastric tooth and the second along the dorsal median margin within cardiac region, with smaller pair posterolateral juxtaposed to second sensory dorsal organ ..... Barbouriinae

Infraorbital angle of the carapace depressed and inconspicuous below small antennal tooth, subocular tooth absent; eye highly reduced with eyestalks fused basally; rostrum, if present, unarmed, not reaching past eyestalk; palp and incisor process of mandible, if present, highly reduced; third maxilliped and first pereiopod notably robust; sensory dorsal organs, if present, highly reduced ..... Calliasmatinae

KEY TO SPECIES OF *CALLIASMATA*, SUBFAMILY CALLIASMATINAE (MODIFIED FROM ESCOBAR-BRIONES *ET AL.*, 1997)

1. Rostrum overreaching eyes, antennal spine overreaching distal margin of eyes, third to fifth pleura of abdominal somites with strong ventral tooth, telson margin bearing 3 spines ..... *C. pholidota*

Rostrum not overreaching eyes, antennal spine almost reaching distal margin of eyes, third to fifth pleura of abdominal somites without ventral tooth, telson margin without spines 2

2. Carapace and integument with setules, third to fifth pleura posteroventral angle acute produced into tooth, propodus of fourth pereiopod 5 times longer than dactylus ..... *C. nohochi*

Setules of carapace and integument, if present, highly reduced, posteroventral angle of third to fifth pleura acute without tooth, propodus of fourth pereiopod 4 times longer than dactylus ..... *C. rimolii*

KEY TO GENERA OF SUBFAMILY BARBOURIINAE

1. Eyes large, cornea darkly pigmented, broader than eyestalk 2
Eyes reduced, cornea darkly pigmented, narrower than or subequal to the eyestalk ..... *B. cubensis* (Fig. 5B)
2. Carpus and propodus of third to fifth pereiopods multiarticulate 3
Carpus and propodus of third to fifth pereiopods not multiarticulate ..... *P. sterreri* (Fig. 5D)
3. Anterior 4 pereiopods with arthrobranchs 4
Anterior 4 pereiopods without arthrobranchs ..... *P. antiguensis* (Fig. 5F)
4. Pleuron of fourth abdominal somite rounded or subacute without terminal point 5
Pleuron of fourth abdominal somite acute or subacute with terminal point, fifth and sixth pleuron produced into tooth, appendix masculina of second male pleopod not reaching as far as distal end of appendix interna, terminal margin of telson formed into point, terminating in a strong tooth ..... *P. uveae* (Fig. 5A)
5. Pleuron 5 of abdominal somite unarmed, appendix masculina of second male pleopod shorter than appendix interna ..... *P. cavernicola* (Fig. 5C)
Pleuron 5 of abdominal somite produced into tooth, appendix masculina of second male pleopod longer than appendix interna 6
6. Rostrum armed with more than 1 dorsal and ventral teeth, extending almost to the distal end of basal segment of antennular peduncle, terminal margin of telson formed into point, terminating in a weak tooth ..... *P. misticia* (Fig. 5E)
Rostrum armed with a single dorsal and ventral tooth, not reaching to the distal end of the basal segment of the antennular peduncle ..... *P. rukuensis*

SUPPLEMENTARY MATERIAL

Supplementary material is available at *Journal of Crustacean Biology* online.

S1 Figure. 16S loci phylogeny with support values calculated using RAxML,

S2 Figure. 28S loci phylogeny with support values calculated using RAxML,

S3 Figure. Enolase loci phylogeny with support values calculated using RAxML,

S4 Figure. H3 loci phylogeny with support values calculated using RAxML,

S5 Figure. NaK loci phylogeny with support values calculated using RAxML,

S6 Figure. PEPCK loci phylogeny with support values calculated using RAxML,

S7 Figure. COI loci (amplified with F/10 primers) phylogeny with support values calculated using RAxML,

S8 Figure. COI loci (amplified with LCO1490/HCO2198 primers) phylogeny with support values calculated using RAxML,

S9 Table. Heat map and genetic distances (D_A) for the 16S partial gene region.

S10 Table. Material of Barbouriidae examined.

ACKNOWLEDGEMENTS

We would like to thank Drs. Thomas Iliffe, T.-Y. Chan, Darryl Felder, Craig Layman, Jocelyn Curtis-Quick, and the Cape Eleuthera Institute, The Bahamas for their assistance in the collection of material. We also thank the curators at USNM and MNHN for providing valuable additional material of *Parhippolyte*. We are grateful for the support and assistance of the Gerace Research Centre, San Salvador, Bahamas and the Bahamian citizens during field work. We are grateful to A. Kerstitch, J. Starmer, T. Iliffe and Meerwasser-Aquaristik-Studio-Korallenkiste, Rosbach vor der Höhe, Germany for providing permission to use photos of barbouriids. We would also like to thank the Dr. Sammy De Grave and the anonymous reviewers for their incite and feedback. This study was supported in part by a student research award from the Gerace Research Centre and The Crustacean Society's Graduate Student Fellowship awarded to RED. LMMO thanks the Consejo Nacional de Ciencia y Tecnología (CONACYT), Mexico to support the exploration in karstic areas in Mexico by funding the project CONACYT-258494 (Fondo Sectorial de Investigación para la Educación). Additional support was provided by Florida International University. This is contribution no. 192 from the Coastlines and Oceans Division of the Institute of Environment at Florida International University.

REFERENCES

Ahyong, S. & O'Meally, D. 2004. Phylogeny of the Decapoda Reptantia: Resolution using three molecular loci and morphology. *Raffles Bulletin of Zoology*, **52**: 673–693.

Aznar-Cormano, L., Brisset, J., Chan, T.Y., Corbari, L., Puillandre, N., Utge, J., Zbinden, M., Zuccon, D. & Samadi, S. 2015. An improved taxonomic sampling is a necessary but not sufficient condition for resolving inter-families relationships in Caridean decapods. *Genetica*, **143**: 195–205.

Baeza, J.A. 2010 Molecular systematics of peppermint and cleaner shrimps: phylogeny and taxonomy of the genera *Lysmata* and *Exhippolysmata* (Crustacea: Caridea: Hippolytidae). *Zoological Journal of the Linnean Society*, **160**: 254–265.

Baeza, J.A. 2013. Molecular phylogeny of broken-back shrimps (genus *Lysmata* and allies): A test of the 'Tomlinson-Ghiselin' hypothesis explaining the evolution of hermaphroditism. *Molecular Phylogenetics and Evolution*, **69**: 46–62.

Baeza, J.A. & Anker, A. 2009. *Lysmata hochi* n. sp., a new hermaphroditic shrimp from the southeastern Caribbean Sea (Caridea: Hippolytidae). *Journal of Crustacean Biology*, **28**: 148–155.

Becking, L.E., Renema, W., Santodomingo, N.K., Hoeksema, B.W., Tuti, Y. & de Voogd, N.J. 2011. Recently discovered landlocked basins in Indonesia reveal high habitat diversity in anchialine systems. *Hydrobiologia*, **677**: 89–105.

Bishop, R.E., Humphreys, W.F., Cukrov, N., Žic, V., Boxshall, G.A., Cukrov, M., Iliffe, T.M., Kršinić, F., Moore, W.S., Pohlman, J.W. & Sket, B. 2015. 'Anchialine' redefined as a subterranean estuary in a crevicular or cavernous geological setting. *Journal of Crustacean Biology*, **35**: 511–514.

Borradaile, L.A. 1900. On the Stomatopoda and Macrura brought by Dr. Willey from the South Seas. In: Willey, A., *Zoological results based on material from New Britain, New Guinea, Loyalty Islands and elsewhere, collected during the years 1895, 1896, and 1897…*, pp. 395–428. University Press, Cambridge, UK.

Bracken-Grissom, H.D., Ahyong, S.T., Wilkinson, R.D., Feldmann, R.M., Schweitzer, C.E., Breinholt, J.W., Bendall, M., Palero, F., Chan, T.-Y., Felder, D.L., Robles, R., Chu, K.-H., Tsang, L.-M., Kim, D., Martin, J.W. & Crandall, K.A. 2014. The emergence of the lobsters: phylogenetic relationships, morphological evolution and divergence time comparisons of an ancient group (Decapoda: Achelata, Glypheidea, Polychelida). *Systematic Biology*, **63**: 457–479.

Bracken, H.D., De Grave, S. & Felder, D.L. 2009a. Phylogeny of the infraorder Caridea based on mitochondrial and nuclear genes (Crustacea: Decapoda). In: Decapod crustacean phylogenetics (J.W. Martin, K.A. Crandall & D.L. Felder, eds.). *Crustacean Issues*, **18**: 274–300.

Bracken, H.D., Toon, A, Felder, D.L., Martin, J.W., Finley, M., Rasmussen, J., Palero, F. & Crandall, K. 2009b. The decapod tree of life: compiling the data and moving toward a consensus of decapod evolution. *Arthropod Systematics and Phylogeny*, **67**: 99–116.

Bruce, A.J. 1883. *Lysmata debelius* new species, a new hippolytid shrimp from the Philippines. *Revue française d'Aquariologie*, **9**[1982]: 115–120.

Buden, D.W. & Felder, D.L. 1977. Cave shrimps in the Caicos Islands. *Proceedings of the Biological Society of Washington*, **90**: 108–115.

Burukovsky, R.N. 2007. On some new and rare shrimps from the Indo-Western Pacific. *Zoologicheskii Zhurnal*, **86**: 1–8 [in Russian].

Chace, F.A. 1997. The Caridean shrimps (Crustacea: Decapoda) of the *Albatross* Philippine Expedition, 1907–1910, part 7: families Atyidae, Eugonatonotidae, Rhynchocinetidae, Bathypalaemonellidae, Processidae, and Hippolytidae. *Smithsonian Contributions to Zoology*, **587**: 1–106.

Chace, F.A. Jr. 1975. Cave shrimps (Decapoda: Caridea) from the Dominican Republic. *Proceedings of the Biological Society of Washington*, **88**: 29–44.

Chace, F.A. 1972. The shrimps of the Smithsonian-Bredin Caribbean Expeditions with a summary of the West Indian shallow-water species (Crustacea: Decapoda: Natantia). *Smithsonian Contributions to Zoology*, **98**: 1–179.

Christoffersen, M.L. 1987. Phylogenetic relationships of hippolytid genera, with an assignment of new families for the Crangonoidea and Alpheoidea (Crustacea, Decapoda, Caridea). *Cladistics*, **3**: 348–362.

Christoffersen, M.L. 1990. A new superfamily classification of the Caridea (Crustacea: Pleocymata) based on phylogenetic pattern. *Zeitschrift für Zoologische Systematik und Evoluationsforschung*, **28**: 94–106.

Clark, J. 1989. *Koror misticius*, new genus, new species (Decapoda: Hippolytidae), a cave shrimp from Palau. *Journal of Crustacean Biology*, **9**: 445–452.

Crandall, K.A. & Fitzpatrick, J.F. 1996. Crayfish molecular systematics: Using a combination of procedures to estimate phylogeny. *Systematic Biology*, **45**: 1–26.

De Grave, S., Li, C.P., Tsang, L.M., Chu, K.H. & Chan, T.Y. 2014. Unweaving hippolytoid systematics (Crustacea, Decapoda, Hippolytidae): Resurrection of several families. *Zoologica Scripta*, **43**: 496–507.

De Man, J.G. 1888. Bericht über die von Herrn Dr. J. Brock im indischen Archipel gesammelten Decapoden und Stomatopoden. *Archiv für Naturgeschichte*, **53**: 289–600, pls. 11–22a.

Ditter, R.E., Erdman, R.B., Goebel, A.M. & Bracken-Grissom, H.D. 2019. Widespread phenotypic hypervariation in the enigmatic anchialine shrimp *Barbouria cubensis* (Decapoda: Barbouriidae). *Zootaxa* [doi: 10.11646/Zootaxa.5648.1.1].

Escobar-Briones, E., Camacho, M.E. & Alcocer, J. 1997. *Calliasmata nohochi*, new species (Decapoda: Caridea: Hippolytidae), from Anchialine Cave

systems in continental Quintana Roo, Mexico. *Journal of Crustacean Biology*, **17**: 733–744.
Fabricius, J.C. 1798. *Supplementum Entomologiae Systematicae*. Proft & Storch, Hafniae [= Copenhagen].
Felsenstein, J. 1985. Confidence limits of phylogenies: an approach using the bootstrap. *Evolution*, **39**: 783–791.
Felsenstein, J. 1989. PHYLIP - Phylogeny Inference Package (Version 3.2). *Cladistics*, **5**: 164–166.
Felsenstein, J. & Churchill, G.A. 1996. A hidden Markov model approach to variation among sites in rate of evolution. *Molecular Biology and Evolution*, **13**: 93–104.
Fiedler, G.C., Rhyne, A.L., Segawa, R., Aotsuka, T. & Schizas, N.V. 2010. The evolution of euhermaphroditism in caridean shrimps: a molecular perspective of sexual systems and systematics. *BMC Evolutionary Biology*, **10**: 297 [doi: 10.1186/1471-2148-10-297].
Folmer, O., Black, M., Hoeh, W., Lutz, R. & Vrijenhoek, R. 1994. DNA primers for amplification of mitochondrial cytochrome c oxidase subunit I from diverse metazoan invertebrates. *Molecular Marine Biology and Biotechnology*, **3**: 294–299.
Fransen, C.H.J.M. & Tomascik, T. 1996. *Parhippolyte uveae* Borradaile, 1899 (Crustacea: Decapoda: Hippolytidae) from Kakaban Island, Indonesia. *Zoologische Mededelingen*, **70**: 227–233.
Gibbes, L.R. 1850. Catalogue of the Crustacea in the Cabinet of the Academy of Natural Sciences of Philadelphia. *Proceedings of the Academy of Natural Sciences of Philadelphia*, **5**: 22–30.
Hart, C.W. & Manning, R.B. 1981. The cavernicolous caridean shrimps of Bermuda (Alpheidae, Hippolytidae, and Atyidae). *Journal of Crustacean Biology*, **1**: 441–456.
Hobbs, H.H. Jr., Hobbs, H.H. III & Daniel, M.A. 1977. A review of the troglobitic decapod crustaceans of the Americas. *Smithsonian Contributions to Zoology*, **244**: 1–177.
Holthuis, L. 1973. Caridean shrimps found in land-locked saltwater pools at four Indo-West Pacific localities (Sinai Peninsula, Funafuti Atoll, Maui and Hawaii Islands): with the description of one new genus and four new species. *Zoologische Verhandelingen*, **128**: 3–48.
Huelsenbeck, J.P. & Ronquist, F. 2001. MrBayes: Bayesian inference of phylogenetic trees. *Bioinformatics*, **17**: 745–755.
Iliffe, T.M. & Kornicker, L.S. 2009. Worldwide diving discoveries of living fossil animals from the depths of anchialine and marine caves. *Smithsonian Contributions to Marine Sciences*, **38**: 269–280.
Iliffe, T.M. 1996. *Somersiella sterreri. The IUCN Red List of Threatened Species* 1996 e.T20371A9192483 [doi: 10.2305/IUCN.UK.1996.RLTS.T20371A9192483.en].
Katoh, K. & Standley, D.M. 2013. MAFFT Multiple Sequence Alignment Software Version 7: Improvements in performance and usability. *Molecular Biology and Evolution*, **30**: 772–780.
Kemp, S. 1914. Hippolytidae. Notes on Crustacea Decapoda in the Indian Museum, V. *Records of the Indian Museum*, **10**: 81–129.
Kingsley, J.S. 1878. Notes on the North American Caridea in the Museum of the Peabody Academy of Science at Salem, Mass. *Proceedings of the Academy of Natural Sciences of Philadelphia*, **1878**: 89–98.
Lanfear, R., Frandsen, P.B., Wright, A.M., Sendfeld, T. & Calcott, B. 2016. PartitionFinder 2: New methods for selecting partitioned models of evolution for molecular and morphological phylogenetic analyses. *Molecular Biology and Evolution*, **34**: 772–773.
Leigh, J.W. & Bryant, D. 2015. PopART: Full-feature software for haplotype network construction. *Methods in Ecology and Evolution*, **6**: 1110–1116.
Legall, N. & Poupin, J. 2018. CRUSTA: Database of Crustacea (Decapoda and Stomatopoda), with special interest for those collected in French overseas territories [http://crustiesfroverseas.free.fr/].
Li, C.P., De Grave, S., Chan, T.-Y., Lei, H.C. & Chu, K.H. 2011. Molecular systematics of caridean shrimps based on five nuclear genes: Implications for superfamily classification. *Zoologischer Anzeiger*, **250**: 270–279.
Manning, R.B. & Hart, C.W. 1984. The status of the hippolytid shrimp genera *Barbouria* and *Ligur* (Crustacea: Decapoda): A Reevaluation. *Proceedings of the Biological Society of Washington*, **97**: 655–665.
Martens, E., von. Über cubanische Crustaceen nach den Sammlungen Dr. J. Gundlach's. *Archiv für Naturgeschichte*, **38**: 77–147.
Mejía, L.M., Zarza, E. & López, M. 2008. *Barbouria yanezi* sp. nov., a new species of cave shrimp (Decapoda, Barbouriidae) from Cozumel Island, Mexico. *Crustaceana*, **81**: 663–672.
Onaga, H., Fiedler, G. & Baeza, J. 2012. Protandric simultaneous hermaphroditism in *Parhippolyte misticia* (Clark, 1989) (Caridea: Hippolytidae): implications for the evolution of mixed sexual systems in. *Journal of Crustacean Biology*, **32**: 383–394.
Palumbi, S., Martin, A., Romano, S., McMillan, W.O., Stice, L. & Grabowski, G. 1991. *The simple fool's guide to PCR*. Department of Zoology and Kewalo Marine Laboratory, University of Hawaii, Honolulu.
Page, T.J., Short, J.W., Humphrey, C.L., Hillyer, M.J. & Hughes, J.M. 2008. Molecular systematics of the Kakaducarididae (Crustacea: Decapoda: Caridea). *Molecular Phylogenetics and Evolution*, **46**: 1003–1014.
Pérez-Moreno, J.L., Iliffe, T.M. & Bracken-Grissom, H.D. 2016. Life in the underworld: anchialine cave biology in the era of speleogenomics. *International Journal of Speleology*, **45**: 149–170.
Porter, M.L., Perez-Losada, M. & Crandall, K.A. 2005. Model-based multi-locus estimation of decapod phylogeny and divergence times. *Molecular Phylogenetics and Evolution*, **37**: 355–369.
Rafinesque, C.S. 1815. *Analyse de la nature ou Tableau de l'univers et des corps organisés*. Palermo, Italy [English translation by A.J. Cain, 1990, *Tryonia*, **20**: 104–218].
Rathbun, M.J. 1912. Some Cuban Crustacea, with notes on the Astacidae by Walter Faxon, and a list of Isopoda, by Harriet Richardson. *Bulletin of the Museum of Comparative Zoology*, **54** (15): 451–460, pls. 1–5.
Risso, A. 1816. *Histoire naturelle des Crustacés des environs de Nice*. Librairie Grecque-Latine-Allemande, Paris.
Robles, R., Schubart, C.D., Conde, J.E., Carmona-Suarez, C., Alvarez, F., Villalobos, J.L. & Felder, D.L. 2007. Molecular phylogeny of the American *Callinectes* Stimpson, 1860 (Brachyura: Portunidae), based on two partial mitochondrial genes. *Marine Biology*, **150**: 1265–1274.
Sarato, C. 1885. Ligur Edwardsii, Nob. Études sur les Crustacés de Nice. In: *Le Moniteur des Étrangers à Nice*, **9** (222): 2.
Song, H., Buhay, J.E., Whiting, M.F. & Crandall, K.A. 2008. Many species in one: DNA barcoding overestimates the number of species when nuclear mitochondrial pseudogenes are coamplified. *Proceedings of the National Academy of Sciences of the United States of America*, **105**: 13486–13491.
Stamatakis, A., Ludwig, T. & Meier, H. 2005. RAxML-III: a fast program for maximum likelihood-based inference of large phylogenetic trees. *Bioinformatics*, **21**: 456–463.
Swofford, D.L. 2002. PAUP*: phylogenetic analysis using parsimony (* and other methods). Sinauer, Sunderland, MA, USA.
Tsang, L.M., Ma, K.Y., Ahyong, S.T., Chan, T.-Y. & Chu, K.H. 2008. Phylogeny of Decapoda using two nuclear protein-coding genes: origin and evolution of the Reptantia. *Molecular Phylogenetics and Evolution*, **48**: 359–368.
Tuimala, J. 2004. *A primer to phylogenetic analysis using Phylip Package*, Edn. 2. Center for Scientific Computing, Espoo, Finland.
Wicksten, M.K. 1996. *Parhippolye cavernicola*, new species (Decapoda: Caridea: Hippolytidae) from the Tropical Eastern Pacific, with taxonomic remarks on the genera *Somersiella* and *Koror*. *Journal of Crustacean Biology*, **16**: 201–207.

PLOS ONE

RESEARCH ARTICLE

What's the temperature in tropical caves?

Luis Mejía-Ortíz[1], Mary C. Christman[2], Tanja Pipan[3], David C. Culver[4]*

1 Lab. de Bioespeleología y Carcinología, División de Desarrollo Sustentable, Universidad de Quintana Roo, Cozumel, Mexico, **2** Departments of Biology and Statistics, MCC Statistical Consulting LLC, University of Florida, Gainesville, Florida, United States of America, **3** ZRC SAZU Karst Research Institute, Ljubljana, Slovenia, **4** Department of Environmental Science, American University, Washington, DC, United States of America

* dculver@american.edu

OPEN ACCESS

Citation: Mejía-Ortíz L, Christman MC, Pipan T, Culver DC (2020) What's the temperature in tropical caves? PLoS ONE 15(12): e0237051. https://doi.org/10.1371/journal.pone.0237051

Editor: Delei Li, Institute of Oceanology Chinese Academy of Sciences, CHINA

Received: July 15, 2020

Accepted: December 17, 2020

Published: December 31, 2020

Data Availability Statement: All relevant data are within the manuscript and its Supporting information files.

Funding: LMMO was supported by CONACYT (www.conacyt.gob.mx) grant 258494 (Fondo Sectorial de Investigacion para la Educacion). The funders had no role in study design, data collection and analysis, decision to publish, or preparation of the manuscript. MCC Statistical Consulting LLC provided support in the form of salaries for MCC, but did not have any additional role in the study design, data collection and analysis, decision to publish, or preparation of the manuscript. The

Abstract

Hourly temperature was measured for approximately one year at 17 stations in three caves in Quintana Roo, Mexico. Thirteen of these stations were in the extensive twilight zones of all three caves. All seventeen stations showed seasonality in temperature with a 3˚C drop during the Nortes season. Two of the caves, Muévelo Sabrosito and Muévelo Rico, showed greater variability during the winter months while in Río Secreto (Tuch) variability was greatest during the rainy season. Río Secreto is less open to the surface than the other two. All sites also showed a daily temperature cycle, although it was very faint in some Río Secreto (Tuch) sites. While temperature variability is diminished relative to surface variation, its temporal pattern is worthy of further study.

Introduction

Besides the absence of light, caves are distinguished from surface habitats by their relative constancy of temperature. For example, Eigenmann [1] divided a cave into three zones—twilight, a region of fluctuating temperature, and the inner cave region of constant temperature, excluding the entrance itself. Gèze [2] proposed that there is a zone of constant temperature (*practiquement invariable*) in most caves. Given this view of invariance of cave temperature, much of the early interest in cave temperature was how it changed from cave to cave with respect to latitude and altitude rather than how it varied within a cave [2, 3]. Cave temperature should be the mean annual temperature of the surface [3] although other factors such as air flows, water flows, and percolating water can cause deviations. This relative constancy of cave temperature makes the stable isotopic composition of cave speleothems a useful proxy for paleoclimate [4]. Cave temperatures have also been used directly to evaluate shorter term natural and anthropogenically induced climate changes on the scale of decades [5, 6].

The relatively low precision of mercury thermometers and their fragility limited the scope of cave temperature studies, a problem which has been solved by the widespread availability of accurate, sturdy digital temperature probes [7, 8]. This, together with a growing interest in the physics of cave temperature, has resulted in a large increase in the understanding of our knowledge of cave temperature and its dynamics. Analytical mathematical models appeared early in the 20th century [9] and continue to have a robust presence in the field [10–12]. As

specific role of this author is articulated in the author contribution section.

Competing interests: I have read the journal's policy and the authors of this manuscript have the following competing interests: MCC Statistical Consulting LLC provided support in the form of salaries for MCC. The commercial affiliation of MCC to MCC Statistical Consulting LLC does not alter our adherence to PLOS ONE policies on sharing data and materials.

Cigna [7] points out, a renaissance of cave temperature and climate studies in general would not be possible without an increase in the accuracy and automation of measuring devices, i.e., dataloggers. These physical studies have addressed a series of questions, including:

- Mean temperature prediction using passage size, entrance size, and exterior temperature [13].
- Time lags between exterior and cave temperatures [7, 11, 14]. These lags are often weeks to months.
- Temperature effects on wall condensation and evaporation [12].
- The relationship between ventilation and temperature [15].

In addition, there are extensive published cave temperature series, some covering multiple years. Most prominent among these are the temperature time series for multiple sites in and near Postojna Planina Cave System (Slovenia) by Šebela and her associates [16, 17].

While physicists have been concerned with equilibration of air masses, water, and the surrounding rock [11, 12, 18] they have not focused on detection of cycles, either daily or yearly, although Stoeva et al. [6] did analyze data for the presence of multi-year cycles correlated with sunspot cycles. Physicists have focused on the fate of a temperature pulse, rather than on the regularity of such pulses, e.g. daily cycles. With the exception of studies focusing on non-cave shallow subterranean habitats [19], very little attention has been paid to daily, monthly, or seasonal cycles.

We know of no cases where temperatures are truly constant although there likely are some, but the amplitude of variation of all caves is reduced compared to surface temperatures, at least on an annual scale [20]. In deep cave sites, amplitude of change has been reported to be approximately 1 to 2˚C, as is the case in Kartchner Caverns in Arizona [7] and at 1100 m depth in Sistema J2 in Slovenia [11]. Kartchner Caverns is anomalous because its temperature is elevated due to geothermal heating [21]. Culver and Pipan [19] report on extensive temperature measurements in the lava tube Pahoa Cave, Hawaii, where annual variation is less than 1˚C less than 100 m inside the cave, and similar measurements for Cueva del Mulo, a lava tube in the Canary Islands [22]. As far as we have been able to determine, these are the only detailed analyses of temperature in a tropical cave, in both cases small lava tubes.

In contrast to physicists, until recently biologists have been largely content to assume temperature constancy, and to make some important assumptions about this constancy. The standard view is that constancy (1) makes cave dwellers highly vulnerable to environmental change because they have had little opportunity to adapt to a varying environment and (2) that neither temperature nor light provide any cues, either daily or seasonally, to set circadian and annual rhythms. The Romanian biologist Emil Racovitza, widely held to have ushered in the modern study of cave biology [23], a very discerning and skeptical chronicler of the science of biospeleology, stated [24, 25]:

> "*We can admit that temperature is constant and it corresponds generally to the mean annual temperature of that place in deep caves, in fissured massifs, in phreatic sheets and groundwater.*
>
> *Surely meteorologists armed with ultra-sensitive instruments will discover without a doubt, variation, that in absolute, can be considered important, but relative to the place and their influence on living beings, these variations are lower than those observed in the surface environment, and therefore it is agreed not to bring them into account*" . . .

After mentioning a few anomalies, such as open air pits, he concludes:

"*No matter these exceptional facts, we can consider the subterranean environment as a habitat with constant and low temperature, but not identical in all its extent*" . . .

That is, temperature variation in caves was held to be without biological interest. It is fair to say that this opinion is still widely held by speleobiologists except as it makes the cave fauna vulnerable to climate change [20].

An exception to this lack of interest in temperature variation by biologists is an approach pioneered by Mammola and Isaia [26, 27] with their study of niche separation in cave dwelling spiders. In one study, they demonstrated that *Meta menardi* and *Meta bourneti* occurred at different temperatures, but that the differences were sometimes less than 1˚C. Pipan et al. [17] argue that temperature is one of the five key factors that should be measured to assess subterranean ecosystem health and change, in part because it is a surrogate for many more difficult to measure environmental parameters.

Goals of the present study

We propose to close the distance between the physical and biological approaches to cave temperature by an emphasis on the temporal, and to a lesser extent, spatial pattern that results from the fluxes and pulses of temperature studied by physicists. The observed temporal (and spatial) patterns, especially repeated ones, are the conditions faced by cave inhabitants. We do this in a tropical limestone cave, a previously unstudied habitat with respect to temperature. Tropical caves are of special interest not only because they are both common and harbor a rich fauna [28], but also because they are likely to be less variable than better studied temperate caves where surface (and by implication cave) conditions are much more variable.

The advent of dataloggers that measure temperature to the hundredths of a degree and relative humidity to a tenth of a percent allows for a more detailed look at the subterranean environment itself. In spite of the overall reduction in amplitude of variation in subterranean habitats, it is possible to detect differences among closely adjoining sites [16] and to detect the presence of daily and annual cycles [19, 22]. In this study, we begin a characterization of the cave environment in terms of temperature. To this end we examine year long temperature records at both photic and aphotic stations, taken hourly, and compare these records, both between different dataloggers in the same cave and among three different caves in Quintana Roo, Mexico. Light intensity provides the backdrop for comparisons.

Our purpose in this paper is two-fold. First, we demonstrate that variation in temperature, although damped relative to surface habitats, shows cyclical patterns, including seasonal and daily cycles. These patterns are relevant not only to biologists studying cave life, but to paleoclimate studies [4] and climate change heat transfer in the environment [18]. Second, we suggest some protocols for the analysis from data loggers put in caves and other aphotic habitats, including an emphasis on cyclical variation.

Methods and materials

The study caves

The three caves are located in the Quintana Roo in the Yucatan Peninsula (Fig 1) in an area, with one of the highest densities of cave passages (mostly flooded) in the world [29, 30]. Air filled caves are also numerous and they are constrained to a relatively thin layer of flat-bedded limestone with a depth of 5 to 10 m to the water table, and a surface topography of gentle ridges and swales with an overall relief of 1–5 m [30, 31]. The area has an annual cycle of

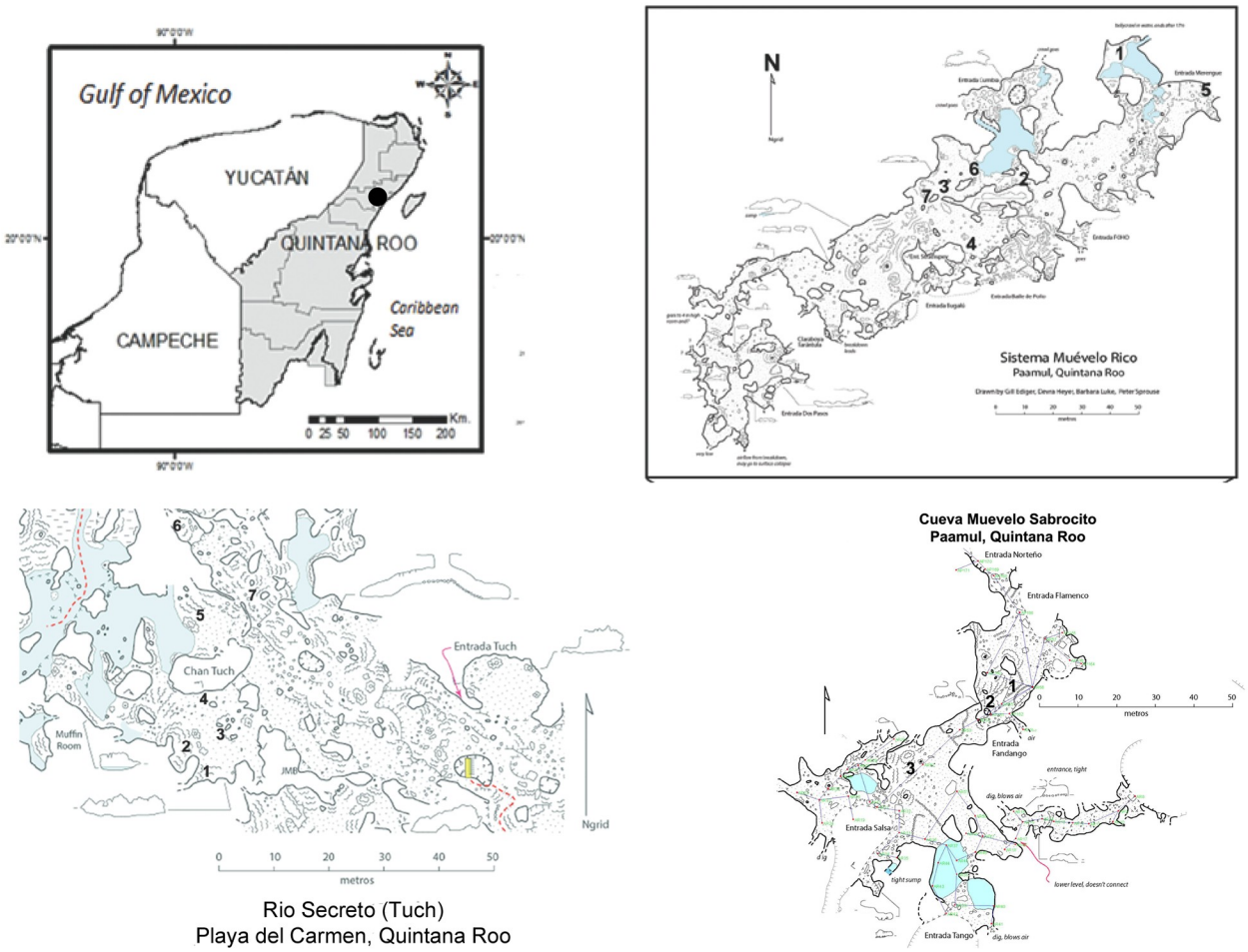

Fig 1. Locator map for caves and sampling sites in the study area. The upper two parts of the figure are from [32]. Maps courtesy of Peter Sprouse.

https://doi.org/10.1371/journal.pone.0237051.g001

precipitation characterized by three seasons: Nortes (cold front season between November and February), dry season (March to May), and rainy season (June to October) which is the hurricane season [32]. During the rainy season 70% of the precipitation occurs. The annual mean temperature is 25.8˚C and the overall precipitation at Playa del Carmen averages 1500 mm over a period of 2005 to 2014 [32].

Sistema Muévelo Rico (20˚32'05.1"N, 87˚12'16.5"W) is located near the settlement of Paamul, in the Mexican state of Quintana Roo (Fig 1). Its surveyed length is 1151 m with a vertical extent of only 4 m [29]. Sistema Muévelo Rico has a large number of entrances, more than 12, if skylights are included. Because of the close proximity of the water table to the surface, vertical development and subterranean terrestrial habitats are very restricted. The cave, with an elevation of 7 m at the entrance, is less than 2 km from the Caribbean Sea. It was originally chosen for study by Mejía-Ortíz et al. [33] because of its extensive twilight zone and extremely small aphotic zone. There were seven monitoring points in the cave. Alberto Rivero gave permission to visit the Sistema Muévelo Rico. No permits were needed since no organisms were collected for this study.

Muévelo Sabrosito (20˚53'N, 87˚20'W) is a small cave immediately adjacent to Sistema Muévelo Rico. It has six entrances and no aphotic zone. Its surveyed length is 400 m with a

depth of 4 m [29]. It has a more open aspect than Sistema Muévelo Rico. There were three monitoring points, all near the Perro Negro section of the cave (Fig 1). Alberto Rivero gave permission to visit Muévelo Sabrosito. No permits were needed since no organisms were collected for this study.

Río Secreto (20˚35'27"N, 87˚8'3"W) is a shallow, horizontally developed cave with 42 km of surveyed passages. It is a tourist cave and the tours are conducted in a small section of the cave. The main entrance is 5 km from the Caribbean coast and 12 km NE of the other two caves. Tides can affect the water table in Río Secreto up to several cm [32]. There were seven monitoring points clustered in the vicinity of the Tuch entrance (Fig 1), and we refer to the cave as Río Secreto (Tuch) throughout. Tania Ramirez of Rio Secreto Natural Preserve gave permission to visit the Tuch entrance of Río Secreto and provided logistical support. No permits were needed since no organisms were collected for this study.

Taken together, the three caves represent a range of cave sizes and cave environments, ranging from small and highly connected with the surface (Muévelo Sabrosito) to large and less connected with the surface (Rio Secreto [Tuch]). The differences in surface connectivity should result in differences in temperature variability, with less surface-connected sites being less variable.

Temperature measurement

Temperature was measured at hourly intervals for the following dates:

- Sistema Muévelo Rico—5 April 2015 to 28 March 2016, n = 8593
- Sistema Muévelo Sabrosito—24 September 2018 to 24 October 2019, n = 9477
- Río Secreto (Tuch entrance)—25 September 2018 to 26 October 2019, n = 9515

We did not include detailed surface measurements because the reduction of variation in caves relative to the surface is well known. Our focus was on variation within caves and the persistence of cyclical patterns. Onset Computer Corporation HOBO™ U23 Pro v2 data loggers were used to measure temperature and readings were accurate to ±0.21˚C with a resolution of 0.02˚C.

Data analysis

Spectral analysis, periodograms, autocorrelations and partial autocorrelations were done on the hourly data to detect possible cycles. Cycles up to a period of 600 hours (25 days) were reported. Analyses were done using JMP® Pro 13.2.0 (©2016 SAS Institute, Inc. Cary, NC). Basic statistics (mean and ranges) were done using EXCEL™.

For estimating monthly means, the hourly data were first averaged over each day to obtain daily means for input to the analyses. In addition, for Río Secreto, the sensors were identified as belonging to two sensor groupings depending on whether light was present. General linear models (GLM) with non-constant variance and covariances among observations were used to estimate the monthly temperature means for each cave separately. The model included fixed effects of month within year and sensor group; temporal autocorrelation of the observations was captured by assuming the residuals were correlated according to a autoregressive process with a lag of one (AR(1)); and variance was assumed to differ by month. The AR(1) covariance was chosen because temporal autocorrelations showed a strong value at a 1 day lag but a small partial autocorrelation value for a lag of 2 days (results not shown). It was expected that some months would have more variable values than others. Other fixed effects were also considered, namely season and sensor but were found to be non-informative and statistically non-significant so were dropped from the model.

Overall, we did four analyses: (1) daily variation of hourly data at each station; (2) long-term variation in hourly data via spectral analysis; (3) variation in each cave of hourly data with a generalized linear mixed model; and (4) variation at each station of monthly averages using a generalized linear mixed model.

Results

Overall temperature patterns

Basic statistics for the 17 sites in the three caves are shown in Table 1 and Fig 2. Raw temperature data for the three caves are given in S1 Table (Sistema Muévelo Rico), S2 Table (Sistema Muévelo Sabrosito), and S3 Table (Río Secreto [Tuch]). Overall, cave temperatures were slightly lower (approximately 1˚C) than the ten-year mean temperature for Playa del Carmen of 25.8˚C for 2005 to 2014 [31].

Temperatures at the seven cave stations in Sistema Muévelo Rico had an amplitude of between 6.7 and 12.9˚C, and the three cave stations in Muévelo Sabrosito had a temperature range of between 6.4 and 11.3˚C. In the Tuch section of Río Secreto, where there was a large dark zone (Table 1), temperature ranges at the seven stations varied between 2.0 and 7.4˚C. For all stations in all caves, temperature extremes occurred at the low end, with no high temperature extremes (Fig 2).

Spatial-temporal variation

Plots of temperature through the year are shown in Figs 3 and 4. For all stations, there was a drop in temperature during the winter months of about 3˚C from the summer high. The other difference was that there was differential variability, usually short term, including daily

Table 1. Basic temperature (˚C), and light intensities (lux) for the 17 monitoring stations.

		Temperature			Light
Cave	**Station**	**Mean**	**Min**	**Max**	**Lux**
Sistema Muévelo Rico	1	24.6	18.7	30.0	<0.1
	2	24.9	20.3	27.2	<0.1
	3	24.5	17.5	26.1	<0.1
	4	24.6	15.2	28.1	<0.1
	5	24.5	12.8	29.4	466
	6	24.5	19.2	25.9	0.2
	7	24.5	18.7	26.0	<0.1
Sistema Muévelo Sabrosito	1	25.0	16.7	28.0	<0.1
	2	24.7	18.4	28.1	<0.1
	3[a]	23.5	19.3	25.7	0.3
Río Secreto (Tuch)	1	24.8	22.2	26.3	0
	2	25.5	22.8	27.3	0
	3	25.8	22.3	27.7	0
	4	25.6	25.4	27.4	0
	5	24.9	22.1	26.9	<0.1
	6	25.2	20.6	27.7	0.8
	7	24.6	19.0	26.4	7.7

Station 5 in Sistema Muévelo Rico is at the entrance.

[a] sensor moved on 27 January 2018, n = 2999

https://doi.org/10.1371/journal.pone.0237051.t001

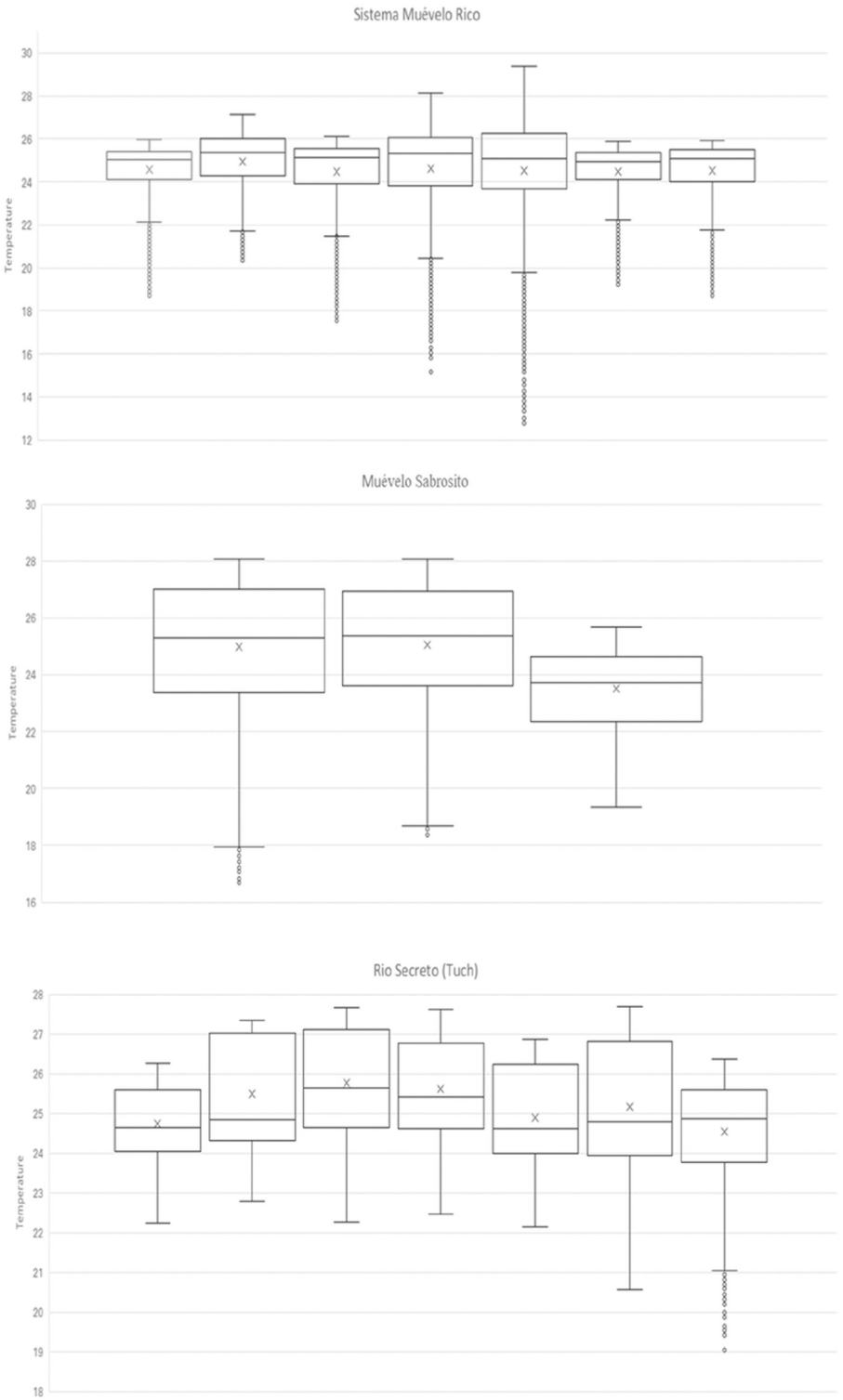

Fig 2. Box and whiskers plots of temperature variation in the individual stations. Order is by number of the station. X's indicate means; the horizontal line within the box, the median; the boxes, the inter-quartile range; whiskers, 1.5 times the interquartile range beyond the box; and small circles are outliers.

https://doi.org/10.1371/journal.pone.0237051.g002

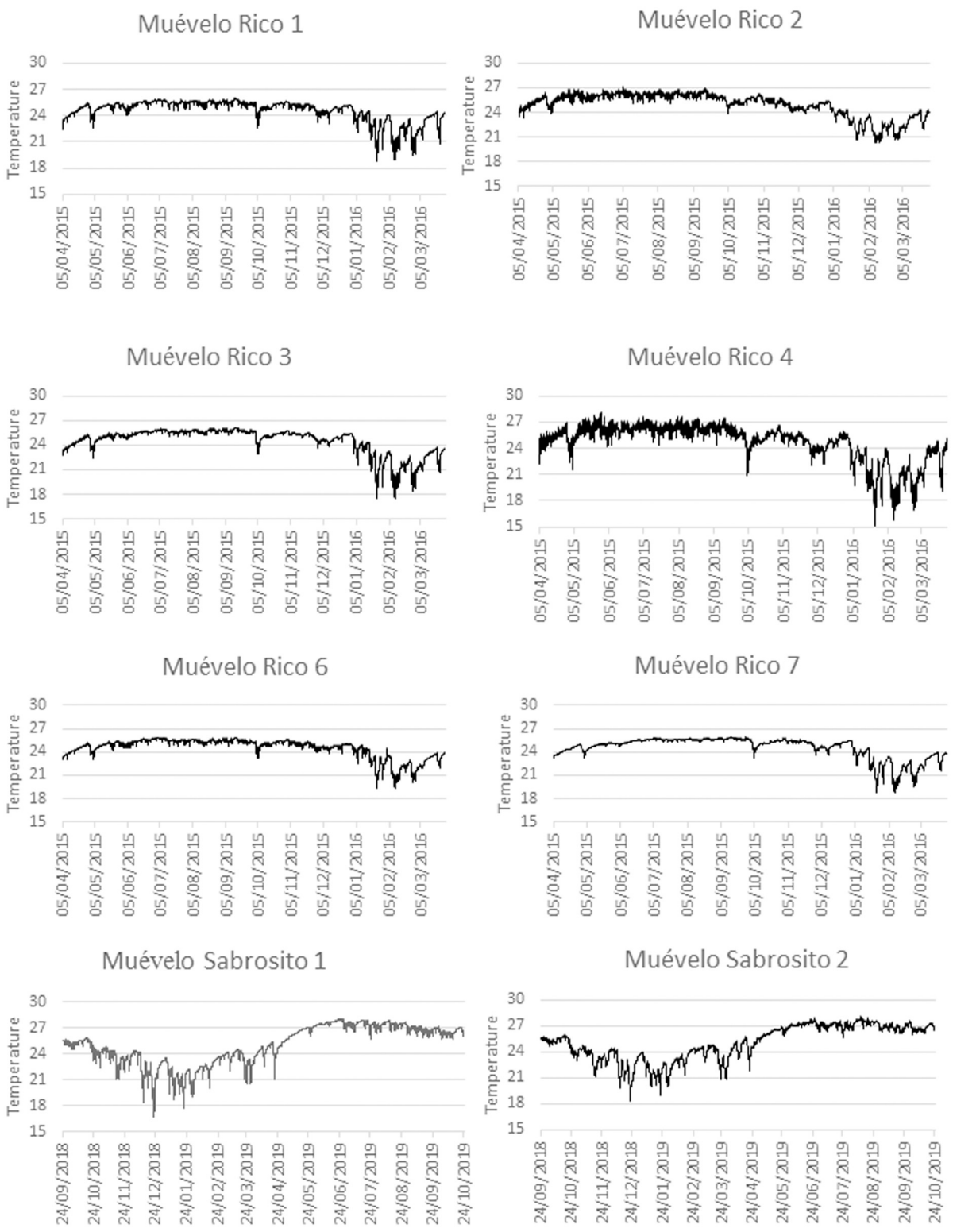

Fig 3. Plot of hourly temperature at stations in Sistema Muévelo Rico and Muévelo Sabrosito. Each station is plotted separately, showing all hourly data. Note that the minimums and higher variability all occur in winter. The patterns appear to be different because of the dates of measurement in the two caves.

https://doi.org/10.1371/journal.pone.0237051.g003

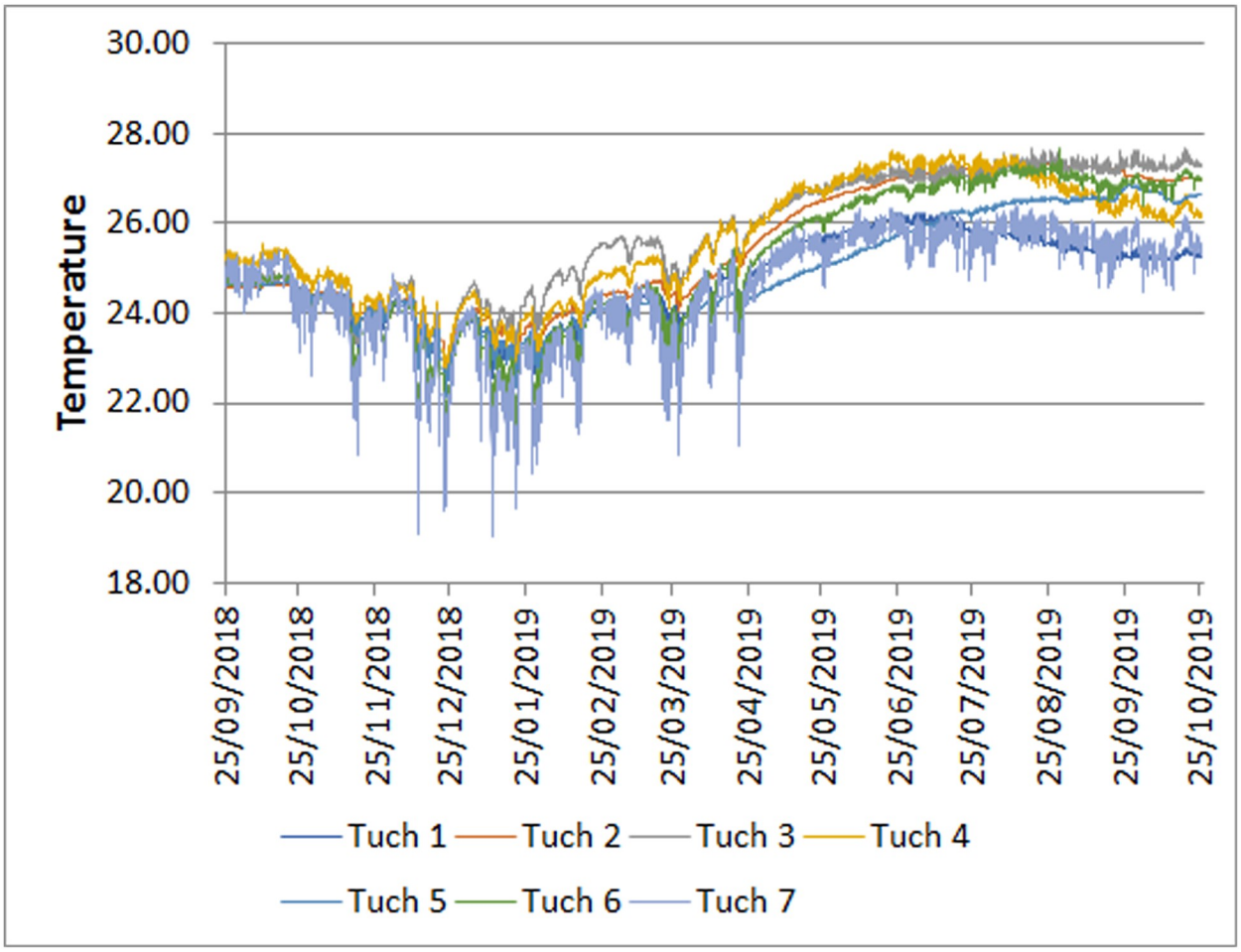

Fig 4. Plot of hourly temperature at stations in Río Secreto near the Tuch entrance. All stations are plotted together for comparison. Only daily means are shown for clarity. Note that the minimums and higher variability all occur in winter.

https://doi.org/10.1371/journal.pone.0237051.g004

fluctuations, that depended on the season. Short term variability was highest during the Nortes season, when a series of cold fronts come through the region [32].

For each of the three caves, the best temperature model included month within a year fixed effects with allowance for monthly unequal variances, and autocorrelation among error terms with a lag of 1 day. Station (and season) had no effect, which was surprising, especially for Río Secreto, where a dark zone was present. The month/year effect was strong, as can be seen in Fig 5, and was highly significant ($p < .0001$) in all cases. In addition, the residuals were well-behaved, being approximately normally distributed. For Muévelo Sabrosito and Muévelo Rico, standard errors were less during the summer months.

Since the temperature measurements for Río Secreto (Tuch) and Muévelo Sabrosito were done at the same time, their patterns can be compared by a generalized linear mixed model. In this case, the interaction of cave x month x sampling site within a cave had a significant effect (Table 2), where sampling sites in Río Secreto (Tuch) were grouped into dark and light sites. When the sites are compared, the seasonal effects remain the most obvious (Fig 6), largely masking differences among stations and caves. The variation is greatest during the winter months.

One especially interesting and contrasting comparison is between the dark and light sites in Río Secreto (Fig 7). Dark zone temperatures tended to be higher throughout the year. This relationship would likely reverse during hotter than normal years.

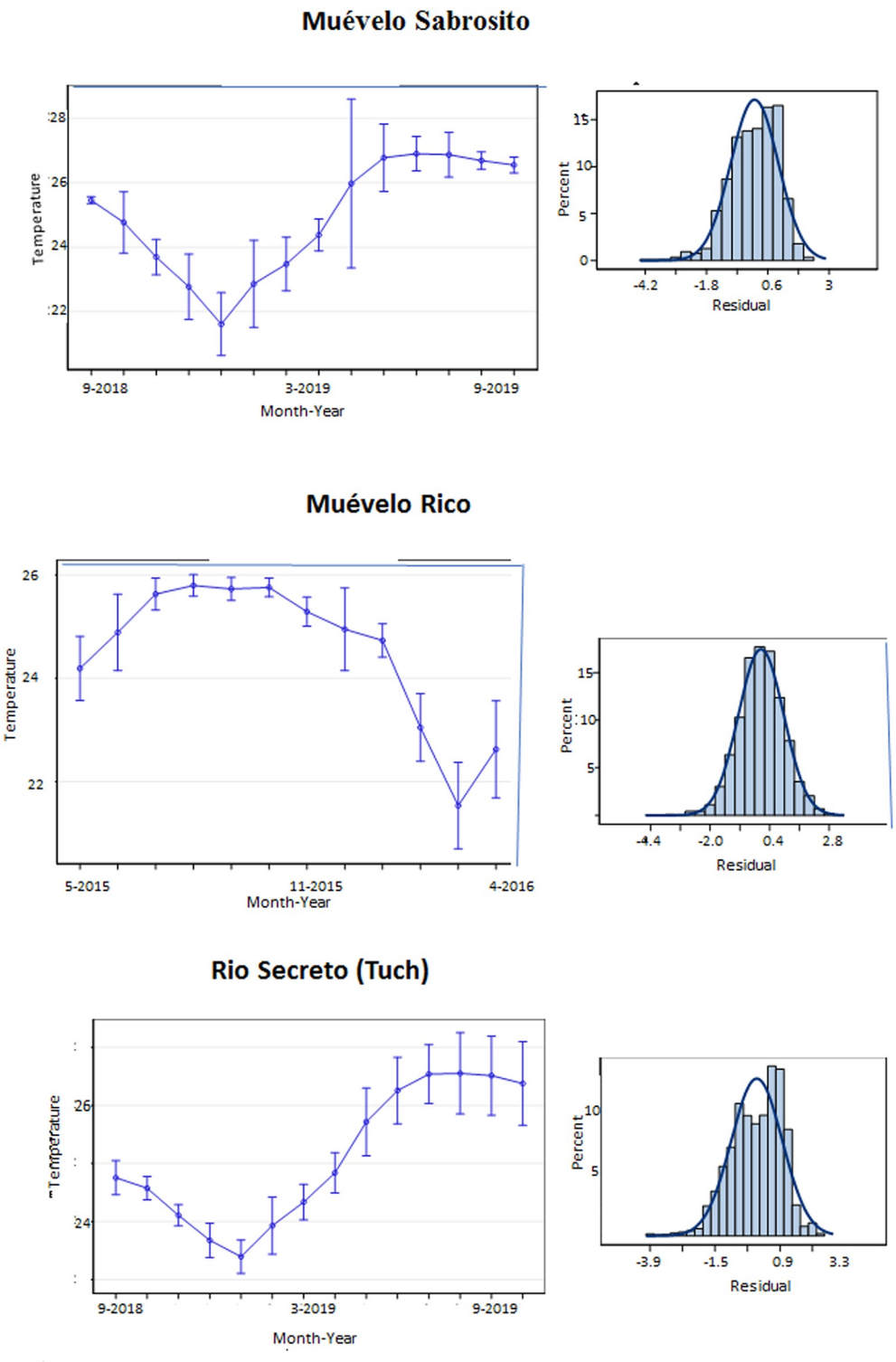

Fig 5. Least Square Means for temperature estimated in the GLM. Left panels are estimates of mean temperature with 95% confidence intervals. Note that the graph for Sistema Muévelo Rico begins at a different month. The entrance station for Sistema Muévelo Rico is not included. Right hand panels are plots of the residuals, compared to a normal distribution.

https://doi.org/10.1371/journal.pone.0237051.g005

Table 2. Type III Tests of Fixed Effects based on GLIMMIX model.

Effect	Numerator DF	Denominator DF	F value	Probability
Cave*site*month	69	25.54	10.43	<0.001

https://doi.org/10.1371/journal.pone.0237051.t002

Daily cycles

Spectral analyses of the 17 sites in the three caves are shown in Figs 8–10, for cycles up to 600 hours in length. For all sites in all caves, the pattern was significantly different than white noise (Fisher's kappa test and Barlett's K-S test).

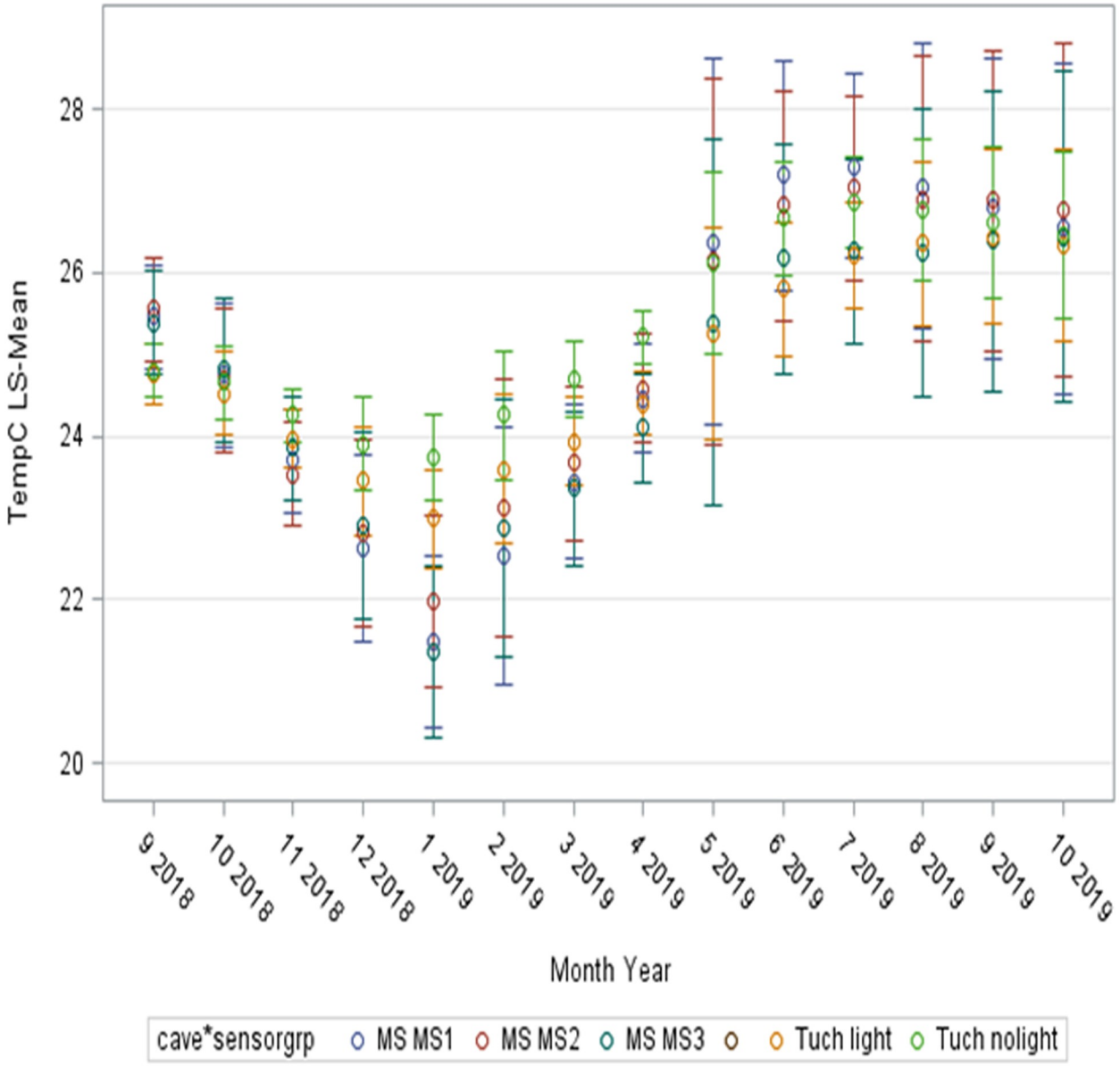

Fig 6. Comparison daily temperatures grouped by month of Río Secreto (labelled as Tuch in figure) and Muévelo Sabrosito (labelled as MS in figure) based on a generalized linear mixed model (see Table 2). Least Square means are shown as circles and 95% confidence limits are shown as lines. The overall impression is that seasonal differences dominate.

https://doi.org/10.1371/journal.pone.0237051.g006

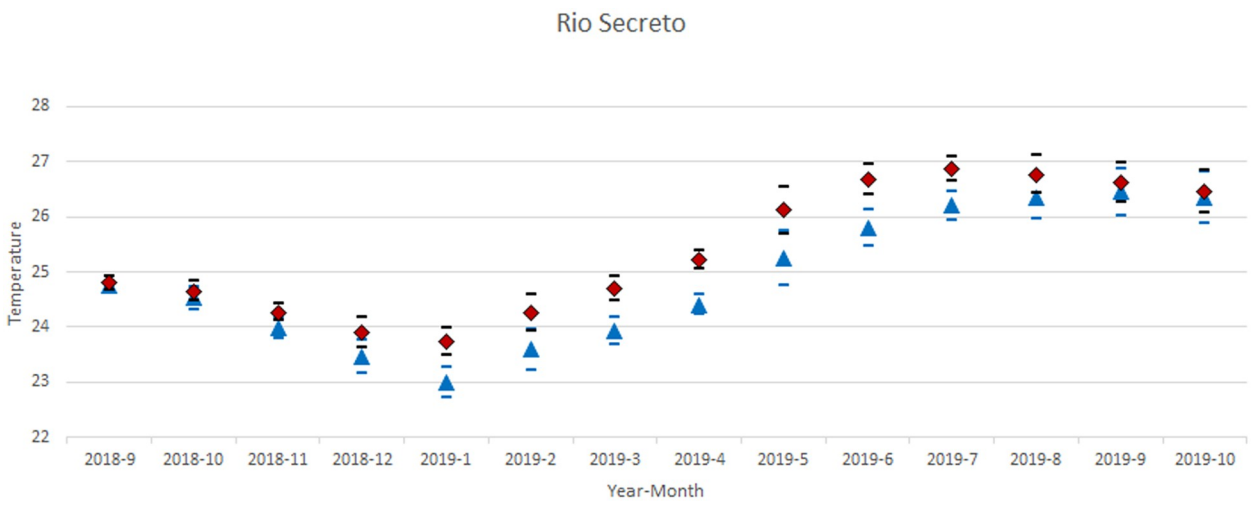

Fig 7. Comparison of GLIMMIX models of aphotic and photic zones in Río Secreto (Tuch). The diamonds and black error bars are for the dark zone and the blue triangles and error bars are for the light zone. The seasonal cycle is apparent as is the greater variation during the winter months.

https://doi.org/10.1371/journal.pone.0237051.g007

Sistema Muévelo Rico (Fig 8) and Muévelo Sabrosito (Fig 9) showed a 24 hour spike at all stations, with a much smaller 12 hour spike at several stations (stations 2, 4, and 5 in Sistema Muévelo Rico and station 3 in Muévelo Sabrosito). There was a strong jump in the spectral density at around 425 hours (17–18 days). It was more prominent than the 24 hour spike in all stations except the entrance in Muévelo Rico. In Muévelo Sabrosito, it was equally prominent in #1 and #2, but the 24 hour spike was more prominent in #3.

Río Secreto (Tuch) showed a different pattern (Fig 10). All stations had a 24 hr spike but it was generally weak. The spike in Tuch #2 was barely evident. The 425 hour spike was also less prominent and not really clear in Tuch #3 and #5 where it became bimodal. There was a more or equally prominent jump at 300 hours (12–13 days). Note these were run at the same time as Muévelo Sabrosito. All these sites showed a seasonal cycle, and the weakness of the daily cycle indicates that the daily temperature flux is not as strong as the seasonal flux.

Discussion

Overall temperature variability

The range of temperature variability in the three study caves varied from 2˚C in Rio Secreto (Tuch) site 4 to 12.9˚C in Sistema Muévelo Rico site 4. Compared to other sites with similar measurements in Slovenia, the Canary Islands, and Hawaii, variation was surprisingly high (Fig 11). Part of this is the result of the geographical context of caves in Quintana Roo, which tend to have multiple entrances and little depth [29, 30]. The largest cave, Rio Secreto (Tuch), had the least variability, and we suspect that there are more isolated sites in the system, with less variation than site 4. Outside of Quintana Roo, the least variable sites were lava tubes in Hawaii [19] and the Canary Islands [16], as well as the large Slovenian show cave, Postojna Planina Cave System [16]. The most variable cave was Jama v Kovačiji, a high altitude snow cave in Slovenia [22]. Many more records are needed before more generalization is possible.

Temporal and spatial patterns

In all three caves there was a marked seasonal effect in temperature, and all stations showed a daily cycle of temperature although the signal was extremely faint in stations 2 and 5 of Río

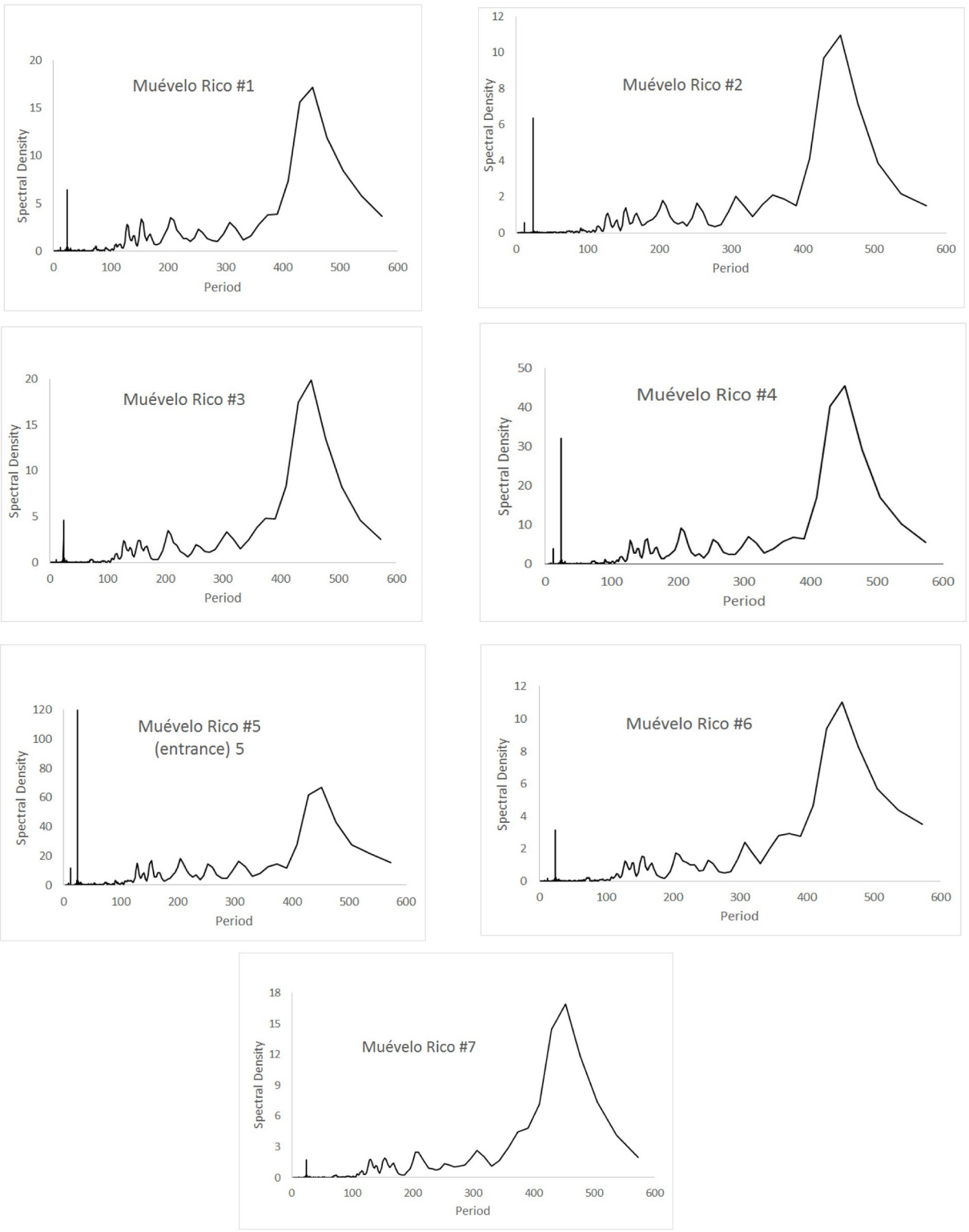

Fig 8. Spectral densities of temperature at the Muévelo Rico sampling stations. Note that the scale of the y-axis is different for different stations. Period is measured in hours.

https://doi.org/10.1371/journal.pone.0237051.g008

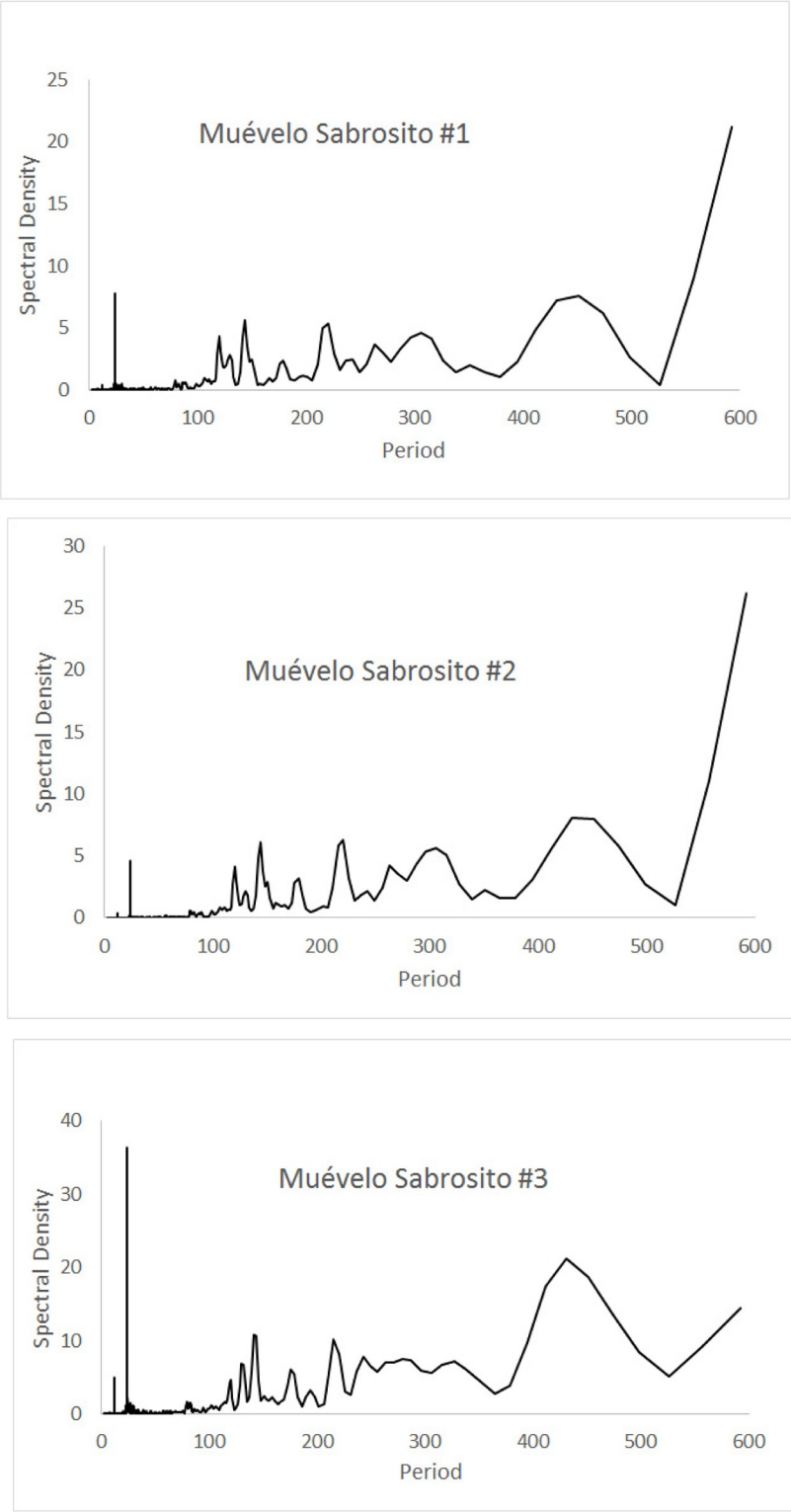

Fig 9. Spectral densities of temperature at the Muévelo Sabrosito sampling stations. Note that the scale of the y-axis is different for different stations. Period is measured in hours.

https://doi.org/10.1371/journal.pone.0237051.g009

Fig 10. Spectral densities of temperature at the Río Secreto (Tuch) sampling stations. Note that the scale of the y-axis is different for different stations. Period is measured in hours.

https://doi.org/10.1371/journal.pone.0237051.g010

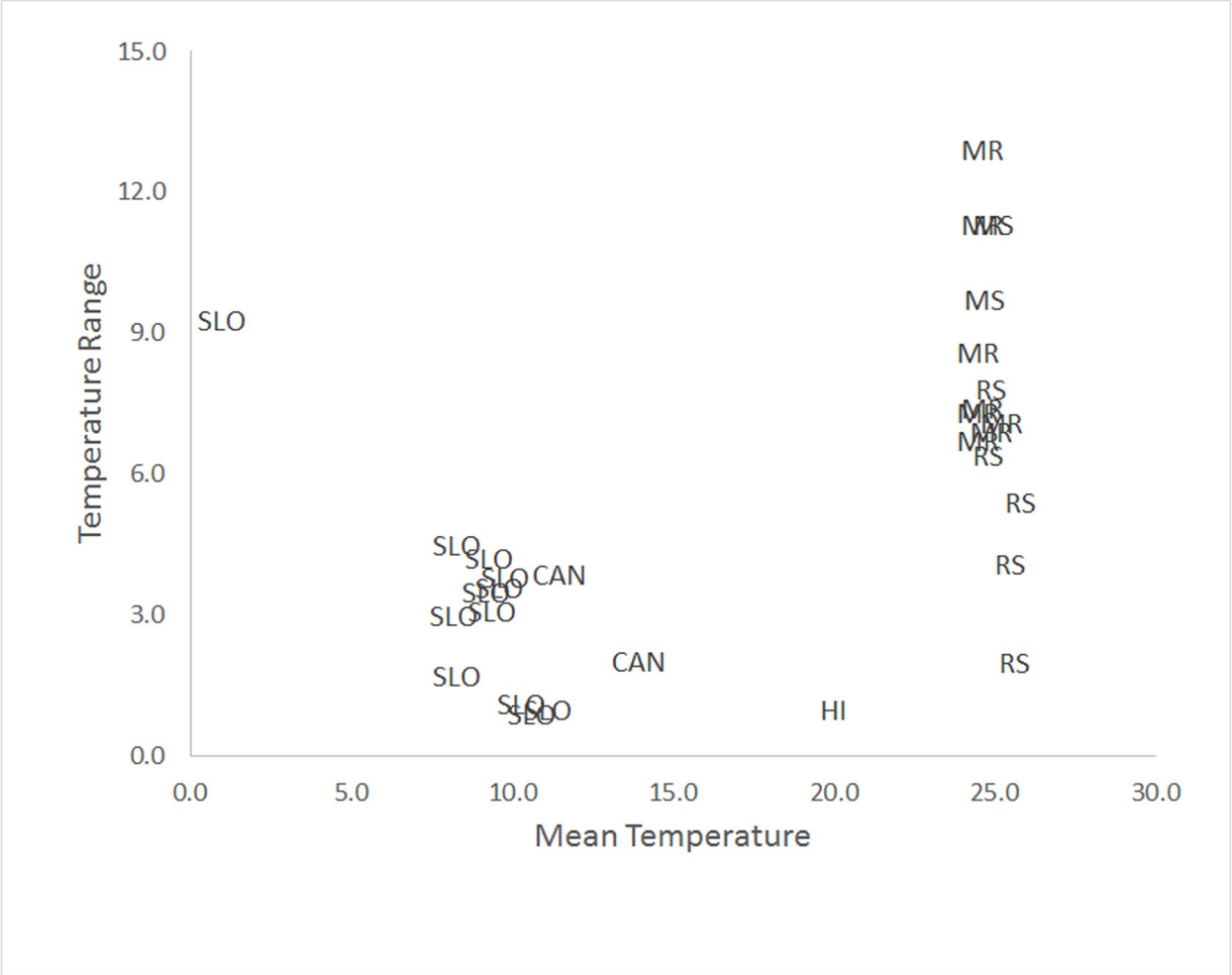

Fig 11. Comparison of overall temperature variability in caves for which year long hourly temperature records are available. Abbreviations are SLO (Slovenia), CAN (Canary Islands), HI (Hawaii), MR (Muévelo Rico), MS (Muévelo Sobrosito), and RS (Rio Secreto [Tuch]). Data from present study and [14, 16, 19, 22].

https://doi.org/10.1371/journal.pone.0237051.g011

Secreto (Tuch) (Fig 10). Some stations in Sistema Muévelo Rico and Muévelo Sabrosito had an odd 12 spike. It is now known what the environmental driver for this is. None of the stations in Río Secreto (Tuch) were particularly deep in the cave, and it seems certain that deeper sites would have no discernible daily temperature cycle. We do not have detailed surface temperature data available. The estimated monthly means for the interior of Río Secreto (Tuch) had a range of 21.5 to 25.8˚C. By contrast, surface monthly temperatures in nearby Playa del Carmen ranged from 21 to 30˚C for a 14 year period [32]. In this case the percent reduction in amplitude was 52 percent. The surface and cave data sets are not strictly comparable but do give a sense of the amount of attenuation of temperature. However, it also seems unlikely that there is anywhere in this river cave without temperature variation throughout the year. For example, there is a detectable annual temperature cycle in Kartchner Caverns, Arizona, with an amplitude of less than 2˚C [4, 7]. Kartchner Caverns is a large desert cave with no stream and a single entrance [34], and thus likely to be less variable than river caves like Río Secreto. While we did not directly demonstrate the reduction of temperature variation in caves relative to surface conditions, this reduction has been recognized for over a century [1, 24]. What has not been

recognized by biologists studying caves is that the reduced temperature variation still carries the cyclical signals present on the surface, including daily cycles.

There are also subtle differences in overall temperature in the three caves we studied, as well as differences among sites within a cave, The highest mean temperature was at site 3 in Río Secreto (Tuch) (25.8˚C) and the lowest was at several sites in Sistema Muévelo Rico (Table 1). Fairchild and Baker [4] outline the many factors that result in spatial and temporal differences in temperature in caves. This variation is of considerable importance to climatologists attempting to use speleothems as proxies for climate change. Some of the differences may be the result of differences in equilibration rates and time. The rate of equilibrium of cave temperature has been measured at 0.04˚C per year in Villars Cave in France [35], indicating equilibration takes a rather long time. Time lags also imply a different phase for surface and cave temperature cycles [16].

We would expect different caves in different regions to have different patterns with respect to the temporal variation and co-variation of light and temperature. The caves we studied were very shallow with numerous surface connections making variation in temperature on the surface a strong signal in the caves. It is likely that in temperate regions, with greater surface variation, that the attenuation in caves is greater, but we suspect that temporal patterning persists, as it does for some non-cave shallow subterranean habitats [27].

Is the temperature variation observed biologically significant?

We do not know what the biological response, if any, is to the relatively small amplitude of temperature variation. Large-scale differences in temperatures may well be lethal to many cave organisms since they do not encounter large scale changes, and put cave animals at special risk with respect to global warming [20]. Smaller differences may be important in niche separation, as Mammola and Isaia [26, 27] show for subterranean spiders. They found that differences of 1˚C or less can be important in determining microdistribution of spiders, which suggests that the temperature differences within a cave documented in this study may be biologically important. Mammola and Isaia [26, 27] did not study seasonality and cyclicity but we conjecture that they may also be important determinants of microdistributions.

There is also a disconnect between lux values observed in caves and shallow subsurface habitats with the lux values typically used in experiments with subterranean animals [36]. The scarcity of surface dwellers and the relative abundance of cave animals in dimly lit Muévelo Rico [33] suggests that very low light levels are in some ways equivalent to no light, at least in terms of faunal composition. Low temperature variation may likewise be equivalent to no temperature variation for the cave inhabitants.

It is well documented that for species limited to caves and other aphotic habitats, that eyes and pigment tend to be reduced or absent compared to related surface-dwelling species [37]. A similar reduction with respect to thermal tolerance may be expected for species living in environments that are nearly thermally constant, such as caves [20, 38]. One hypothesis is that the thermal tolerance of cave-limited species should correspond to the temperature variation in the subterranean habitats where the species are found. The actual pattern, and it is hard to even find a pattern, is quite different [20]. There are a very few cases where temperatures out of the range of those encountered have been reported to be lethal, most notably two species of *Proasellus* isopods living in caves and springs in the French Jura Mountains [39]. However, a third species showed broad thermal tolerances. A more common finding is that thermal tolerances of subterranean species are less than species found on the surface but that the range of thermal tolerance is much greater than the temperature range currently encountered by the species [40–42]. Pallares et al. [38] present data on thermal acclimation of beetles of differing

dependence on caves and show that the loss of acclimation in cave specialist may make these species especially sensitive to climate change.

Nearly all the studied examples are from temperate zone caves and the situation may be different in tropical caves, where surface variation intemperature is less, where phenotypic plasticity may be reduced in general [43]. The effect of reduced thermal variation may well have other effects, such as a reduction in phenotypic plasticity, but this has been little studied.

The possible reasons for this confusion of results are many. First, testing conditions vary, and it may well be that there are long term effects of temperature change not detected in the experimental protocol. Second, genes for thermal tolerance may have pleiotropic effects, a common situation for eye and pigment loss [44, 45]. This is likely the case for heat shock proteins [46]. Third, there may not have been sufficient evolutionary time for the thermal tolerance to attenuate.

The utility of temperature measurements

The widespread availability of dataloggers to measure temperature provide an unprecedented opportunity to understand the physical environment of caves. At present there is a gap between the views of biologists and physical scientists studying caves—biologists stress constancy and physical scientists stress differences. Physicists, especially Badino [18] and Covington and Perne [11], frame cave temperature around the question of the fate of fluxes of temperature, how far they penetrate and how long they last. They and others [12, 46] have looked at what affects fluxes (e.g., airborne vs. water borne). We have shown what the impact of these fluxes is on temperature trends.

What is clear from the analyses presented here is that there is a muted variability in caves, but variability with a rich temporal and spatial pattern, even in supposedly constant tropical caves. The mapping of organisms onto this pattern should provide new insights into the ecology of cave organisms.

It is also clear that a simple description of variability does not capture the patterns, especially of temperature. It is not the total amount of variability that is likely to be important, but rather its temporal pattern. We found generalized linear models especially useful for the analysis of this pattern and there are of course other statistical tools available. Rather rely on overall measures such as means and standard deviations, we suggest that analysis of temporal patterns is more likely to yield new insights into the cave environment.

Supporting information

S1 Table. Hourly temperature data for Sistema Muévelo Rico.
(XLSX)

S2 Table. Hourly temperature data for Muévelo Sabrosito.
(XLSX)

S3 Table. Hourly temperature data for Río Secreto (Tuch entrance).
(XLSX)

Acknowledgments

Benjamin Schwartz, Christian Martinez, Ximena Rosales, Jesus Cupul, Alex Contreras, Vanessa Tafoya, Rodrigo Cisneros, Fernanda Lases, and Raúl Padilla assisted with field work. Anonymous reviewers greatly improved the manuscript.

Author Contributions

Conceptualization: Luis Mejía-Ortíz, Mary C. Christman, Tanja Pipan, David C. Culver.

Data curation: Mary C. Christman, Tanja Pipan.

Formal analysis: Mary C. Christman.

Funding acquisition: Luis Mejía-Ortíz.

Investigation: Luis Mejía-Ortíz, Tanja Pipan, David C. Culver.

Methodology: Tanja Pipan.

Writing – original draft: David C. Culver.

Writing – review & editing: Luis Mejía-Ortíz, Mary C. Christman, Tanja Pipan, David C. Culver.

References

1. Eigenmann CH. Cave vertebrates of America. A study in degenerative evolution. Washington: Carnegie Institution of Washington; 1909.
2. Géze B. La spéléologie scientifique. Paris: Editions du Seuil; 1965.
3. Moore GW. Cave temperature. Nat Speleological Soc News. 1964; 22: 57–60.
4. Fairchild IJ, Baker A. Speleothem Science. From process to past environments. Chichester, UK: Wiley-Blackwell; 2012.
5. Šebela S, Turk J, Pipan T. Cave micro-climate and tourism: towards 200 years (1819–2015) at Postojnska jama (Slovenia). Cave Karst Sci. 2015; 42: 78–85.
6. Stoeva P, Stoev A, Kiskinova N. Long-term changes in the cave atmosphere air temperature as a result of periodic heliophysical processes. Phys Chem Earth. 2006; 31: 123–128.
7. Cigna AA. Modern trend[s] in cave monitoring. Acta Carsologica. 2002; 31: 35–54.
8. Cigna AA. Climate of caves. In: Gunn J, editors. Encyclopedia of caves and karst science. New York: Fitzroy Dearbor; 2004. pp. 228–230.
9. Bock H. Mathematisch-physikalische Untersuchung der Eishöhlen und Windrören, pp. 102–144. In: Simonys F, editor, Höhlen in Dachstein. Graz: Deutsche Vereins-Druckerei; 1913. pp. 102–144.
10. Wigley T, Brown M. The physics of caves. pp. 329–358. In: Ford T, Cullingford C, editors. The science of speleology. New York: Academic Press; 1976. pp. 329–358.
11. Covington MD, Perne M. Consider a cylindrical cave: a physicists's view of cave and karst science. Acta Carsologica. 2015; 44: 363–380
12. Guerrier B, Doumenc AF, Roux A, Mergui S, Jeannin PY. Climatology in shallow caves with negligible ventilation: Heat and mass transfer. Int J Thermal Sci. 2019; 146: 106066.
13. Jernigan JW, Swift RJ. A mathematical model of air temperature in Mammoth Cave, Kentucky. J Cave Karst Stud. 2001; 63: 3–8.
14. Liu W, Zhou C, Liu Z, Yang C, Brancelj A. The temperature variation in an epikarstic cave and its impact factors: a case from Velika Pasica Cave, Central Slovenia. Arab J Geosci. 2017; 10: 2.
15. Gregorič A, Vaupotič J, Šebela S. The role of cave ventilation in governing cave air temperature and radon levels (Postojna Cave, Slovenia). Int J Climatol. 2013; 34: 1488–1500.
16. Šebela S, Turk J. Air temperature characteristics of the Postojna and Predjama cave systems. Acta Geog Slovenica. 2011; 51: 44–64.
17. Pipan T, Petrič M, Šebela S, Culver DC. Analyzing climate change and surface-subsurface interactions using the Postojna Planina Cave System (Slovenia) as a model system. Regional Env Change. 2018; 19: 179–189.
18. Badino G. Underground meteorology–"what's the weather underground?". Acta Carsologica. 2010; 39: 427–448.
19. Culver DC, Pipan T. Shallow subterranean habitats. Ecology, evolution and conservation. Oxford: Oxford University Press; 2014.

20. Mammola S, Piano E, Cardoso P, Vernon P, Domìnguez-Viller D, Culver DC, et al. Climate change going deep: the effects of global climatic alterations on cave ecosystems. Anthropocene Rev. 2019; 6: 98–116.

21. Hill CA. Mineralogy of Kartchner Caverns, Arizona. J Cave Karst Stud. 1999; 61: 73–78.

22. Pipan T, López H, Oromí P, Polak S, Culver DC. Temperature variation and the presence of troglobionts in shallow subterranean habitats. J Nat Hist. 2011; 45: 253–273.

23. Sket B. An essay about *the essai*. Un hommage a Emil Racoviță. In: Moldavan OT, editor. Essay on biospeleological problems—French, English, Romanain Versions. Cluj-Napoca: Casa Cărții de Ştiință; 2006. pp. 119–125.

24. Racovitza EG. Essai sur les problems biospéologiques. Arch Zool Exp Gén. 1907; 6: 371–488.

25. Racovitza EG. Essay on biospeological problems, translated in English by D.C. Culver and O.T. Moldavan. In: Moldovan OT, editor. Essay on biospeological problems. French, English, Romanian Versions. Cluj-Napoca: Casa Cărții de Ştiință; 2006, pp. 122–183.

26. Mammola S, Isaia M. Niche differentiation in Meta bourneti and M. menardi (Araneae, Tetragnathidae) with notes on the life history. Int J Speleol. 2014; 43: 343–353.

27. Mammola S, Isaia M. The ecological niche of a specialized subterranean spider. Invert Bio. 2016; 135: 20–30.

28. Deharveng L, Bedos A. Biodiversity in the tropics. In: White WB, Culver DC, Pipan T, editors. Encyclopedia of caves, Third edition. London: Academic Press (Elsevier): 2019. pp. 146–162.

29. QRSS. Quintana Roo Speleological Survey.(accessed: May 22, 2020). 2017. https://caves.org/project/qrss/qrss.htm

30. Kambesis PN, Coke JG. Overview of the controls on eogenetic and karst development in Quintana Roo, Mexico, In: Lace MJ, Mylroie JE, editors. Coastal karst landforms. Dordrecht, The Netherlands: Springer; 2013. pp. 347–374.

31. Ward WC. Quaternary geology of northeastern Yucatan Peninsula, part 2. In: Ward WC, Weidie AE, Back W, editors. Geology and hydrogeology of the Yucatan and Quaternary geology of the northeastern Yucatan Peninsula. New Orleans Geological Society: New Orleans: 1985. pp. 23–53.

32. Lases-Hernandez F, Medina-Elizalde M, Burns S, DeCesare M. Long-term monitoring of drip water and groundwater stable isotopic variability in the Yucatán Peninsula: Implications for recharge and speleothem rainfall reconstruction. Geochim Cosmochim Acta. 2019; 246: 41–59.

33. Mejía-Ortíz LM, Pipan T, Culver DC, Sprouse P. The blurred line between photic and aphotic environments: a large Mexican cave with almost no dark zone. Int J Speleol. 2018; 37: 69–80.

34. Buecher RH. Microclimate study of Kartchner Caverns. J Cave Karst Stud. 1999; 61:108–120.

35. Genty D. Palaeoclimate research in Villars Cave (Dordogne, SW-France). Int J Speleology. 2008; 37: 173–191.

36. Fišer Ž, Novak L, Luštrik R, Fišer C. 2016. Light triggers habitat choice of eyeless subterranean but not surface amphipods. Sci Nat. 2016; 103: 7.

37. Fong DW, Kane TC, Culver DC. Vestigialization and loss of nonfunctional characters. Ann Rev Ecol Syst. 1995; 26: 249–268.

38. Mermillod-Blondin F, Lefour G, Lalouette L, Renault D, Malard F, Simon L, et al. Thermal tolerance breadths among crustaceans living in a thermally constant environment. J Exp Bio. 2013; 216: 1683–1694.

39. Novak T, Šajna N, Antolinc E, Lipovšek S, Devetak D, Janžekovič F. Cold tolerance in terrestrial invertebrates inhabiting subterranean habitats. Int J Speleol. 2014; 43: 265–272.

40. Raschmanová N., Miklisová D., Kováč L., et al. Testing the climate variability hypothesis in edaphic and subterranean Collembola (Hexapod). Journal of Thermal Biology. 2018; 78:391–400. https://doi.org/10.1016/j.jtherbio.2018.11.004 PMID: 30509663

41. Pallarés S., Colado R, Pérez-Fernández T, Wesener T, Ribera I, Sánchez-Fernádez D. Heat tolerance and acclimation capacity in subterranean arthropods living under common and stable thermal conditions. Ecol Evol. 2019; 9: 13731–13739. https://doi.org/10.1002/ece3.5782 PMID: 31938477

42. Angilletta MJ. Thermal adaptation. A theoretical and empirical synthesis. New York: Oxford University Press; 2009.

43. Jeffery WR. Evolution of eye degeneration in cavefish: the return of pleiotropy. Subt Bio. 2005; 3: 1–11.

44. Bilandžija H, Ma L, Parkhurst A, Jeffery WR. A potential benefit of albinism in *Astyanax* cavefish: downregulation of the oca2 gene increases tyrosine and catecholamine levels as an alternative to melanin synthesis. PLoS ONE. 2013; 8: e80823. https://doi.org/10.1371/journal.pone.0080823 PMID: 24282555

45. Rohner N, Jarosz DF, Kowalko JE, Yoshizawa M, Jeffery WR, Borowsky RL, et al. Cryptic variation in morphological evolution: HSP90 as a capacitor for loss of eyes in cavefish. Science. 2013; 342: 1372–1375. https://doi.org/10.1126/science.1240276 PMID: 24337296

46. Brookfield AE, Macpherson GL, Covington MD. Effects of changing meteoric precipitation patterns on groundwater temperature in karst environments. Ground Water. 2017; 55: 227–236. https://doi.org/10.1111/gwat.12456 PMID: 27643637